DOI 10.1007/s10778-017-0833-3
International Applied Mechanics, Vol. 53, No. 5, September, 2017

DYNAMICS OF INHOMOGENEOUS SHELL SYSTEMS UNDER NON-STATIONARY LOADING (SURVEY)

P. Z. Lugovoi[*] and V. F. Meish[**]

Experimental works on the determination of dynamics of smooth and stiffened cylindrical shells contacting with a soil medium under various non-stationary loading are reviewed. The results of studying three-layer shells of revolution whose motion equations are obtained within the framework of the hypotheses of the Timoshenko geometrically nonlinear theory are stated. The numerical results for shells with a piecewise or discrete filler enable the analysis of estimation of the influence of geometrical and physical-mechanical parameters of structures on their dynamics and reveal new mechanical effects. Basing on the classical theory of shells and rods, the effect of the discrete arrangement of ribs and coefficients of the Winkler or Pasternak elastic foundation on the normal frequencies and modes of rectangular planar cylindrical and spherical shells is studied. The number and shape of dispersion curves for longitudinal harmonic waves in a stiffened cylindrical shell are determined. The equations of vibrations of ribbed shells of revolution on Winkler or Pasternak elastic foundation are obtained using the geometrically nonlinear theory and the Timoshenko hypotheses. On applying the integral-interpolational method, numerical algorithms are developed and the corresponding non-stationary problems are solved. The special attention is paid to the statement and solution of coupled problems on the dynamical interaction of cylindrical or spherical shells with the soil water-saturated medium of different structure.

Keywords: experimental studies, dynamical problems, impulsive loads, discretely ribbed shells of revolution, three-layer elements of shell structures, Timoshenko geometrically nonlinear shell theory, Winkler and Pasternak elastic foundation, soil medium system, harmonic waves, dispersion curves, normal frequencies, non-stationary vibrations, numerical method

Introduction. The analysis of the dynamical behavior of modern shell systems is evidence of the considerable influence of inhomogeneities such as stiffening ribs, layering, and the interaction of shells with the environment on their strength. Theoretical and experimental studies of the dynamics of shells of revolution are reviewed in [6, 10, 24, 25, 33, 34, 71, 144]. However, aspects of experimental evaluation of vibrations and stress–strain state (SSS) of shell structures contacting with a continuum and subject to impulsive loading have been studied inadequately. In the present survey, considerable attention is paid to experimental investigations of the dynamics of inhomogeneous cylindrical shells in soil medium under non-stationary loading. The obtained experimental data make it possible to evaluate the applicability of the theoretical approaches used.

Three-layer shell elements consisting of two bearing layers and piecewise homogeneous filler providing their combined operation have received considerable distribution in technology. On calculating the strength of these shell structures with a piecewise homogeneous filler under dynamic loading, it is necessary to determine the SSS both in the domain of and at a considerable distance from the inhomogeneities. It follows from the analysis of the publications [14, 15, 28, 32, 40, 43, 51] that there are few publications on dynamical processes in three-layer shells with piecewise homogeneous filler; they mainly address

S. P. Timoshenko Institute of Mechanics, National Academy of Sciences of Ukraine, 3 Nesterova St., Kyiv, Ukraine 03057, e-mail: [*]plugovyy@inmech.kiev.ua; [**]vfmeish@gmail.com. Translated from Prikladnaya Mekhanika, Vol. 53, No. 5, pp. 3–65, September–October, 2017. Original article submitted June 5, 2015.

steady vibrations. The study of the effect of parameters of piecewise-homogeneous filler on oscillatory processes in three-layer shells of revolution is one of the areas for further investigations. To this end, we formulate nonlinear dynamical problems of the theory of three-layershells of revolution with piecewise-homogeneous filler and derive (using the Reissner variational principle) of the vibrations equations, contacting conditions by the structure length in the domain of variation of the filler parameters and boundary conditions for independent kinematic and static hypotheses for each layer of the shell, considering transversal normal and shearing deformations in filler. Use is made of assumptions corresponding to (in the geometrically nonlinear theory of shells) the Timoshenko hypotheses [138] and an efficient numerical technique for solving problems of this class. The obtained solutions for axisymmetric problems for three-layer shells of revolution with piecewise-homogeneous filler under non-stationary loading enable investigation of the effect of the geometrical and physical-mechanical parameters of the initial structures on their SSS and discover new mechanical effects [62, 63, 101].

The analysis of the dynamical behavior of three-layer shells of revolution with allowance for the discreteness of the filler necessitates the development of refined computer methods for thin-walled systems. Based on this we obtain the equations of vibrations and the corresponding natural boundary conditions on the basis of the Hamilton–Ostrogradsky variational principle within the geometrically nonlinear shell theory corresponding to the Timoshenko hypotheses in quadratic approximation. Efficient numerical methods and algorithms for solving problems of non-stationary axisymmetric and nonaxisymmetric vibrations of three-layer shells of revolution with discrete filler were developed. The numerical method used for solving the dynamical problems of the theory of three-layer shells is based on use of the integral-interpolation method for constructing difference schemes with respect to spatial variables and an explicit finite-difference scheme with respect to the time coordinate [33].

Based on the initial computational model and the developed numerical algorithms, we obtained solutions of dynamical problems in the case of axisymmetric and nonaxisymmetric vibrations and perform the SSS analysis of three-layer shells of revolution under non-stationary loading over a wide range of geometrical and physical-mechanical parameters. Numerical results, regularities and mechanical effects peculiar for wave processes in such three-layer shells are analyzed. In the case of cylindrical shells, numerical results for deflection magnitudes obtained according to the theory of three-layer shells with discrete filler and structurally orthotropic shells are compared. Computations are evidence of the fact that the deflection magnitudes according to the structurally-orthotropic model take place within the limits of variation of the deflection magnitudes of the inner and outer layers according to the theory allowing for the discreteness of ribs.

Investigations of the dynamics of inhomogeneous shell systems on elastic foundation are intensively developed due to the practical use of such structures. Aspects of the dynamics of smooth and stiffened plates and shells of revolution are sufficiently fully covered in [6, 33].

In the present survey starting from the equations of vibration of the classical theory of beams, plates, and shells [3] with discrete ribs, a technique is stated and natural frequencies and modes of vibrations of rectangular planar shells on Winkler and Pasternak elastic foundation [13, 35, 95] are determined. Similar problems were solved for the stiffened cylindrical shell on elastic foundation [36]. The numbers and shapes of dispersion curves for harmonic waves propagating along the longitudinally stiffened cylindrical shell on elastic foundation were determined [100]. The problem statement of vibrations of ribbed shells on elastic foundation is given with the use of the geometrically nonlinear theory of beams and shells with considering assumptions corresponding to the Timoshenko hypothesis, the equations of vibrations of discretely stiffened shells of revolution on the Winkler of Pasternak elastic foundation were obtained by means of the Hamilton–Ostrogradsky variational principle. For discretely stiffened shells of revolution on elastic foundation, we obtain finite-difference schemes using integral-differential interpolation method for construction of difference schemes and solve the corresponding non-stationary problems [8, 9, 74, 27, 97]. Particular attention is paid to the statement of coupled problems of interaction of cylindrical and spherical shells with soil medium modeled by nonlinear three-component ground. For the motion equations and boundary conditions of soil medium interacting with cylindrical or spherical shells, correspondingly, the MacCormack finite-difference schemes were constructed. The numerical algorithms for solving dynamical problems of discretely stiffened shells of revolution on the elastic foundation as well as for coupled problems of interaction on the action of impulsive loading on cylindrical and spherical shells in water-saturated ground massif were developed. Solving coupled problems of vibrations of discretely stiffened shells of revolution under impulsive loading [6, 10, 15, 17, 22, 25, 26, 28] enables investigation of the influence of the properties of the elastic medium on the mechanical effects in inhomogeneous shell systems. The similarity of the structure of the equations of cylindrical and spherical shells on elastic foundation and in soil medium enables performing the theoretical estimation of the

TABLE 1.1

l, mm	0	10	20	30	40	50	60	70
$\varepsilon_{av} \cdot 10^5$	–0.8	0.2	0.5	1.5	2.0	3.0	4.0	5.0
l, mm	80	85	90	95	100	110	120	130
$\varepsilon_{av} \cdot 10^5$	6.0	7.0	8.0	9.5	8.0	6.0	5.0	3.0

Winkler coefficient. New data about the action of impulsive loading on cylindrical cavities and cylindrical shells in periodic ground media were obtained in [41, 42, 54].

In the present survey, preference is given to the results obtained by the authors of the present article, as well as executed in collaboration with colleagues. It is necessary to note that the survey does not reflect results of investigations obtained by other authors. In particular, we note that investigations on the dynamic behavior of multilayered shells are not completely presented in the survey.

1. Experimental Investigations of Environmental Effect on the Dynamics of Inhomogeneous Shell Structures under Impulse Loading. Publications on experimental investigations of vibrations and SSS of shell structures are reviewed in [6, 10, 33, 34, 71]. However, aspects of experimental evaluation of the dynamics of shell systems contacting with continuum and subject to non-stationary loading have been studied inadequately. Therefore, in the present survey considerable attention will be paid to experimental investigations of the dynamics of inhomogeneous cylindrical shells in soil medium under impulsive loading. It is expedient to combine the use of theoretical methods of investigation of shell systems with experimental approaches to substantiate their efficiency and ascertaining the limits of their applicability.

1.1. Investigation of the Phenomenon of Quasi-total Internal Reflection (QTIR) in Shells with Liquid. The analysis of the conducted research of the QTIR phenomenon [4] enables drawing the conclusion that similar QTIR phenomena can take place in different structures filled with liquid. For example, in performing perforating-explosive operations in casing pipes filled with liquid, when an explosion occurs on the axis of the orthotropic cylindrical shell, the QTIR angles [18, 19] are determined from the equation $\cos\beta_k = a / V_k$ (β_k is the QTIR angle, a is the sound velocity in liquid, V_k is the velocity of quasi-longitudinal wave in the cylindrical shell). It is known [7, 102] that if the stiffness parameter of elastic foundation ($0 < C <$) and the shell geometry ($0 < R <$) vary substantially, the critical velocities of quasi-longitudinal waves in the orthotropic casing pipe on elastic foundation vary slightly, since they are bounded by the range $V_1 < V_k < V_3$ for $G_{13} < E_1$. The angles of reflection β_k in the domain $\beta_1 < \beta_k < \beta_3$ change similarly. This fact points out that the most dangerous is the pipe segment $l \le R(1-\cos\beta_3)/\cos\beta_3$. Thus, the conducted theoretical investigations gives the possibility to refine parameters of safe explosive processing of boreholes, which is desirable to validate experimentally.

In the experiments, an orthotropic pipe of length $L = 0.35$ m, radius $R = 0.138$ m, and thickness $h = 0.008$ m is used as testing sample. The moduli of elasticity for the material of the shell $E_1 = 4.3 \cdot 10^{10}$ Pa and $E_2 = 0.76 \cdot 10^{10}$ Pa [11]. In the middle of its inner surface along the generatrix, a strain gage was pasted on for measuring longitudinal deformations. The capacitor discharge on the pipe axis serves as a source of shock waves. The signal from a bridge circuit (from the strain gage) was recorded by a C9-8 oscillograph. The shell with strain gage was immersed in water and placed at the reservoir center; therefore, the reservoir walls and water day surface did not affect the results of experiments. The point of electric discharge fixedly moved along the axis of the tube from the beginning (above the gage) to 0.13 m. The orthotropic pipe was filled with water and placed in water; therefore, water was an elastic foundation for it.

Table 1.1 gives the distances l along the generatrix from the epicenter of the explosion and mean values of maximal tensile strains ε_{av}.

It follows from Table 1.1 that the maximal deformations of the inner surface of the shell occur at the point $l = 0.095$ m, which correspond to a QTIR angle of 55.8°. According to the theory stated above, the QTIR angle is equal to 50.3°. The difference between theoretical results and experimental data does not exceed 11%. Thus, we conclude that when drawing up

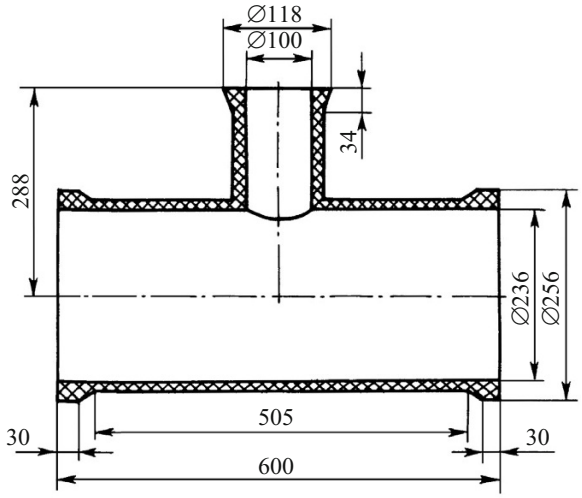

Fig. 1.1

projects for safe explosive-perforating operations in wells with liquid, it is necessary to take into account the obtained theoretically and experimentally confirmed effect of abrupt increase in the strains and stresses at the points defining the QTIR angle.

1.2. Dynamics of Fiberglass Shell Structure under Transverse Impulsive Loading. The effect of impulsive loading of a fiberglass shell structure, consisting of a closed cylindrical shell and a cylindrical joining pipe, on its natural frequencies and modes, as well as its SSS is studied. Investigations of the influence of the environment on the minimal natural frequency of vibrations and SSS of the shell with joining pipe under impulsive loading is of interest [99].

1.3. Frequencies and Modes of Resonant Vibrations. The shell (Fig. 1.1) was used for the experimental investigation. The thickness of the shell and joining pipe is $h = 0.003$ m. According to the conclusions drawn in [11], the moduli of elasticity for the material of the shell $E_1 = 4.3 \cdot 10^{10}$ Pa and $E_2 = 0.76 \cdot 10^{10}$ Pa. The system, consisting of a shell, attached rigidly with the help of rings to the mass brackets, was installed in a metal container with dimensions 0.80×0.45×0.45 m. The container was filled with a material such that the joining pipe does not contact with it. The vibrations of the shell were excited kinematically by means of VEDS-10A vibration electrical dynamical stand. The frequency of forced vibrations was checked by F3-32 electronic frequency counter. The amplitudes of the shell were measured in a contact-free way by means of a vibrator inverter, on which a signal from aluminum plate with the center at the distance $L/4$ from the shell edge (L is the shell length) was supplied. a similar plate was pasted at the point $L/2$. The results of determination of amplitude-frequency characteristics (AFC) of the shell are given in Fig. 1.2*a* for the shell without sand and in Fig. 1.2*b* for the shell contacting with the medium. The modes in the middle cross-section of the shell $L/2$ are shown in Fig. 1.3*a* and in the cross-section $L/4$ from the shell edge in Fig. 1.3*b*. The maximum natural frequency of the shell not contacting with the medium is equal to 230 Hz, and the associated natural modes $n = 4$ (at the points $L/2$ and $L/4$) are presented in Fig. 1.3*a*, *b*, respectively. The minimum natural frequency of the shell contacting with sand is equal to 49 Hz.

It was ascertained that contact of the shell with the medium has a considerable influence on both minimal natural frequency of the shell and the natural frequencies of the whole system.

1.4. Experimental Determination of the SSS of the Shell under Impulsive Loading. Impulsive loading was by generated by dropping a monolith weight on a diaphragm. The diaphragm is a cone with a base of radius $R = 0.10$ m. The cone is attached by means of three screws to the upper edge of the joining pipe such that the cone axis coincides with the joining pipe axis. A pad done of vacuum rubber of 6 mm thickness is installed on the cone bottom. A steel cylinder with a weight of 4.78 kg is used as a monolith. The drop height h was equal to 0.05, 0.10, 0.15, and 0.20 m. Strain gages were used to measure deformations, which were pasted at the points $L/2$ and $L/4$. The strain gages were alternatively connected with bridge circuit, consisting of three MSR-63 resistance banks. The voltage of the bridge disbalance was determined by a V3-56 millivoltmeter. This voltage was used to determine circumferential and longitudinal strains on both outer and inner surfaces. The strains were calculated as in [6].

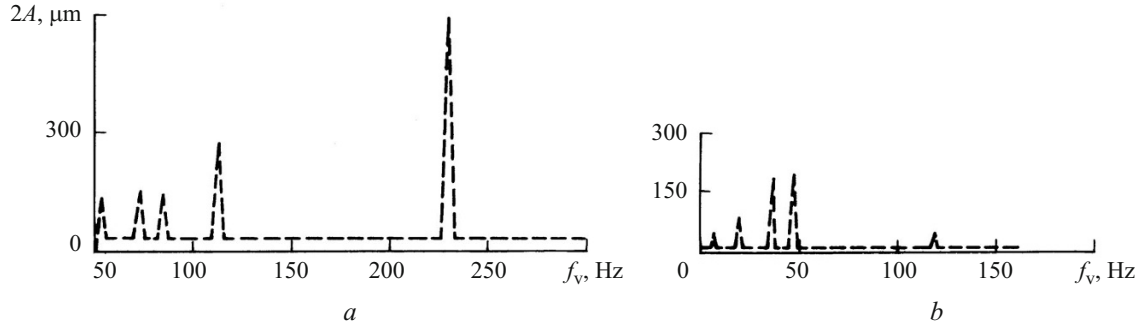

a *b*

Fig. 1.2

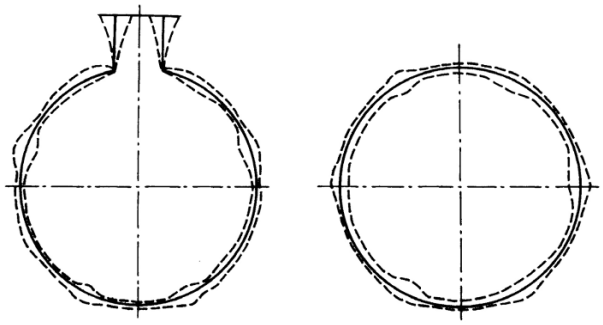

a *b*

Fig. 1.3

The disbalance voltage of the bridge circuit was supplied to the input of a F8-17 oscillograph with memory and was recorded on its screen. Vibrorecords at the point $L/2$ in the circumferential and longitudinal directions due to the action of impulsive loading are given in Fig. 1.4*a*, *b*, respectively. The maximum strains at the places of strain gages were determined from the vibrorecords. Here the maximal values for a drop height of 0.20 m were used as the amplitude of the impulse acting on the structure. According to the conclusion drawn in [18], it is possible to assume the impulsive loading constant during the entire period of impact, and its value is determined as

$$F = \frac{m\sqrt{2gh}}{\tau}, \tag{1.1}$$

where m is the mass of the falling monolith; g is the free-falling acceleration; h is the drop height; τ is the impact duration.

Table 1.2 shows the dependence of vibrostresses ($\sigma^1_{1\text{dist}}$ for the shell without a medium, $\sigma^2_{1\text{dist}}$ for the shell with medium) on the magnitude of the total impulse for variant $L/2$. The table indicates that the shell structure response to impulsive loading is strongly dependent on whether the structure is in contact with a medium or not. In the absence of continuum, the vibrostresses are considerably smaller than for the shell with medium (Table 1.2). For the fourth variant, the difference is about 13%.

1.5. Experimental Investigation of the Influence of a Medium on the Vibroaccelerations of a Shell Structure Subject to Dynamical Loading. The accelerations of the shell structure were measured with a standard D14 accelerometer rigidly fixed to the shell wall at the point $L/2$. The maximal values of accelerations at the point of accelerometer fixing were determined. The dependence of maximal accelerations on the maximum of the total impulse for two variants of acceleration is presented in Table 1.3: where accelerations a correspond to excitation of the shell without interaction with medium and accelerations a^1 are for the shell contacting with the medium.

The dependences of accelerations at the point $L/2$ on the level of the shell excitation by a vibrator in resonant mode are shown in Tables 1.4 and 1.5. Note that the obtained data (Tables 1.4 and 1.5) are evidence of the fact that the shell structure response to impulsive loading considerably depends on whether the structure is in contact with a medium. The dependence of vibroaccelerations a on the level of excitation of the shell (without medium), which was regulated by a milliampere meter, is

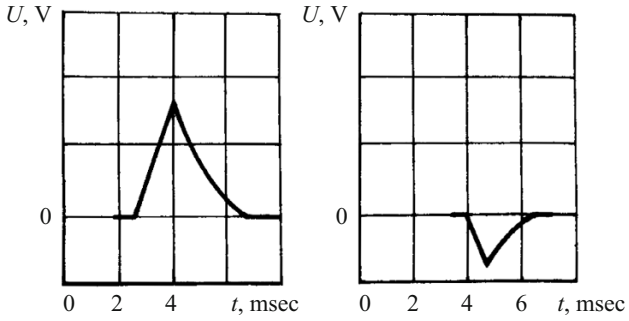

Fig. 1.4

TABLE 1.2

F, H	$\sigma^1_{1\text{dist}} / 10^5$, Pa	$\sigma^2_{1\text{dist}} / 10^5$, Pa
675.9	245.53	384.14
956.0	552.98	687.73
1170.8	737.02	893.41
1352.0	882.90	996.45

TABLE 1.3

F, H	a, m/sec^2	a^1, m/sec^2
675.9	30	25
956.0	50	36
1170.8	70	50
1352.0	90	70

given in Table 1.4. The same dependence of vibroaccelerations a^1 on the level of excitation of the same shell but contacting with medium is given in Table 1.5.

It follows from Tables 1.3–1.5 that in the absence of medium, the vibroaccelerations are considerably greater than in the presence of liquid.

1.6. Experimental Investigation of Vibrations of Cylindrical Shells Contacting with Medium under Impulsive Loading. The natural frequencies and modes of vibrations and vibroaccelerations of a cylindrical shell filled with a medium were determined in [94, 98]. For the execution of experiments a special installation was developed, where water, clay, and sand were working media. The natural frequencies and modes of vibrations of the model were determined and compared with the results of experimental investigations [17].

1.7. Experimental Investigations of Natural Frequencies and Modes of Vibrations of a Stiffened Cylindrical Shell. A stiffened cylindrical shell of radius $R = 0.20$ m, length $L = 0.45$ m, and thickness $h = 0.0005$ m was used as an experimental sample [98]. On the outer surface, the shell was stiffened by 32 stringers of angle profile 0.004×0.0035×0.0005 m, uniformly distributed along the circumference. The stringer length was 0.45 m. The shell and stringers were made of AMg-6M aluminium alloy. The shell edges were placed into circumferential slots of steel disks, filled with molten paraffin, on which solidification the conditions of rigid fixing of the shell edges were realized. During the experiments, the shell was filled with liquid, clay, or sand. For determination of the natural frequencies and modes of vibrations, the resonance method was used. The natural modes of the shell were determined by measuring the amplitudes of deflection in the circumferential and longitudinal directions. The amplitudes of vibrations were determined with a vibrator inverter of eddy-current type and VVV-302 electronic unit. The testing shell was installed on a mass foundation. The contact-free vibrator inverter was fixed to a rigid holder installed on a mass plate. The vibrations of the shell were excited using a VEDS-10A vibration electrodynamic stand. To plot the AFC, the electric current in the coil was kept constant and was checked by an amperemeter. The frequency of forced vibrations was recorded with F3-32 electronic counting frequency meter with accuracy up to 1 Hz. The results of measurements of AFC for $H_1 = 0$ and $H_1 = 1$ ($H_1 = H / L$, where H is the height of the medium in the shell) for $n = 8$ (n is the number of circumferential waves) are shown in Fig. 1.5. The AFC for the shell filled with clay, empty shell, and shell with dry sand are given in Fig. 1.5*a–c* correspondingly. The

TABLE 1.4

f_e, Hz	I, mA	a, m/sec^2
112	22	260
	28	185
	35	150
	42	105
230	22	190
	28	162
	35	135
	42	110

TABLE 1.5

f_e, Hz	I, mA	a^1, m/sec^2
38	22	32
	28	24
	35	20
	42	13
49	22	35
	28	29
	35	22
	42	14

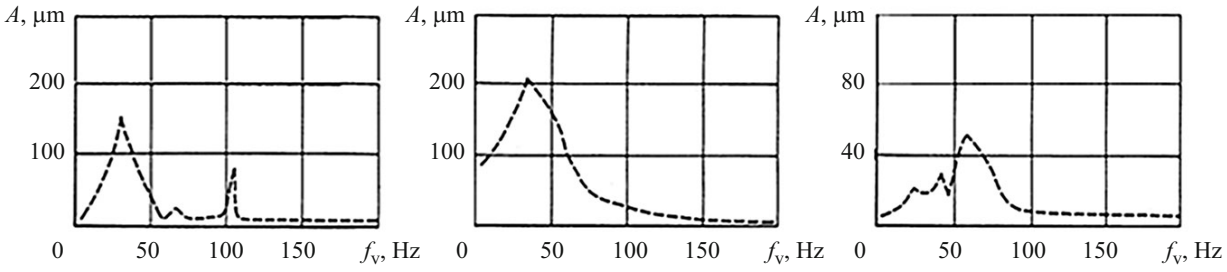

a *b* *c*

Fig. 1.5

number of half-waves was always constant ($m = 1$). It follows from the analysis of results in Fig. 1.5 that with increase in the specific weight of the medium, the amplitudes of vibrations of the shell decrease and the resonant frequencies slightly increase.

1.8. Experimental Investigations of the Effect of Medium on Vibroaccelerations in the Shell under Impulsive Loading. A ribbed cylindrical shell of radius $R = 0.20$ m, length $L = 0.45$ m, and thickness $h = 0.0005$ m is made of AMg-6M alloy and rigidly fixed in disks. The shell is placed in a container installed on a mass foundation. Impulsive loading was generated by dropping a weight on the shell at the point at a distance of 0.12 m from the shell edge and the accelerometer (the point of a weight impact and accelerometer are on a common generatrix). The weight was 0.8 kg. The drop height h was equal to 0.05, 0.10, 0.15, 0.20, 0.25, 0.30 m. To measure the vibroaccelerations of the system, a standard accelerometer D14 was used, which was rigidly fixed to the shell wall in its middle cross-section. The maximum values of accelerations a at the point of the accelerometer fixing were measured. The dependences of maximal accelerations a on the maximum total impulse F for variants of impulsive loading are given in Table 1.6. The impulse amplitude was assumed constant during the impact, and its value was determined by formula (1.1). Table 1.6 gives the values of acceleration of the shell interacting with no medium (a_1), with clay (a_2), with dry sand (a_3), and with wet sand (a_4).

The dependencies of maximal vibroaccelerations a on the total impulse for different specific weights of sand (ρ, kg/cm^3) are shown in Table 1.7. The specific weight of sand was changed by adding water.

Based on the analysis of experimental data given in Table 1.7 it follows that the increase of sand moisture results in considerable decrease of the vibroaccelerations. Vibrorecords obtained on the excitation of impulses in the "empty" shell and the shell filled with clay, dry sand, and wet sand (for the same drop height $h = 0.2$ m) are given in Fig. 1.6*a–d*. Here the direction of

TABLE 1.6

F, N	a_1, m/sec^2	a_2, m/sec^2	a_3, m/sec^2	a_4, m/sec^2
158.3	28	15	23	14
224.0	35	20	29	24
273.6	45	23	40	30
316.8	60	27	46	35
353.6	70	31	58	38
387.2	80	34	65	42

TABLE 1.7

F, N	a, m/sec^2						
	ρ = 1.87 g/cm^3	ρ = 1.94 g/cm^3	ρ = 2.02 g/cm^3	ρ = 2.09 g/cm^3	ρ = 2.16 g/cm^3	ρ = 2.24 g/cm^3	ρ = 2.31 g/cm^3
158.3	23	23	23	20	17	16	14
224.0	33	33	33	33	32	28	24
273.6	40	40	40	38	36	33	30
316.8	46	46	46	46	44	40	35
353.6	58	58	57	52	48	44	38
387.2	65	65	58	58	52	50	42

measurements of accelerations coincides with the normal to the shell. Signals from accelerometers were supplied to GDS-806S oscillograph and were recorded on its screen.

It was ascertained from the analysis of the obtained vibrorecords that the increase of specific weight of medium contacting with the outer side of the shell results in a considerable decrease of vibroaccelerations and a slight increase of impulse duration.

For similar investigations of the effect of moisture of the medium on the vibroaccelerations of the shell under impulsive loading [94], we used also a cylindrical shell with radius $R = 0.09$ m, length $L = 0.58$ m, and thickness $h = 0.003$ m. The shell was made of OT4-1 titanium alloy with modulus of elasticity $E = 1.1 \cdot 10^5$ MPa and Poisson's ratio $\nu = 0.34$ (density $\rho = 4400$ kg/m^3). The conditions of rigid fixing of the shell edges and impulsive loading were similar to the previous tests. Table 1.8 presents the dependences of accelerations a at the middle point of the shell on the maximum total impulse for the considered variants of dynamic loading ($h = 0.05$, 0.10, 0.15, 0.20 m).

Here the following notation is used: a_1 is vibroacceleration of the shell without medium; a_2 is vibroacceleration of the shell contacting with medium; ρ is the specific weight of sand; F is the impact force defined by formula (1.1).

It follows from the analysis of experimental data given in Table 1.8 that the increase of sand moisture results in a considerable decrease of vibroaccelerations at the point for the same value of the maximum impact impulse.

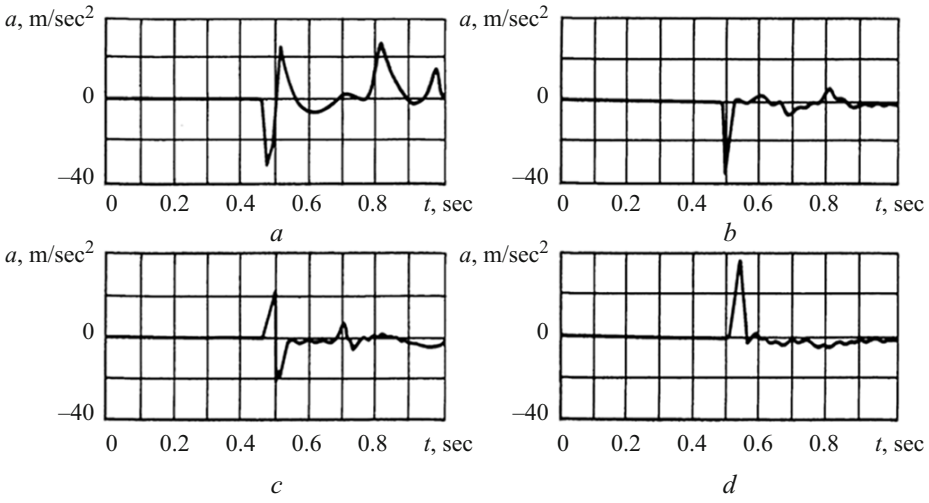

Fig. 1.6

TABLE 1.8

F, N	a_1, m/sec^2	a_2, m/sec^2					
		ρ = 1.87 g/cm^3	ρ = 1.96 g/cm^3	ρ = 2.05 g/cm^3	ρ = 2.13 g/cm^3	ρ = 2.22 g/cm^3	ρ = 2.31 g/cm^3
158.3	25	3.3	3.1	3.0	2.8	2.7	2.5
224.0	32	9.0	8.0	7.0	6.5	6.0	5.5
273.6	39	14	13	11	10	9	8
316.8	45	17	16	15	14	13	11

Vibrorecords obtained on disturbance of impulses in the "empty" shell and the shell contacting with dry and wet sand (for the same drop height $h = 0.05$ m) for variants where the accelerometers are at distances 0.28 and 0.40 m from the point of the weight impact are shown in Fig. 1.7*a–c* and Fig. 1.8*a–c*, respectively. In Figs. 1.7 and 1.8, the upper curve is obtained for the point of fixing of accelerometer 0.28 m, and the lower one at the point 0.40 m.

It follows from the analysis of the obtained experimental data that the dependence of vibroaccelerations on the impact loading is nearly linear. It was found that with increase in the specific weight of sand due to moister, the velocity of elastic waves in the system increases. The increase of the velocity of waves occurs due to the reduction of the air component of the wet sand, which is confirmed by theoretical computations. It follows from the analysis of the obtained vibrorecord that the increase in the specific weight of the medium from the outer side of the shell results in a considerable reduction of vibroaccelerations.

1.9. Experimental Investigation of the Dynamics of a Stiffened Cylindrical Shell during Its Depressurization. It is of interest to measure the natural frequencies and modes of vibrations and vibroaccelerations upon depressurization of a stiffened cylindrical shell contacting with a medium. For the execution of experiments, a special installation was produced, in which dry sand is the environment for the cylindrical shell. The phenomenon of depressurization was modeled in the following way. Air was pumped into the shell. The vibrations of the shell were excited by removing the rubber cork from the upper disk. For experimental investigations, we used a cylindrical shell with radius $R = 0.15$ m, length $L = 0.5$ m, and thickness $h = 0.0005$ m. The shell was stiffened on the outer surface by seven frames spaced by 0.0625 m. The thickness of Z-shaped frames was the same as for the shell; the height of the vertical post was 0.005 m, and of the horizontal flanges was 0.008 m. The shell and frames were made of AMg-6M alloy. The edges of the shell were installed on gaskets of vacuum rubber to provide simple support conditions.

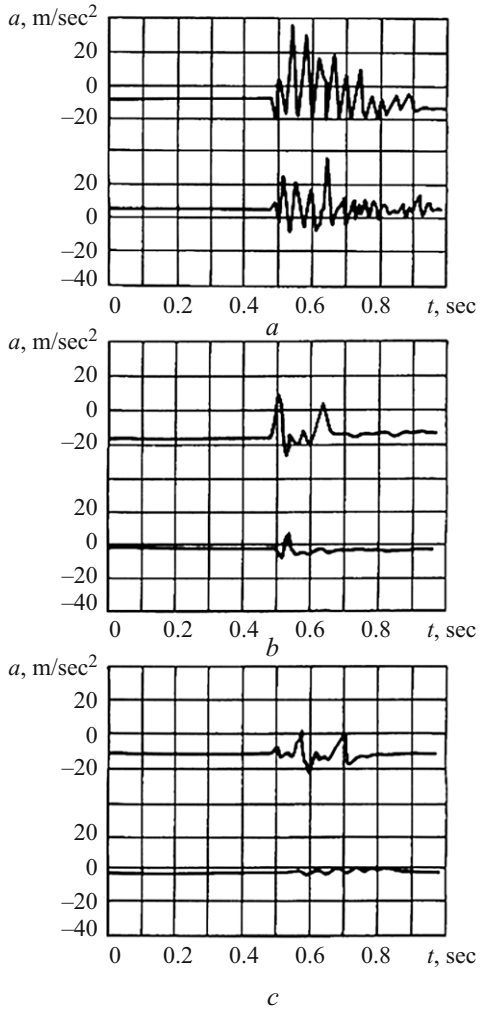

Fig. 1.7

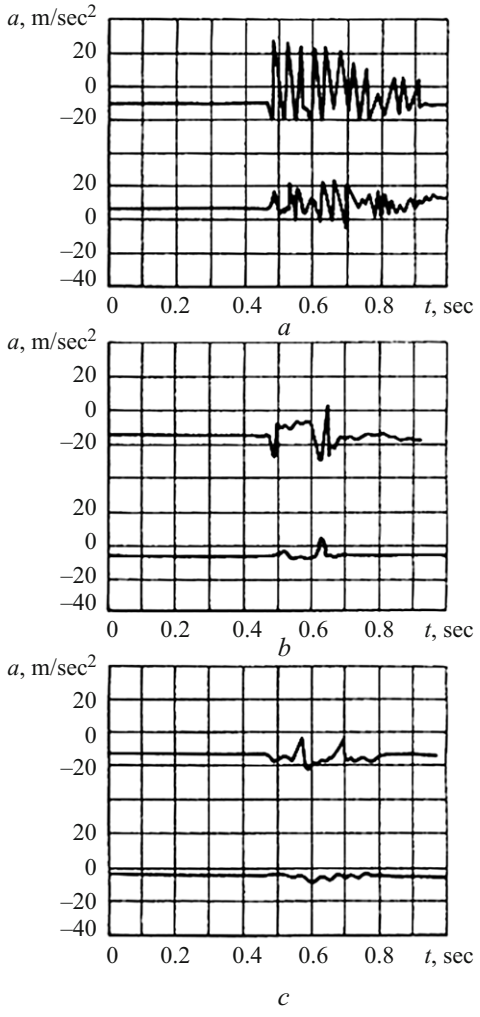

Fig. 1.8

The tested shell was installed inside the container filled with sand. The container was installed on a mass foundation. The experimental values of natural frequencies and natural modes were determined by the resonance method. The vibrations of the shell were excited with a G3-110 generator and measured with a contact-free vibroinvertor and VVV-302 measuring unit. The contact-free vibroinvertor was used to determine the natural modes. Here the amplitudes of vibrations were measured at 20 points along the circumference (in the middle cross-section) and at 15 points along the meridian. The dependence of the natural frequencies f_{mn} on the number n of circumferential waves for the empty shell is shown in Fig. 1.9. We obtained one longitudinal half-wave $m = 1$ ($f^{\min}{}_e = 475$ Hz). The minimum natural frequency of the shell filled with sand was determined. It was ascertained that the minimal natural frequency of the ribbed shell with sand is equal to $f^{\min}{}_e = 250$ Hz. It was discovered that the natural frequencies of the shell contacting with medium with inner or outer side differ insignificantly. It was ascertained that on contact with outer side, the natural frequencies are somewhat higher than for the variant of inner filing of the shell by the medium.

It follows from the analysis of the obtained results that the medium considerably reduces the minimal natural frequency.

Impulsive loading, which models depressurization of the shell, is generated by removing the cork from the hole in the upper disk. The diameter of the hole is 0.017 m. The initial pressure inside the shell was measured by a standard pressure gage and was equal to $(0.1, 0.15, 0.20, 0.25, 0.30)\cdot 10^5$ Pa. To measure the vibroaccelerations of the system, two standard accelerometers D14 were used. One accelerometer 1 is in the middle cross-section of the shell, and the second one 2 is at a distance of 0.31 m from the upper edge of the shell. The maximum values of accelerations a at the point of fixing of accelerometers were measured. The dependences of maximum vibroaccelerations a on the initial pressure for two variants of

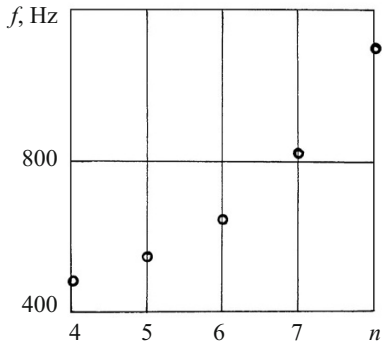

Fig. 1.9

TABLE 1.9

$P \cdot 10^{-5}$, Pa	a, m/sec^2			
	$m = 0$		$m = 1$	
	1	2	1	2
0.10	3.5	0.8	3.0	0.3
0.15	4.0	1.2	5.0	0.5
0.20	5.0	1.5	6.0	0.7
0.25	6.5	1.9	7.0	0.9
0.30	7.5	2.1	8.0	1.0

loading (without and with sand) are given in Table 1.9. The following notation is used: m is variant of installation ($m = 0$, when only the shell without sand was in the container; $m = 1$ for the shell whose outer surface is in contact with sand); P is the initial pressure inside the shell.

It follows from the analysis of experimental data (Table 1.9) that the increase of the initial pressure inside the shell results in a considerable increase of vibroaccelerations. It was ascertained that by filling the container with sand, vibroaccelerations in the middle cross-section of the shell somewhat increase, and on the shell edge they, decrease.

The amplified signals from accelerometers *1* and *2* were supplied to GDS-806S oscillograph. Vibrorecords obtained on excitation of impulses for the initial pressure $P = 0.3 \cdot 10^5$ Pa in the shell without sand are given in the middle cross-section (Fig. 1.10*a*) and on the shell edge (Fig. 1.10*b*), and they are given for the shell contacting with dry sand in Fig. 1.10*c*, *d*, respectively.

It follows from the analysis of the obtained vibrorecords that on contact of the ribbed cylindrical shell with medium, the vibroaccelerations in the middle cross-section after depressurization slightly increase, and they decrease on the edge of the shell.

Experimental modeling of depressurization of the ribbed cylindrical shell in sand allows us to state that the dependence of the vibroaccelerations on the internal initial pressure is nearly linear.

2. Three-Layer Shells of Revolution with Piecewise-Homogeneous Filler. Two-dimensional theories of deformation of multilayered shells can be conventionally represented as theories based on the application of an analytical method of reduction of three-dimensional problems of elasticity to a two-dimensional one and the shell theory constructed based on the method of hypotheses.

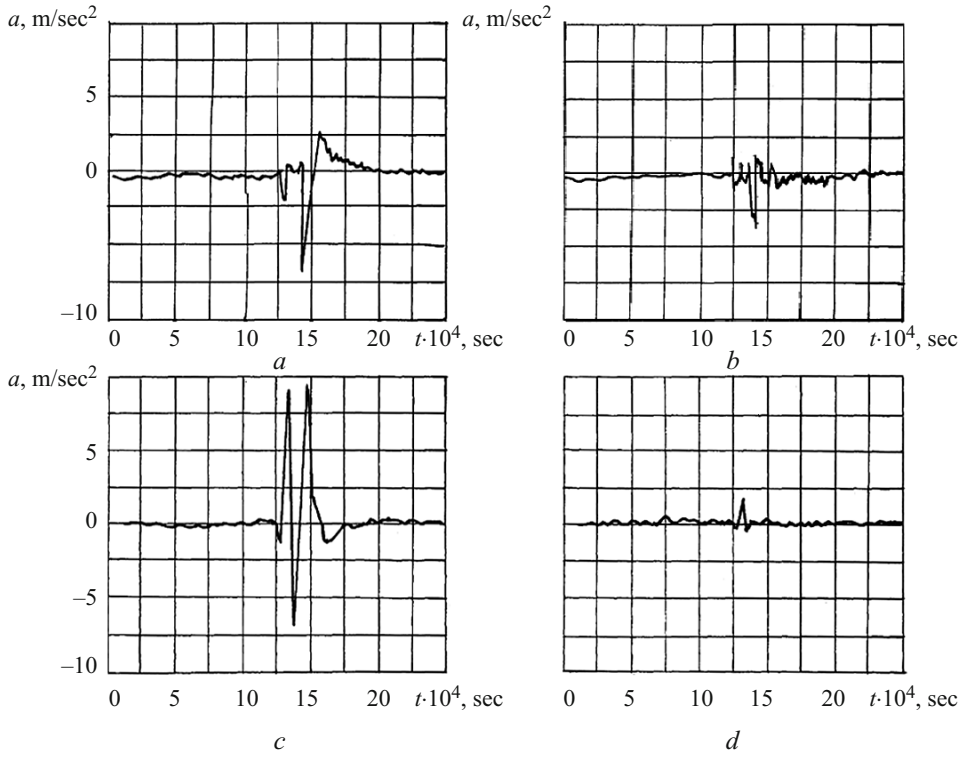

Fig. 1.10

In the first case, two-dimensional theories are constructed by expanding the desired displacements into series with respect to the thickness coordinate. The order of the resulting equations depends on both the number of layers and on the number of terms retained in the series.

In deriving the equations of multilayered shells, the method of hypotheses was widely used owing to its simplicity, clearness, and potential for the construction of algorithms for solving a wide class of practically important problems. Considerable successes in the development of the theory of multilayered shells and solving the problems of their vibrations were achieved in [2, 82, 110–113, 139]. In such theories, there are two approaches. The first approach is to investigate the behavior of shell structures using theories of layered shells based on the application of hypotheses for the entire package of layers [2, 28, 32, 40, 43, 51, 59, 72–77, 82, 105, 106, 110–116, 118–128, 131, 137, 139–141]. This approach was widely used in the case of a small difference between the physical-mechanical parameters of layers and small gradients of SSS. In this case, the order of the governing system of equations does not depend on the number of layers. Theories constructed using the generalized hypotheses for the entire package of layers considerably enlarge the class of problems compared with the classical theory; however, they do not allow accurate analysis of the SSS of multilayered shells with physical and mechanical characteristics that differ considerably. The other approach is to investigate the SSS of shells using theories based on hypotheses applied to each layer individually. This approach is used when the difference of the physical and mechanical characteristics of layers is significant. Note that the order of the governing system of equations depends on the number of layers, and the form of the governing system is complicated considerably [14, 15, 52, 55–57, 60, 61, 64, 104, 144].

In the most publications, the problems of static or quasistatic deformation of shell structures are considered. Publications dealing with dynamical processes are much fewer and they mainly address steady-state vibrations. The publications [14, 15, 52, 55–57, 60, 61, 64, 104, 144] deal with non-stationary problems of the theory of three-layer shells and hypotheses applied to each layer separately. Refined models of shells and assumptions, corresponding to the Timoshenko hypotheses for every layer are used in the second approach. In publications of the mentioned authors, three-layer shells of different geometry with homogeneous layers relative to the length of the shell structures are considered. Publications on the investigation of forced vibrations of three-layer shells with piecewise-homogeneous filler with hypotheses applied to each layer separately are practically absent in the literature.

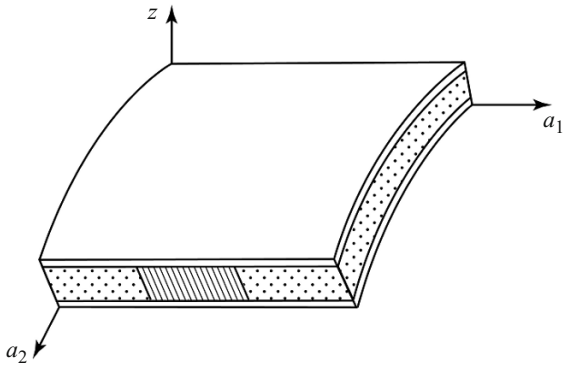

Fig. 2.1

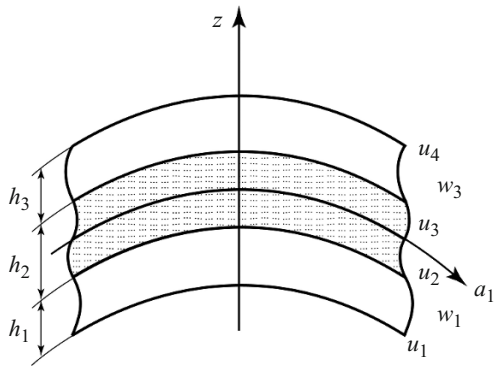

Fig. 2.2

Below we will consider problems and study forced vibrations of three-layer shells of revolution with piecewise-homogeneous filler under non-stationary axisymmetric loading using hypotheses for each of the layers whoso physical and mechanical parameters differ considerably.

2.1. Statement of the Initial Problems. The equations of vibrations of three-layer shells of revolution with homogeneous and piecewise-homogeneous filler with the use of hypotheses for each layer are presented in [14, 15, 52, 55–57, 60, 61, 64, 104, 144]. For a three-layer shell of revolution of constant thickness consisting of outer layers (boarding) and inner piecewise-homogeneous layer (filler) (Fig. 2.1), it was assumed that its SSS can be completely determined within the simplest nonlinear variant of the theory of elastic shells with considering transversal linear and angular deformations in quadratic approximation. It is assumed that the layers are continuous and that they deform without slip and separation.

In deriving the equations of vibrations of three-layer shells of revolution, we accept independent kinematic and static hypotheses for each layer and account for the transverse normal and shear deformations in the filler. The kinematic hypotheses have the form

$$u_1^{kz}(\alpha_1, z) = u_1^k(\alpha_1) + z\varphi_1^k(\alpha_1) \quad (k = \overline{1,3}),$$

$$u_3^{kz}(\alpha_1, z) = u_3^k(\alpha_1) \quad (k = 1,3),$$

$$u_3^2(\alpha_1, z) = u_3^2(\alpha_1) + z\varphi_3^2(\alpha_1), \quad u_1^k(\alpha_1) = (u_{k+1}(\alpha_1) + u_k(\alpha_1))/2 \quad (k = \overline{1,3}),$$

$$u_3^k(\alpha_1) = w_k(\alpha_1) \quad (k = 1,3), \quad u_3^2(\alpha_1, z) = (w_3(\alpha_1) + w_1(\alpha_1))/2,$$

$$\varphi_1^k(\alpha_1) = (u_{k+1}(\alpha_1) - u_k(\alpha_1))/h_k \quad (k = \overline{1,3}),$$

$$\varphi_3(\alpha_1) = (w_3(\alpha_1) - w_1(\alpha_1))/h_2. \tag{2.1}$$

The components of the generalized vector of displacements on the surfaces of layers, $\overline{U} = (u_1(\alpha_1), u_2(\alpha_1), u_3(\alpha_1), u_4(\alpha_1), w_1(\alpha_1), w_3(\alpha_1))^T$ (Fig. 2.2) are selected as independent desired functions.

The transverse shearing stresses change across thickness of a layer as

$$\sigma_{13}^{kz}(\alpha_1, z) = f_k(z)\sigma_{13}^k(\alpha_1) \quad (k = \overline{1,3}). \tag{2.2}$$

The functions $f_k(z)$ are selected so that the transverse shearing stresses are continuous in the absence of surface loading. We specify the transverse normal stress σ_{33} in the filler as

$$\sigma_{33}^z(\alpha_1, z) = f(z)\sigma_{33}(\alpha_1). \tag{2.3}$$

The function $f(z)$ is selected so that $\sigma_{33}^z(\pm h_2/2) = P_3^{\pm}(\alpha_1)$ where $P_3^{\pm}(\alpha_1)$ is the transverse normal loading.

The physical and mechanical parameters in the initial equations are piecewise-homogeneous along the length of the structure:

$$\begin{bmatrix} E_{fil}(\alpha_1) \\ \nu_{fil}(\alpha_1) \\ \rho_{fil}(\alpha_1) \end{bmatrix} = \sum_{i=1}^{N} \left[\eta(\alpha_1 - \alpha_{1i}) - \eta(\alpha_1 - \alpha_{1i-1})\right] \begin{pmatrix} E_i(\alpha_1) \\ \nu_i(\alpha_1) \\ \rho_i(\alpha_1) \end{pmatrix}, \tag{2.4}$$

where $\eta(\alpha_1)$ is the Heaviside function; E_i, ν_i, ρ_i are the physical and mechanical parameters of the homogeneous filler; $\alpha_{1\,i}$ are the contact lines of the filler; $\alpha_{1\,0}$ and $\alpha_{1\,N}$ are the boundaries of the shell.

To derive the equations of vibrations of a three-layer shell, we use the Reissner variational principle for dynamical processes [33]:

$$\int_{t_1}^{t_2} [\delta(R - T) - \delta A]dt = 0, \tag{2.5}$$

where R is the Reissner functional; T is kinetic energy; A is the work done by the external forces. The expressions for the functional R and the kinetic energy have the form

$$R = \int_s \left\{ \sum_{i=1,3} \int_{z_i} \left\{ \sigma_{11}^{iz}\varepsilon_{11}^{iz} + \sigma_{22}^{iz}\varepsilon_{22}^{iz} + \sigma_{13}^{iz}\varepsilon_{13}^{iz} - \frac{1}{2}\frac{(\sigma_{13}^{iz})^2}{G_{13}^{i}} \right\} dz_i \right.$$

$$+ \int_{z_2} \left\{ \sigma_{11}^{2z}\varepsilon_{11}^{2z} + \sigma_{22}^{2z}\varepsilon_{22}^{2z} + \sigma_{33}^{2z}\varepsilon_{33}^{2z} + \sigma_{13}^{2z}\varepsilon_{13}^{2z} \right.$$

$$-\frac{1}{2}\left[\frac{(\sigma_{11}^{2z})^2}{E_{fil}(s)} + \frac{(\sigma_{22}^{2z})^2}{E_{fil}(s)} + \frac{(\sigma_{33}^{2z})^2}{E_{fil}(s)} - 2\nu_{fil}(s)\frac{\sigma_{11}^{2z}\sigma_{22}^{2z}}{E_{fil}(s)} \right.$$

$$\left.\left.\left. -2\nu_{fil}(s)\frac{\sigma_{11}^{2z}\sigma_{33}^{2z}}{E_{fil}(s)} - 2\nu_{fil}(s)\frac{\sigma_{22}^{2z}\sigma_{33}^{2z}}{E_{fil}(s)} + \frac{\sigma_{13}^{2z}}{G_{fil}(s)} \right] \right\} dz_2 \right\} ds, \tag{2.6}$$

$$T = \frac{1}{2}\int_s \left\{ \sum_{i=1,3} \rho_i \int_{z_i} \left(\left(\frac{\partial u_1^{iz}}{\partial t} \right)^2 + \left(\frac{\partial u_3^{iz}}{\partial t} \right)^2 \right) dz_i + \rho_{fil}(s) \int_{z_2} \left(\left(\frac{\partial u_1^{2z}}{\partial t} \right)^2 + \left(\frac{\partial u_3^{2z}}{\partial t} \right)^2 \right) dz_2 \right\} ds.$$

In (2.6), z_i correspond to domains of integration over thicknesses of the corresponding layers; ρ_i, ρ_{fil} are the densities of the material of the layers; $E_1^2, E_2^2, E_3^2, \nu_{21}^2, \nu_{31}^2, \nu_{32}^2$ are the physical and mechanical characteristics of the filler (superscript "2"); δ_{i2} is the Kronecker symbol.

The use of the Reissner variational principle enables elimination of formal contradictions in the equations of the generalized Hooke's law for transverse and shear stresses of the layers by accepting independent hypotheses for the approximation of the displacements (2.1) and stresses (2.2), (2.3). In using the Reissner principle, both displacements and stresses are subject to variation. After standard transformations in functional (2.5) considering the independence of variations of components of the generalized displacement vector, we obtain a system of differential equations of vibrations of three-layer shells of revolution.

The equations of vibrations of the initial shell structure for the independent functions of displacements u_1, u_2, u_3, u_4, w_1, w_3 on the surfaces of layers have the form

$$L_{3m+1}(\overline{U}) = \frac{\rho_{2m+1} h_{2m+1}}{2} \frac{\partial^2}{\partial t^2}\left(\frac{u_{2m+1} + u_{2m+2}}{2}\right) + (-1)^{m+1} \frac{\rho_{2m+1} h_{2m+1}^2}{12} \frac{\partial^2}{\partial t^2}\left(\frac{u_{2m+2} - u_{2m+1}}{h_{2m+1}}\right) \quad (m = 0, 1),$$

$$L_3(\overline{U}) = \frac{\rho_{fil}(s) h_2}{2} \frac{\partial^2}{\partial t^2}\left(\frac{u_1 + u_2}{2}\right) - \frac{\rho_1 h_1^2}{12} \frac{\partial^2}{\partial t^2}\left(\frac{u_2 - u_1}{h_1}\right) + \frac{\rho_{fil}(s) h_2}{2} \frac{\partial^2}{\partial t^2}\left(\frac{u_3 + u_2}{2}\right) + \frac{\rho_{fil}(s) h_2^2}{12} \frac{\partial^2}{\partial t^2}\left(\frac{u_3 - u_2}{h_2}\right),$$

$$L_4(\overline{U}) = \frac{\rho_3 h_3}{2} \frac{\partial^2}{\partial t^2}\left(\frac{u_2 + u_3}{2}\right) + \frac{\rho_{fil}(s) h_2^2}{12} \frac{\partial^2}{\partial t^2}\left(\frac{u_3 - u_2}{h_2}\right) - \frac{\rho_3 h_3}{2} \frac{\partial^2}{\partial t^2}\left(\frac{u_4 + u_3}{2}\right) + \frac{\rho_3 h_3^2}{12} \frac{\partial^2}{\partial t^2}\left(\frac{u_4 - u_3}{h_3}\right),$$

$$L_{m+5}(\overline{U}) = \rho_{2m+1} h_{2m+1} \frac{\partial^2 w_{2m+1}}{\partial t^2} + \frac{\rho_{fil}(s) h_2}{2} \frac{\partial^2}{\partial t^2}\left(\frac{w_1 + w_3}{2}\right) + (-1)^{m+1} \frac{\rho_{fil}(s) h_2^2}{12} \frac{\partial^2}{\partial t^2}\left(\frac{w_3 - w_1}{h_2}\right) \quad (m = 0, 1), \quad (2.7)$$

where the operators $L_m(\overline{U}), m = \overline{1, 6}$, have the following form, considering the integral characteristics over the layer thickness:

$$L_{3m+1}(\overline{U}) = \frac{1}{2A_1A_2}\left[\frac{\partial}{\partial \alpha_1}(A_2 T_{11}^{2m+1}) - T_{22}^{2m+1} \frac{\partial A_2}{\partial \alpha_1}\right]$$

$$-(-1)^m \frac{1}{h_{2m+1} A_1 A_2}\left[\frac{\partial}{\partial \alpha_1}(A_2 M_{11}^{2m+1}) - M_{22}^{2m+1} \frac{\partial A_2}{\partial A_1}\right] + (-1)^m \frac{1}{h_{2m+1}} T_{13}^{2m+1} + \frac{1}{2} \overline{T}_{13}^{2m+1} k_1 \quad (m = 0, 1),$$

$$L_{m+1}(\overline{U}) = \frac{1}{2A_1A_2}\left[\frac{\partial}{\partial \alpha_1}(A_2 T_{11}^m) + \frac{\partial}{\partial \alpha_1}(A_2 T_{11}^{m+1}) - (T_{22}^m + T_{22}^{m+1}) \frac{\partial A_2}{\partial \alpha_1}\right]$$

$$+ \frac{1}{h_m A_1 A_2}\left[\frac{\partial}{\partial \alpha_1}(A_2 M_{11}^m) - M_{22}^m \frac{\partial A_2}{\partial \alpha_1}\right] - \frac{1}{h_{m+1} A_1 A_2}\left[\frac{\partial}{\partial \alpha_1}(A_2 M_{11}^{m+1}) - M_{22}^{m+1} \frac{\partial A_2}{\partial \alpha_1}\right]$$

$$-\frac{1}{h_{m+1}} T_{13}^m + \frac{1}{h_{m+1}} T_{13}^{m+1} + \frac{k_1}{2}(\overline{T}_{13}^m + \overline{T}_{13}^{m+1}) \quad (m = 1, 2),$$

$$L_{m+5}(\overline{U}) = \frac{1}{A_1A_2} \frac{\partial}{\partial \alpha_1}\left[A_2\left(\overline{T}_{13}^{2m+1} + \frac{1}{2}\overline{T}_{13}^2\right)\right]$$

$$-(T_{11}^{2m+1} k_1 + T_{22}^{2m+1} k_2) - \frac{1}{2}(T_{11}^2 k_1 + T_{22}^2 k_2) + (-1)^m \frac{1}{h_2} T_{33}^2 - (-1)^m \frac{1}{h_2}(M_{11}^2 k_1 + M_{22}^2 k_2) \quad (m = 0, 1),$$

$$\overline{T}_{13}^i = T_{13}^i + T_{11}^i \theta_1^i \quad (i = \overline{1, 3}). \quad (2.8)$$

The integral characteristics of stresses for each layer are given by

$$(T_{11}^k, T_{22}^k, T_{13}^k, T_{33}^2) = \int_z (\sigma_{11}^{kz}, \sigma_{22}^{kz}, \sigma_{13}^{kz}, \sigma_{33}^2) dz,$$

$$(M_{11}^k, M_{22}^k) = \int_z (z^k \sigma_{11}^{kz}, z^k \sigma_{22}^{kz}) dz \quad (k = \overline{1, 3}), \quad z \in [-h/2, h/2].$$

The equations of vibrations of three-layer shells of revolution with piecewise-homogeneous filler are supplemented by the corresponding natural contact conditions, boundary, and the initial conditions. In particular, boundary conditions for free edge for $s = 0$ or $s = L\,(s = A_1\alpha_1)$ have the following form [132]:

$$\frac{1}{2}T_{11}^{2m-1}-\frac{M_{11}^{2m-1}}{h_{2m-1}}=F_{3m-2},\qquad \frac{1}{2}T_{11}^{m}+\frac{M_{11}^{m}}{h_m}+\frac{1}{2}T_{11}^{m+1}-\frac{M_{11}^{m+1}}{h_{m+1}}=F_{m+1},$$

$$\overline{T}_{13}^{2m+1}+\frac{1}{2}\overline{T}_{13}^{2}=\Phi_m \qquad (m=1,2). \tag{2.9}$$

Boundary conditions for rigidly fixed edge have the form

$$S=0 \quad \text{or} \quad s=L:\ \overline{U}=0. \tag{2.10}$$

The initial conditions for

$$t=0,\quad \overline{U}=0,\quad \frac{\partial\overline{U}}{\partial t}=0. \tag{2.11}$$

2.2. Numerical Algorithm. Consider the construction of a numerical algorithm for solving non-stationary dynamical problems of three-layer shells of revolution with piecewise-homogeneous filler. Selection of the method for solving problems of the theory of layered shells depends on a specific statement (design model, boundary conditions, piecewise-homogeneous filler, type of loading). The literature data indicate that numerical methods are widely used to solve problems of the non-stationary behavior of layered structures. The finite-difference method was applied to problems of the dynamics of layered shells under non-stationary loading [6, 33, 69].

The numerical algorithm for solving non-stationary problems of the theory of three-layer shells with piecewise-homogeneous filler using independent kinematic and static hypotheses for each layer and accounting for transverse normal and shear deformations in the filler is based on one of the variants of difference approximation of the initial variational functional (2.5). Due to the arbitrariness of variations of displacements and stresses, after standard transformations in the variational functional, we obtain two groups of equations. One group is the equations of vibrations of three-layer shells for forces and moments written for the domains of homogeneous filler, while the second one is the relations of the generalized Hooke's law.

The basis of the numerical algorithm is an explicit finite-difference scheme of „cross" type with respect to spatial and time coordinates. The transition from the continuous system of equations to a finite-difference one is done in two stages. The first stage consists in a finite-difference approximation of divergent equations of vibrations for forces and moments in the domain of homogeneous filler, which is equivalent to the use of integral-interpolation method of approximation of the motion equations [6, 33, 69]. After standard transformations considering relations (2.1)–(2.5), (2.7)–(2.9), we obtain difference equations of vibrations of three-layer shell of revolution for independent functions of displacements on the surface of the layer $u_1, u_2, u_3, u_4, w_1, w_3$:

$$L_{3m+1}(\overline{U}_i^n)=\frac{\rho_{2m+1}h_{2m+1}}{4}[(u_{2m+1,i}^n)_{\bar{t}\,t}+(u_{2m+2,i}^n)_{\bar{t}\,t}]$$

$$+(-1)^{m+1}\frac{\rho_{2m+1}h_{2m+1}}{12}[(u_{2m+2,i}^n)_{\bar{t}\,t}-(u_{2m+1,i}^n)_{\bar{t}\,t}] \qquad (m=0,1),$$

$$L_{3m+1}(\overline{U}_i^n)=\frac{\rho_{m+1}h_{m+1}}{4}[(u_{m,i}^n)_{\bar{t}\,t}+(u_{m+1,i}^n)_{\bar{t}\,t}]$$

$$+(-1)^m\frac{\rho_m h_m}{12}[(u_{m+1,i}^n)_{\bar{t}\,t}-(u_{m,i}^n)_{\bar{t}\,t}]+(-1)^m\frac{\rho_{m+1}h_{m+1}}{4}[(u_{m+2,i}^n)_{\bar{t}\,t}+(u_{m+1,i}^n)_{\bar{t}\,t}]$$

$$+\frac{\rho_{m+1}h_{m+1}}{12}[(u_{m+2,i}^n)_{\bar{t}\,t}-(u_{m+1,i}^n)_{\bar{t}\,t}] \qquad (m=1,2),$$

$$L_{m+5}(\overline{U}_i^n)=\rho_{2m+1}h_{2m+1}(w_{2m+1,i}^n)_{\bar{t}\,t}+\frac{\rho_2 h_2}{4}[(w_{1,i}^n)_{\bar{t}\,t}+(w_{3,i}^n)_{\bar{t}\,t}]$$

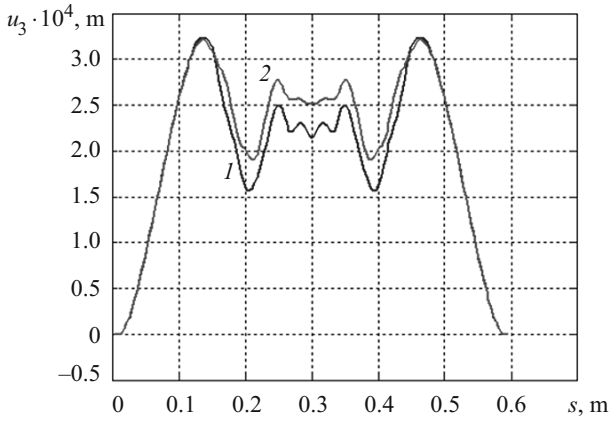

Fig. 2.3

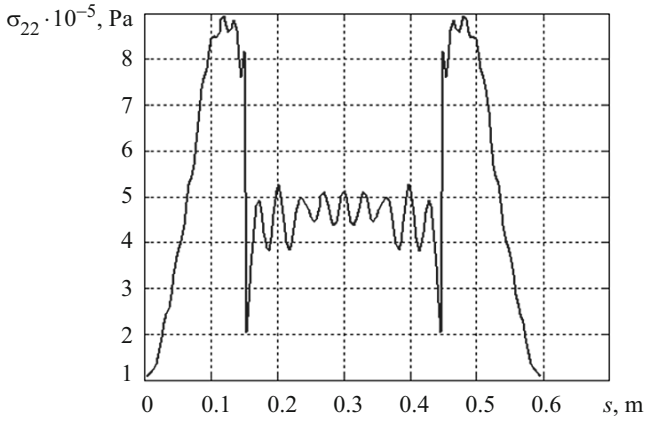

Fig. 2.4

$$+(-1)^m \frac{\rho_2 h_2}{12}[(w^n_{3,i})_{\bar{t}\,t} - (w^n_{1,i})_{\bar{t}\,t}] \qquad (m = 0, 1). \tag{2.12}$$

In (2.12), $L_j(\overline{U}_i^n)$, $j = \overline{1,6}$, are difference operators according to (2.9) at the ith discrete point with respect to spatial variable s and the nth discrete layer with respect to time coordinate t. The notation of the difference derivatives is taken from [69].

The second stage of approximation of the equations is to select energy-agreed finite-difference approximations of the forces and moments and the corresponding deformations in the domains of homogeneous filler so that the finite-difference analog of the energy equation holds. Using the explicit "cross" scheme, we approximate the components of the generalized vector of displacements at the integer point of the computational mesh, we approximate the components of the generalized strain tensor and forces and moments at the half-integer points of the mesh [6, 33]. Such an approach enables maintaining the divergent form of difference representation of differential equations as well as the fulfillment of the law of conservation of total mechanical energy at the difference level.

2.3. Forced Vibrations of Three-Layer Shells. A number of dynamical problems of the theory of three-layer shells of revolution with continuous and piecewise-homogeneous filler under axisymmetric non-stationary loading are considered. Problem statements and numerical algorithms for solving equations of three-layer shells of revolution using independent hypothesis for each layer are given below. Numerical results of solving of dynamic problems of the non-stationary behavior of three-layer shells of revolution with a piecewise-homogeneous filler (cylindrical, spherical, conic, and ellipsoidal shells) over a wide range of physical, mechanical, and geometrical parameters are presented for different types of boundary conditions and types of loading. We consider the problems of dynamical deformation of three-layer cylindrical shells with piecewise-homogeneous filler in the case of rigid fixing of the shell edges under internal distributed loading, when one edge of the shell is rigidly fixed and the second one is free for internal distributed loading; the problems of non-stationary behavior of the open three-layer spherical, conical, and ellipsoidal shells in the case of rigid fixing of edges and free edges for internal distributed loading [14, 15, 52, 55–57, 60, 61, 104, 132].

We consider the problem of the dynamical behavior of a three-layer cylindrical shell with inhomogeneous filler under distributed loading. It is assumed that the cylindrical shell is rigidly fixed at the edges. The problem is solved for the following geometrical, physical, and mechanical parameters:

$$R/h = 30, \quad h = h_1 + h_2 + h_3, \quad h_1 = h_3, \quad h_2/h_1 = 8, \quad L/R = 2,$$

$$\rho_1 = \rho_3 = 2.7 \cdot 10^3 \text{ kg/m}^3, \quad E_1^1 = E_2^1 = E_1^3 = E_2^3 = 7 \cdot 10^{10} \text{ Pa}.$$

Let $E_1 / E_{fil} = 100$, $\rho_1 / \rho_{fil} = 4$ in the domains $0 \le x \le L/4$ and $3/4L \le x \le L$ and $E_1 / E_{fil} = 400$, $\rho_1 / \rho_{fil} = 8$ in the domain $L/4 \le x \le 3/4L$, where E_1^1, ρ_1 refer to the shell, and E_{fil}, ρ_{fil} to the filler.

Loading is defined by

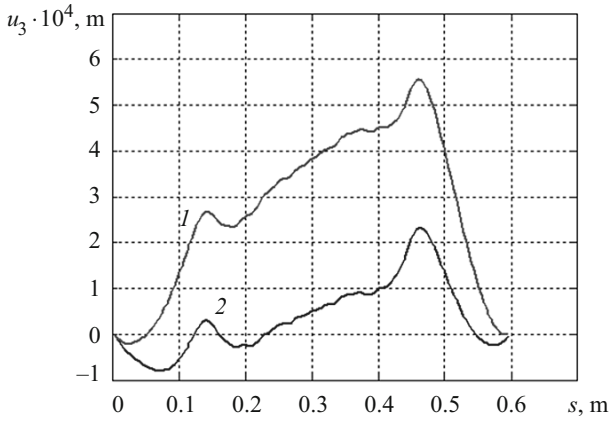

Fig. 2.5

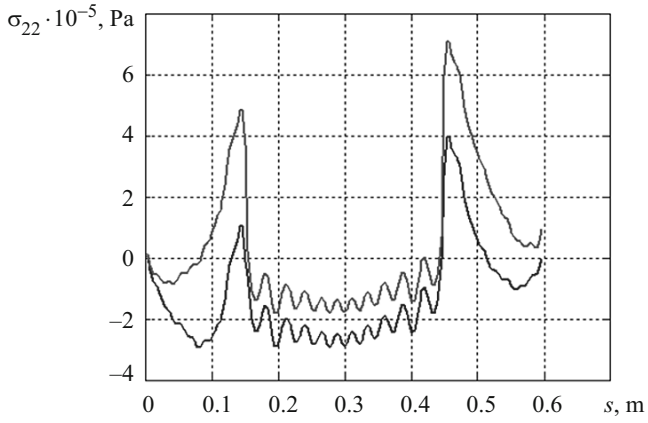

Fig. 2.6

$$P_3(t) = A \sin \frac{\pi t}{T} \left[\eta(t) - \eta(t-T)\right], \tag{2.13}$$

where $A = 10^6$ Pa is the loading amplitude, $T = 50 \cdot 10^{-6}$ sec is loading duration, η is the Heaviside function.

Characteristic distributions of magnitudes of deflections w_1, w_3 and stresses σ_{22} in the filler over the spatial variable x at instant $t = 7T$ are presented in Figs. 2.3 and 2.4. The graphycal representation allows analyzing the qualitative and quantitative distribution of the deflection and stresses along the length of the cylindrical shell. The domain with filler $E_1 / E_{fil} = 400$, $L/4 \le x \le 3/4L$ manifests clearly. In the domains $0 \le x \le L/4$ and $3/4L \le x \le L$, the deflections for the internal layer (curve *1*) and external layer (curve *2*) practically coincide. The difference is observed in the domain $L/4 \le x \le 3/4L$. For the values of σ_{22} (Fig. 2.4) in the domain $L/4 \le x \le 3/4L$ high-frequency vibrations occur, which are explained by the effect of transverse normal stress σ_{33} and, correspondingly, normal transverse strains in the initial equations of vibrations. The domains of contact of the filler with different physical and mechanicsl properties are clearly manifested.

We consider the problem of the dynamical behavior of a rigidly fixed three-layer conic shell with inhomogeneous filler under distributed normal internal loading $P_3(t)$ for the following geometrical, physical, and mechanical parameters of the initial structure: $R_0 / h = 30$, $h = h_1 + h_2 + h_3$, $h_1 = h_3$, $h_2 / h_1 = 8$, $L/R = 2$, $\rho_1 = \rho_3 = 2.7 \cdot 10^3$ kg/m^3, $E_1^1 = E_2^1 = E_1^3 = E_2^3 = 7 \cdot 10^{10}$ Pa, $\nu_1^1 = \nu_2^1 = \nu_1^3 = \nu_2^3 = 0.3$,

1) in the domains $0 \le s \le L/4$ and $3L/4 \le s \le L$ the filler parameters are $E_{fil} = E_1^1 / 100$, $\rho_{fil} = \rho_1 / 4$, $\nu_{fil} = 0.34$,

2) in the domain $s/4 \le s \le 3L/4$ the filler parameters are $E_{fil} = E_1^1 / 500$, $\rho_{fil} = \rho_1 / 8$, $\nu_{fil} = 0.34$.

Here E_1^1, ν_1^1, ρ_1 refer to the material of the shell and $E_{fil}, \nu_{fil}, \rho_{fil}$ to the material of the filler. The distributed normal loading is specified as (2.13).

Computations were done in the case $\beta = \pi/12$ and $\beta = \pi/6$ (β is the cone angle). In particular, the characteristic distribution of u_3 depending on the spatial coordinate s for internal layer at $t = 7T$ is presented in Fig. 2.5. Curve *1* corresponds to $\beta = \pi/6$, and curve *2* to $\beta = \pi/12$.

The dependencies of σ_{22} for the filler are shown in Fig. 2.6 (the notation is the same as in Fig. 2.5). The graphycal representation allows analyzing the qualitative and quantitative distribution of u_3 and σ_{22} along the length of the conic shell (contact lines, caused by inhomogeneity of the filler, the effect of the cone angle on the distribution of SSS of the structure, and so on).

We consider the problem of the dynamical behavior of a rigidly fixed segment of an ellipsoidal shell ($\alpha_{10} \le \alpha_1 \le \alpha_{1N}$) with piecewise-homogeneous filler under distributed normal internal loading $P_3(t)$. Geometrical, physical, and mechanical parameters of the initial structures are the following: $a/h = 20$, $\alpha_{10} = \pi/12$, $\alpha_{1N} = 11\pi/12$, $h = h_1 + h_{fil} + h_3$, $b/a = 1.25$, $h_1 = h_3$, $h_{fil} / h_1 = 8$, $\rho_1 = \rho_3 = 2.7 \times 10^3$ kg/m^3, $E_1^1 = E_2^1 = E_1^3 = E_2^3 = 7 \cdot 10^{10}$ Pa, $\nu_1^1 = \nu_2^1 = \nu_1^3 = \nu_2^3 = 0.3$;

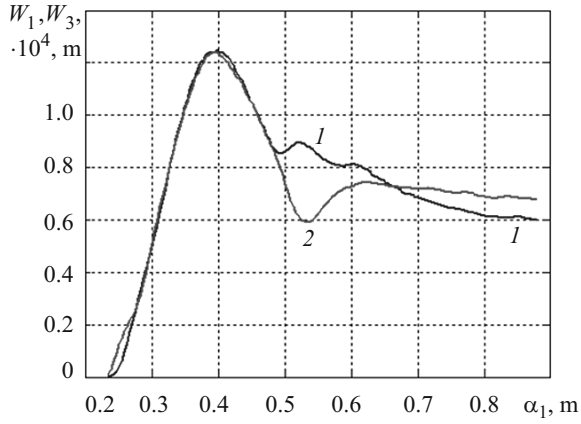

Fig. 2.7

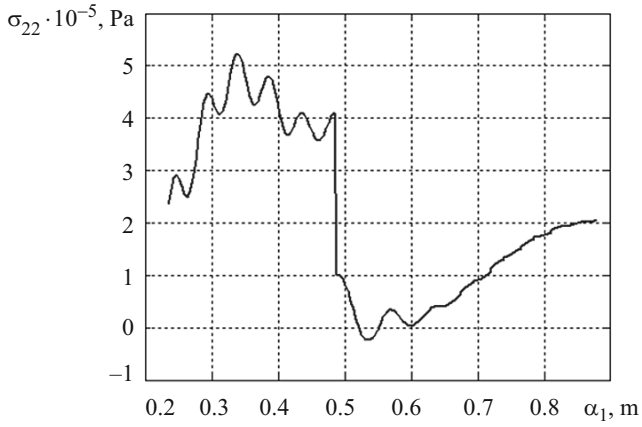

Fig. 2.8

1) in the domains $s_0 \le s \le s_0 + \Delta s/4$ and $s_N - \Delta s/4 \le s \le s_N$, $\Delta s = s_N - s_0$, $E_{fil} = E_1^1/100, \rho_{fil} = \rho_1/4, \nu_{fil} = 0.34$;

2) in the domain $s_0 + \Delta s/4 \le s \le s_N - \Delta s/4$, $E_{fil} = E_1^1/400, \rho_{fil} = \rho_1/4, \nu_{fil} = 0.34$.

Here E_1^1, ν_1^1, ρ_1 refer to the material of the shell, and $E_{fil}, \nu_{fil}, \rho_{fil}$ to the material of the filler. The distributed normal loading is specified as (2.13).

Computations were performed for $t = 20T$. The obtained results enable performing the detailed analysis of SSS of the investigated inhomogeneous shell at an arbitrary time of the time interval. In particular, Fig. 2.7 shows typical distribution of w_1 and w_3 (internal and external deflections) depending on the spatial coordinate at $t = 7.5T$ (due to the symmetry of the initial structure about $\alpha_1 = \pi/2$, the results are given only for $\alpha_{10} \le \alpha_1 \le \pi/2$). Curve *1* corresponds to the deflection w_1 for internal layer, curve *2* corresponds to the deflection w_3 for external layer.

The distribution of magnitudes of stresses σ_{22} in the middle surface of the filler depending on the spatial coordinate at $t = 3T$ (time of attaining the maximum value on the time interval) is presented in Fig. 2.8.

The line of discontinuity that separates the domains of the filler with different physical and mechanical parameters ($\alpha_1 \approx 0.8$ rad) is clearly seen. As numerical computations show, in the domain of filler for $E_{fil} = E_1^1/100, \rho_{fil} = \rho_1/4, \nu_{fil} = 0.34$ the deflections w_1 and w_3 hardly differ. The difference begins to manifest for values less that $E_{fil} = E_1^1/100$ (in particular, in the domain $s_0 + \Delta s/4 \le s \le s_N - \Delta s/4$). It is discovered that considering the geometrically nonlinear components can considerably affect the SSS of three-layer shells of revolution. Computations were performed (linear and nonlinear variants) using hypotheses for each layer under internal distributed loading ($E_1/E_{fil} = 1000$). Note that the effect of geometrically nonlinear factors for interval distributed loading manifests considerably (the difference according to linear and nonlinear theories can reach about 15–20%).

2.4. Reliability of Obtained Results. Practical convergence of numerical results is presented in the case of the problem of the dynamical behavior of a three-layer cylindrical shell with piecewise-homogeneous filler under internal distributed loading. Boundary conditions of rigid fixing are used for the left and right edges of the cylindrical shell. Table 2.1 gives the number of discrete intervals of partition in the first column. The maximal values of internal deflection w_1, in the cross-sections $x = L/8$ and $x = L/2$ are given in the second and third columns, respectively. In the fourth and fifth columns, the maximal values of stresses in the filler in the cross-sections $x = L/8$ and $x = L/2$ are presented. As follows from the presented results, sufficiently good convergence takes place.

The dependence of practical convergence on the number of discrete intervals of partition is given in Table 2.1.

Table 2.2 presents the dependence of numerical results on the Courant number K, which connects time dimensionless discrete step Δt with dimensionless spatial discrete step Δx for $N = 160$:

$$\Delta t = K \Delta x / c_{11}, \qquad c_{11} = E_1 / [\rho_1 (1 - \nu_1^2)]. \tag{2.14}$$

TABLE 2.1

Number of partition intervals	$w_1 \cdot 10^{-3}$, m		$\sigma_{22\,fil} \cdot 10^6$, Pa	
	$x = L/8$	$x = L/2$	$x = L/8$	$x = L/2$
$N = 20$	—	—	—	—
$N = 40$	0.245	0.281	0.821	0.445
$N = 80$	0.239	0.275	0.708	0.445
$N = 160$	0.240	0.276	0.701	0.436
$N = 320$	0.240	0.276	0.701	0.439

TABLE 2.2

Value of the Courant number	$w_1 \cdot 10^{-3}$, m		$\sigma_{22\,fil} \cdot 10^6$, Pa	
	$x = L/8$	$x = L/2$	$x = L/8$	$x = L/2$
$K = 1.00$	—	—	—	—
$K = 0.95$	0.240	0.276	0.701	0.436
$K = 0.90$	0.240	0.276	0.701	0.436

In the first column of Table 2.2, the values of the Courant number are given according to formula (2.14). Denotations in other columns correspond to the previous case for $N = 160$. As is seen, for values of the Courant number close to one, satisfactory convergence with respect to the time coordinate takes place.

An indirect comparison is made between the numerical results obtained with the equations for a homogeneous filler and the results obtained with other applied theories (the Kirchhoff–Love theory of three-layer shells and theory based on the Timoshenko hypotheses for the package) with known experimental and analytical data of solving the corresponding problems [1, 57, 66, 104].

The indirect analysis was performed starting from the following assumptions. Known analytical solutions of the problems and experimental data on the theory of three-layer beams in statics (as a particular case of three-layer shells) were considered. For the given geometrical, physical, and mechanical parameters, computations on the dynamical behavior of a three-layer cylindrical shells were done using the equations stated in [57] for homogeneous filler. The problem was considered under the action of the sudden distributed loading in the form $P_3(x,t) = Af(x)f(t)$, where A is the amplitude of loading, $f(t)$ is a function corresponding to the variation of loading in time; $f(x)$ is a function responsible for the shape of loading by the spatial coordinate x. The obtained kinematical and force parameters are compared with known data of solving the corresponding problems of statics via the dynamic amplification coefficient K_d. Values of the dynamic amplification factor are known for a hinged beam under loading $P_3(x,t)$ and the function form $f(t) = (1 - t/T)\cdot\eta(t - T)$, where T is the duration of loading, $\eta(t)$ is the Heaviside function. It was shown that $K_d = 2$ for $\omega T \geq 100$, where ω is the circular frequency of the beam vibraiotns for a given deflection function. For suddenly applied loading and $f(t) = \eta(t)$, $K_d = 2$ was considered a limiting case.

The results of computations are presented and experimental data and theoretical results obtained with applied theories of three-layer beams are compared in Tables 2.3 and 2.4. Indirect comparison of the results according to experiments [1, 66] and according to applied theories of three-layer beams is given in Table 2.3 [1], and comparison according to the experiments [66] is presented in Table 2.4. In computations, it was assumed that $1/R = 0$ for cylindrical shells. The results of Table 2.3 correspond to

TABLE 2.3

Type of results	$U_3 \cdot 10^{-2}$, m	Δ, %
Result according to experiment	0.153	
Result according to analytics	0.160	4.68
Theory according to independent hypotheses	0.1432	6.4
Theory according to the Timoshenko hypothese	0.168	9.8
Kirchhoff theory	0.1155	24.5

TABLE 2.4

Type of results	$U_3 \cdot 10^{-2}$, m	Δ, %
Result according to experiment	0.348	
Result according to analytics	0.363	4.13
Theory according to independent hypotheses	0.354	1.7
Theory according to the Timoshenko hypothese	0.1995	42.7
Kirchhoff theory	0.1902	45.3

the computation variant of a hinged beam under distributed loading $P_3 = Af(x)\eta(t)$, where L is the beam length. The results of the experiment and analytical solution are taken from [1, 66].

We consider a three-layer beam with outside layers made of D16-T alloy and polyfoam filler. The following geometrical, physical, and mechanical parameters are used: $\delta_1 = 0.7 \cdot 10^{-3}$ m is the thickness of the outside layers, $\delta_2 = 0.37 \cdot 10^{-2}$ m is the filler thickness, $E_{out} = 7.03 \cdot 10^{10}$ Pa, $\nu = 0.33$, $E_{out} / E_{fil} = 471$, $A = 0.0996 \cdot 10^5$ Pa, $L = 0.28$ m.

In Table 2.3 *a*) correspond to the results of experiments [66] for deflection U_3 on the outside surface of the beam for $x = L/2$; *b*) to the results of analytical solution; *c*) to computations according to the present survey; *d*) to the Timoshenko theory of three-layer beams (package); *e*) to the Kirchhoff theory of three-layer beams (package). The third column in Table 2.3 corresponds to relative error Δ determined by the formula $|\Delta = (w_m - w_*)/w_m| \cdot 100\%$, where w_m is the experimental value, and w_* are the corresponding values according to different computational schemes.

Comparison of the deflection values according to the experiment [66] is given in Table 2.4. The case of the hinged beam under loading $P_3 = Af(x)\eta(t)$ is considered. Geometrical, physical, and mechanical parameters of the beam are the following: $L/h = 10$, $\delta_1 / \delta_2 = 0.5$, $h = 2\delta_1 + \delta_2$, $E_{out} = 2.02 \cdot 10^{11}$ Pa, $\nu_{out} = 0.3$, $E_{fil} = 0.394 \cdot 10^{10}$ Pa, $\nu_{fil} = 0.35$, $A = 5 \cdot 10^5$ Pa. The notation in Table 2.4 is similar to that in Table 2.3. As follows from the results, computations by the theory of independent approximations are the most consistent with the corresponding experimental and analytical solutions, which indirectly confirms the reliability of the results obtained.

3. Three-Layer Shells of Revolution with Discrete Ribbed Filler. Three-layer shells with discrete ribbed filler under impulsive loading are considered below. As mentioned above, there are two main approaches to the construction of variants of the theory of multilayered shells, i.e., application of common hypotheses to the whole package and the hypotheses that consider kinematical and statical parameters of every layer. It is evident that shells with discrete filler can be related to the second approach. On the other hand, these inhomogeneous shell structures with ribbed filler can be considered as shells with discrete ribs.

The most completely modern state of research in the field of dynamics of stiffened shells is described in [3, 6, 10, 24–26, 33, 34, 36, 37, 40, 43, 51]. Almost all of the investigations use a computational scheme based on the equations of the Kirchhoff–Love applied theory of shells and the Kirchhoff–Clebsch theory of rods. Mainly the problems of natural vibrations are considered. Forced vibrations of stiffened shells are considered for harmonic lading [3]. Application of models of shells and rods, corresponding to the Timoshenko hypotheses in the problems of stiffened shells with discrete ribs is considered in [6, 24,

25, 33] (numerical modeling of axisymmetric and non-axisymmetric vibrations of stiffened shells of revolution under nonstationary loading in linear and geometrically nonlinear statements).

The present analysis of investigations of non-stationary vibrations of inhomogeneous shells [143] showed that the problems of forced axisymmetric and non-axisymmetric vibrations of three-layer shells of revolution with discrete filler under non-stationary loading are urgent.

3.1. Equations of Vibrations of Three-Layer Shells with Discrete Ribbed Filler. A three-layer shell with internal filler is an elastic structure consisting of inner and outer layers and a system of ribs rigidly connected with them. An element of the structure is schematized in Fig. 3.1. We assumed that the SSS of the outer layers can be determined within the framework of the geometrically nonlinear shell theory making the assumptions corresponding to the Timoshenko hypotheses (in quadratic approximation). For computation of ribs, we use the geometrically nonlinear variant of the Timoshenko theory of rods.

3.2. Axisymmetric Equations of Vibrations of Three-Layer Shells of Revolution with Discrete Ribbed Filler. A mathematical model of dynamic deformation of a three-layer elastic structure with discrete filler is a hyperbolic system of nonlinear differential equations corresponding to the Timoshenko hypotheses. In deriving the motion equations of the structure, we use the variant of the geometrically nonlinear theory of thin shells in quadratic approximation [6, 33, 62, 63, 101]. The deformed state of the inner and outer continuous shells of revolution is determined by the corresponding components of the generalized vectors of displacements $\overline{U}_1 = (u_1^1, u_3^1, \varphi_1^1)^T$ and $\overline{U}_2 = (u_1^2, u_3^2, \varphi_1^2)^T$. We model the internal filler by a system of discrete ribs. Moreover, we assume that the deformed state of the *j*th rib is determined by the generalized vector of displacement of the center of gravity of its transverse cross-section $\overline{U}_j = (u_{1j}, u_{3j}, \varphi_{1j})^T$. Starting from the assumption of rigid connection of discrete ribs with the outside shells, we represent the conditions of contact of the centers of gravity of ribs with them as

$$u_{1j} = u_1^i(s_j) \pm h_j^i \varphi_1^i(s_j), \quad u_{3j} = u_3^i(s_j),$$

$$\varphi_{1j} = \varphi_1^i(s_j) \quad (i = 1, 2,\ j = \overline{1, J}), \tag{3.1}$$

where s_j is the coordinate of the coupling line of the center of gravity of the *j*th rib with the middle surface; $h_j^i = 0.5h_i + H_j$, $h_i\ (i = 1, 2)$ are the thicknesses of the inner and outer shells; H_j is the distance from the axis of the *j*th rib to the surfaces of the smooth shells.

To derive the equations of vibrations of the three-layer inhomogeneous structure, we use the Hamilton–Ostrogradsky principle of stationarity:

$$\int_{t_1}^{t_2} [\delta(\Pi - K) - \delta A]\, dt = 0, \tag{3.2}$$

where Π is the potential energy of the elastic system; K is the kinetic energy; A is the work done by external forces.

We write the expressions for the values $\delta\Pi$ and δK as follows:

$$\delta\Pi = \sum_{i=1}^{2} \delta\Pi_{0i} + \sum_{j=1}^{J} \delta\Pi_j, \qquad \delta K = \sum_{i=1}^{2} \delta K_{0i} + \sum_{j=1}^{J} \delta K_j,$$

$$\delta\Pi_{0i} = \int_{s_i} (T_{11}^i \delta\varepsilon_{11}^i + T_{22}^i \delta\varepsilon_{22}^i + T_{13}^i \delta\varepsilon_{13}^i + M_{11}^i \delta\kappa_{11}^i + M_{22}^i \delta\kappa_{22}^i)\, ds_i,$$

$$\delta\Pi_j = T_{22j} \delta\varepsilon_{22j},$$

$$\delta K_{0i} = \rho_i h_i \int_{s_i} \left[\left(\frac{\partial^2 u_1^i}{\partial t^2} \right) \delta u_1^i + \left(\frac{\partial^2 u_3^i}{\partial t^2} \right) \delta u_3^i + \frac{h_i^2}{12} \left(\frac{\partial^2 \varphi_1^i}{\partial t^2} \right) \delta\varphi_1^i \right] ds_i,$$

$$\delta K_j = \rho_j F_j \left[\left(\frac{\partial^2 u_{1j}}{\partial t^2} \right) \delta u_{1j} + \left(\frac{\partial^2 u_{3j}}{\partial t^2} \right) \delta u_{3j} + \frac{I_{twj}}{F_j} \left(\frac{\partial^2 \varphi_{1j}}{\partial t^2} \right)^2 \delta\varphi_{1j} \right], \tag{3.3}$$

where $s_i = \alpha_1 A_1^i$, t are the spatial (for every outside layer) and time coordinates, respectively; A_1^i $(i = 1, 2)$ are the coefficients of the first quadratic form of the middle surfaces of the inner and outer shells; ρ_i, ρ_j are the densities of the shells and the rib; F_j, I_{twj} are the geometrical parameters of the jth rib.

The forces and moments in (3.3) are expressed as follows:

$$T_{11}^i = B_{11}^i(\varepsilon_{11}^i + \nu_2^i \varepsilon_{22}^i), \quad T_{22}^i = B_{11}^i(\varepsilon_{22}^i + \nu_1^i \varepsilon_{11}^i), \quad T_{13}^i = B_{13}^i \varepsilon_{13}^i,$$

$$M_{11}^i = D_{11}^i(\kappa_{11}^i + \nu_2^i \kappa_{22}^i), \quad M_{22}^i = D_{22}^i(\kappa_{22}^i + \nu_1^i \kappa_{11}^i), \quad T_{22j} = B_{22j} \varepsilon_{22j}, \tag{3.4}$$

where

$$\varepsilon_{11}^i = \frac{\partial u_1^i}{\partial s_i} + \frac{1}{2}[\theta_1^i]^2 + k_1^i u_3^i, \quad \varepsilon_{22}^i = \psi^i u_1^i + k_2^i u_3^i, \quad \varepsilon_{13}^i = \varphi_1^i + \theta_1^i,$$

$$\theta_1^i = \frac{\partial u_3^i}{\partial s_i} - k_1^i u_1^i, \quad \kappa_{11}^i = \frac{\partial \varphi_1^i}{\partial s_i}, \quad \kappa_{22}^i = \psi^i \varphi_1^i, \quad \varepsilon_{22j} = \frac{u_{3j}}{R_j}, \quad \psi^i = \frac{1}{A_2^i}\frac{dA_2^i}{ds_i},$$

$$B_{11}^i = \frac{E_1^i h_i}{1 - \nu_1^i \nu_2^i}, \quad B_{22}^i = \frac{E_2^i h_i}{1 - \nu_1^i \nu_2^i}, \quad B_{13}^i = G_{13} K_i^2,$$

$$D_{11}^i = \frac{E_1^i h_i^3}{12(1 - \nu_1^i \nu_2^i)}, \quad D_{22}^i = \frac{E_2^i h_i^3}{12(1 - \nu_1^i \nu_2^i)}, \quad B_{22j} = E_j F_j. \tag{3.5}$$

In (3.5), k_1^i, k_2^i are the curvatures of the middle surfaces of the shells $(i = 1, 2)$; $E_1^i, E_2^i, G_{13}^i, \nu_1^i, \nu_2^i, E_j$ are the physical and mechanical characteristics of the materials of the shells and ribs; K_i^2 is the coefficient of the transverse shear in the theory of shells, corresponding to the Timoshenko hypotheses.

After standard transformations in (3.2) considering (3.1), (3.3)–(3.5), we obtain two groups of equations:

1) in the smooth domain between ribs for $s_{ij} < s_i < s_{ij+1}$:

$$\frac{1}{A_2^i}\frac{\partial}{\partial s_i}(A_2^i T_{11}^i) - \psi^i T_{22}^i + k_1^i \overline{T}_{13}^i = \rho_i h_i \frac{\partial^2 u_1^i}{\partial t^2},$$

$$\frac{1}{A_2^i}\frac{\partial}{\partial s_i}(A_2^i \overline{T}_{13}^i) - k_1^i T_{11}^i - k_2^i T_{22}^i + P_3 = \rho_i h_i \frac{\partial^2 u_3^i}{\partial t^2},$$

$$\frac{1}{A_2^i}\frac{\partial}{\partial s_i}(A_2^i M_{11}^i) - \psi^i M_{22}^i - T_{13}^i = \frac{\rho_i h_i^3}{12}\frac{\partial^2 \varphi_1^i}{\partial t^2}, \tag{3.6}$$

2) on lines of discontinuity $s_i = s_{ij}$:

$$\sum_{i=1}^{2} T_{11}^{i\pm} = \rho_j F_j \frac{\partial^2 u_{1j}}{\partial t^2}, \quad \sum_{i=1}^{2} \overline{T}_{13}^{i\pm} = \rho_j F_j \frac{\partial^2 u_{3j}}{\partial t^2},$$

$$\sum_{i=1}^{2} (M_{11}^{i\pm} \mp h_j T_{11}^{i\pm}) = \rho_j I_{twj} \frac{\partial^2 \varphi_{1j}}{\partial t^2}. \tag{3.7}$$

The motion equations (3.6), (3.7) are supplemented by the corresponding boundary (for $s_i = s_{i0}, s_i = s_{iN}$) and initial conditions.

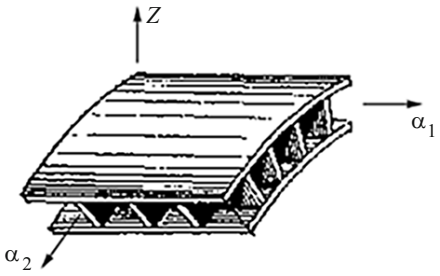

Fig. 3.1

3.3. Equations of Vibrations of Three-Layer Cylindrical Shells with Discrete Longitudinally Transverse Ribbed Filler. Three-layer cylindrical shells with discrete ribbed filler are an elastic system consisting of inner (upper index 1) and outer (upper index 2) shells and a system of discrete ribs rigidly fixed to them. We assume that the SSS of these (cylindrical) shells and ribs can be determined within the framework of the simplest geometrically nonlinear variant of the theory of shells and rods, where the Timoshenko hypotheses are accepted [6, 33, 137]. The elastic structure is schematized in Fig. 3.1.

The deformed state of the inner and outer shells can be determined by the components of the generalized vectors of displacements of the corresponding middle surfaces $\overline{U}_1 = (u_1^1, u_2^1, u_3^1, \varphi_1^1, \varphi_2^1)^T$ and $\overline{U}_2 = (u_1^2, u_2^2, u_3^2, \varphi_1^2, \varphi_2^2)^T$. The deformed state of a rib directed along the axis x is determined by the vector of displacement of the line of the center of gravity of transverse cross-section $\overline{U}_i = (u_{1i}, u_{2i}, u_{3i}, \varphi_{1i}, \varphi_{2i})^T$. Accordingly, for a rib directed along the axis y it is determined by the vector $\overline{U}_j = (u_{1j}, u_{2j}, u_{3j}, \varphi_{1j}, \varphi_{2j})^T$.

To derive the equations of vibrations of the three-layer elastic structure with longitudinally transverse discrete ribbed filler, we use the Hamilton–Ostrogradsky variational principle of stationarity (3.2). We write the expressions for total potential and kinetic energy as

$$\delta\Pi = \delta\sum_{i=1}^{2}\Pi^i + \delta\sum_{i=1}^{I}\Pi_i + \delta, \tag{3.8}$$

$$\delta K = \delta\sum_{i=1}^{2} K^i + \delta\sum_{i=1}^{I} K_i + \delta, \tag{3.9}$$

$$\delta\Pi^i = \int_S (T_{11}^i\delta\varepsilon_{11}^i + T_{22}^i\delta\varepsilon_{22}^i + T_{13}^i\delta\varepsilon_{13}^i + T_{12}^i\delta\varepsilon_{12}^i + M_{11}^i\delta\kappa_{11}^i + M_{22}^i\delta\kappa_{22}^i + H^i\delta\kappa_{12}^i)\,dS, \tag{3.10}$$

$$\delta\Pi_i = \int_{L_i} (T_{11i}\delta\varepsilon_{11i} + T_{12i}\delta\varepsilon_{12i} + T_{13i}\delta\varepsilon_{13i} + M_{11i}\delta\kappa_{11i} + M_{12i}\delta\kappa_{12i})\,dL_i, \tag{3.11}$$

$$\delta\Pi_j = \int_{L_i} (T_{22j}\delta\varepsilon_{22j} + T_{21j}\delta\varepsilon_{21j} + T_{23j}\delta\varepsilon_{23j} + M_{21j}\delta\kappa_{21j} + M_{22j}\delta\kappa_{22j})\,dL_j, \tag{3.12}$$

$$\delta K^i = \int_S \left[\rho_i h_i\left(\frac{\partial^2 u_1^i}{\partial t^2}\delta u_1^i + \frac{\partial^2 u_2^i}{\partial t^2}\delta u_2^i + \frac{\partial^2 u_3^i}{\partial t^2}\delta u_3^i\right) + \rho_i\frac{h_i^3}{12}\left(\frac{\partial^2\varphi_1^i}{\partial t^2}\delta\varphi_1^i + \frac{\partial^2\varphi_2^i}{\partial t^2}\delta\varphi_2^i\right)\right] dS, \tag{3.13}$$

$$\delta K_i = \int_{L_i}\left[\rho_i F_i\left(\frac{\partial^2 u_{1i}}{\partial t^2}\delta u_{1i} + \frac{\partial^2 u_{2i}}{\partial t^2}\delta u_{2i} + \frac{\partial^2 u_{3i}}{\partial t^2}\delta u_{3i}\right) + \rho_i\left(I_{1i}\frac{\partial^2\varphi_{1i}}{\partial t^2}\delta\varphi_{1i} + I_{kri}\frac{\partial^2\varphi_{2i}}{\partial t^2}\delta\varphi_{2i}\right)\right] dL_i, \tag{3.14}$$

$$\delta K_j = \int_{L_j}\left[\rho_j F_j\left(\frac{\partial^2 u_{1j}}{\partial t^2}\delta u_{1j} + \frac{\partial^2 u_{2j}}{\partial t^2}\delta u_{2j} + \frac{\partial^2 u_{3j}}{\partial t^2}\delta u_{3j}\right) + \rho_j\left(I_{twj}\frac{\partial^2\varphi_{1j}}{\partial t^2}\delta\varphi_{1j} + I_{2j}\frac{\partial^2\varphi_{2j}}{\partial t^2}\delta\varphi_{2j}\right)\right] dL_j. \tag{3.15}$$

The notation of the integral characteristics of the shells and ribs in (3.8)–(3.15) is takedn from [6, 33].

After standard transformations in the variational functional (3.2) we have three groups of the equations:

in the smooth domain:

$$\frac{\partial T_{11}^k}{\partial x}+\frac{\partial S^k}{\partial y}+P_1^k=\rho_k h_k\frac{\partial^2 u_1^k}{\partial t^2},\qquad \frac{\partial S^k}{\partial x}+\frac{\partial T_{22}^k}{\partial y}+\frac{\bar{T}_{23}^k}{R_k}+P_2^k=\rho_k h_k\frac{\partial^2 u_2^k}{\partial t^2},$$

$$\frac{\partial \bar{T}_{13}^k}{\partial x}+\frac{\partial \bar{T}_{23}^k}{\partial y}-\frac{T_{22}^k}{R_k}+P_3^k=\rho_k h_k\frac{\partial^2 u_3^k}{\partial t^2},\qquad \frac{\partial M_{11}^k}{\partial x}+\frac{\partial H^k}{\partial y}-T_{13}^k=\rho_k\frac{h_k^3}{12}\frac{\partial^2\varphi_1^k}{\partial t^2},$$

$$\frac{\partial H^k}{\partial x}+\frac{\partial M_{22}^k}{\partial y}-T_{23}^k=\rho_k\frac{h_k^3}{12}\frac{\partial^2\varphi_2^k}{\partial t^2},$$

$$\bar{T}_{13}^k=T_{13}^k+T_{11}^k\theta_1^k+S^k\theta_2^k,\qquad \bar{T}_{23}^k=T_{23}^k+T_{22}^k\theta_2^k+S^k\theta_1^k, \tag{3.16}$$

for the ith discrete filler along the axis OX, in the cylindrical structure:

$$[S]_i+\frac{\partial T_{11i}}{\partial x}=\rho_i F_i\frac{\partial^2 u_{1i}}{\partial t^2},\qquad [T_{22}]_i+\frac{\partial \bar{T}_{12i}}{\partial x}=\rho_i F_i\frac{\partial^2 u_{2i}}{\partial t^2},\qquad [\bar{T}_{23}]_i+\frac{\partial \bar{T}_{13i}}{\partial x}=\rho_i F_i\frac{\partial^2 u_{3i}}{\partial t^2},$$

$$[H]_i+\frac{\partial M_{11i}}{\partial x}-T_{13i}=\rho_i I_{1i}\frac{\partial^2\varphi_{1i}}{\partial t^2},\qquad [M_{22}]_i+\frac{\partial M_{12i}}{\partial x}=\rho_i I_{kri}\frac{\partial^2\varphi_{2i}}{\partial t^2},$$

$$\bar{T}_{12i}=T_{12i}+T_{11i}\theta_{2i},\qquad \bar{T}_{13i}=T_{13i}+T_{11i}\theta_{1i}, \tag{3.17}$$

for the jth discrete element along the axis OY:

$$[T_{11}]_j+\frac{\partial \bar{T}_{21j}}{\partial y}=\rho_j F_j\frac{\partial^2 u_{1j}}{\partial t^2},\qquad [S]_j+\frac{\partial T_{22j}}{\partial y}+k_{2j}\bar{T}_{23j}=\rho_j F_j\frac{\partial^2 u_{2j}}{\partial t^2},$$

$$[T_{13}]_j+\frac{\partial \bar{T}_{23j}}{\partial y}-k_{2j}T_{22j}=\rho_j F_j\frac{\partial^2 u_{3j}}{\partial t^2},$$

$$[M_{11}]_j+\frac{\partial M_{21j}}{\partial y}=\rho_j I_{twj}\frac{\partial^2\varphi_{1j}}{\partial t^2},\qquad [H]_j+\frac{\partial M_{22j}}{\partial y}-T_{23j}=\rho_j F_j\frac{\partial^2\varphi_{2j}}{\partial t^2}. \tag{3.18}$$

The relation between the forces and moments and the deformations for the shells and ribs is used from [6, 33].

The relation between the components of vectors of displacements describing the SSS of the shells and filler elements is given by the following formulas, in particular, for shells and longitudinal ribs:

$$u_{1i}(x)=u_1^k(x,y_i)\pm H_i^k\varphi_1^k(x,y_i),\qquad u_{2i}(x)=u_2^k(x,y_i)\pm H_i^k\varphi_2^k(x,y_i),$$

$$u_{3i}(x)=u_3^k(x,y_i),\qquad \varphi_{1i}(x)=\varphi_1^k(x,y_i),\qquad \varphi_{2i}(x)=\varphi_2^k(x,y_i)\qquad (k=1,2). \tag{3.19}$$

In (3.19) $H_i^k=0.5(h_i+h_k)$; h_i are the heights of the ith element of discrete filler; $h_k\,(k=1,2)$ are the thicknesses of the shells; y_i is the coordinate line of projecting of the centers of gravity of the transverse cross-section of the ith longitudinal discrete element of filler, directed along the axis OX, onto the corresponding middle surface of the shell. The contact conditions for the corresponding shells and transverse ribs are written similarly.

The equations of vibrations of inhomogeneous elastic structure are supplemented by natural boundary and initial conditions, which follow from the variational principle (3.2).

3.4. Numerical Algorithms for Solving Problems of the Dynamical Behavior of Three-Layer Shells with Discrete Ribbed Filler. Let us consider numerical algorithms for solving non-stationary dynamical problems for three-layer shells with discrete ribbed filler.

3.4.1. Numerical Algorithms for Solving Dynamical Axisymmetric Problems for Three-Layer Shells of Revolution with Ribbed Filler. According to the integral-interpolation method for construction of difference schemes [69], for the equations of vibrations of inhomogeneous shells [6, 33] the following difference equations were obtained for (3.6), (3.7):

$$\frac{1}{A^k_{2\,l}}\frac{A^k_{2\,l+1/2}T^{kn}_{11\,l+1/2}-A^k_{2\,l-1/2}T^{kn}_{11\,l-1/2}}{\Delta s}$$

$$-\frac{\Psi_{k\,l}}{2}(T^{kn}_{22\,l+1/2}+T^{kn}_{22\,l-1/2})+\frac{k_{1\,l}}{2}(\overline{T}^{kn}_{13\,l+1/2}+\overline{T}^{kn}_{13\,l-1/2})+P^{kn}_{1\,l}=\rho_k h_k (u^{kn}_{1\,l})_{\bar{t}\,t},$$

$$\frac{1}{A^k_{2\,l}}\frac{A^k_{2\,l+1/2}\overline{T}^{kn}_{13\,l+1/2}-A^k_{2\,l-1/2}\overline{T}^{kn}_{13\,l-1/2}}{\Delta s}-\frac{k_{1\,l}}{2}(T^{kn}_{11\,l+1/2}+T^{kn}_{11\,l-1/2})-\frac{k_{2\,l}}{2}(T^{kn}_{22\,l+1/2}+T^{kn}_{22\,l-1/2})$$

$$+P^{kn}_{3\,l}=\rho_k h_k (u^{kn}_{3\,l})_{\bar{t}\,t},$$

$$\frac{1}{A^k_{2\,l}}\frac{A^k_{2\,l+1/2}M^{kn}_{11\,l+1/2}-A^k_{2\,l-1/2}M^{kn}_{11\,l-1/2}}{\Delta s}-\frac{\Psi_{k\,l}}{2}(M^{kn}_{22\,l+1/2}+M^{kn}_{22\,l-1/2})-\frac{1}{2}(T^{kn}_{13\,l+1/2}+T^{kn}_{13\,l-1/2})$$

$$+m^{kn}_{1\,l}=\rho_k\frac{h_k^3}{12}(\varphi^{kn}_{1\,l})_{\bar{t}\,t},$$

$$\overline{T}^{kn}_{13\,l\pm1/2}=T^{kn}_{13\,l\pm1/2}+T^{kn}_{11\,l\pm1/2}\theta^{kn}_{1\,l\pm1/2},\qquad \Psi_{k\,l}=\frac{1}{A^k_{2\,l}}\frac{A^k_{2\,l+1/2}-A^k_{2\,l-1/2}}{\Delta s}. \tag{3.20}$$

The difference relations between the forces and moments are taken from [6, 33].

3.4.2. Numerical Algorithm for Solving Dynamical Problems for Three-Layer Cylindrical Shells with Longitudinal–Transverse Discrete Ribbed Filler. According to the approach [6, 33, 69], the difference relations for solving Eq. (3.16) have the form

$$\frac{T^{kn}_{11l+1/2,\,m}-T^{kn}_{11l-1/2,\,m}}{\Delta x}+\frac{S^{kn}_{11l,\,m+1/2}-S^{kn}_{11\,l,m-1/2}}{\Delta y}+P^{kn}_{1lm}=\rho_k h_k (u^{kn}_{1lm})_{\bar{t}t},$$

$$\frac{S^{kn}_{l+1/2,\,m}-S^{kn}_{l-1/2,\,m}}{\Delta x}+\frac{T^{kn}_{22l,\,m+1/2}-T^{kn}_{22l,\,m-1/2}}{\Delta y}+\frac{\overline{T}^{kn}_{23l,\,m+1/2}+\overline{T}^{kn}_{23l,\,m-1/2}}{2R_k}+P^{kn}_{2lm}=\rho_k h_k (u^{kn}_{2lm})_{\bar{t}t},$$

$$\frac{\overline{T}^{kn}_{13l+1/2,\,m}-\overline{T}^{kn}_{13l-1/2,\,m}}{\Delta x}+\frac{\overline{T}^{kn}_{23l,\,m+1/2}-\overline{T}^{kn}_{23l,\,m-1/2}}{\Delta y}-\frac{T^{kn}_{22l,\,m+1/2}+T^{kn}_{22l,\,m-1/2}}{2R_k}+P^{kn}_{3lm}=\rho_k h_k (u^{kn}_{3lm})_{\bar{t}t},$$

$$\frac{M^{kn}_{11l+1/2,\,m}-M^{kn}_{11l-1/2,\,m}}{\Delta x}+\frac{H^{kn}_{l,m+1/2}-H^{kn}_{l,m-1/2}}{\Delta y}-\frac{T^{kn}_{13l+1/2,\,m}+T^{kn}_{13l-1/2,\,m}}{2}+m^{kn}_{1\,lm}=\rho_k\frac{h_k^3}{12}(\varphi^{kn}_{1\,lm})_{\bar{t}t},$$

$$\frac{H^{kn}_{l+1/2,\,m}-H^{kn}_{l-1/2,\,m}}{\Delta x}+\frac{M^{kn}_{22l,\,m+1/2}-M^{kn}_{22l,\,m-1/2}}{\Delta y}-\frac{T^{kn}_{23l,\,m+1/2}+T^{kn}_{23l,\,m-1/2}}{2}+m^{kn}_{2\,lm}=\rho_k\frac{h_k^3}{12}(\varphi^{kn}_{2\,lm})_{\bar{t}t},$$

$$\overline{T}^{kn}_{13l\pm1/2,\,m} = T^{kn}_{13l\pm1/2,\,m} + T^{kn}_{11l\pm1/2,\,m}\theta^{kn}_{1l\pm1/2,\,m} + S^{kn}_{l\pm1/2,\,m}\theta^{kn}_{2l\pm1/2,\,m},$$

$$\overline{T}^{kn}_{23l,\,m\pm1/2} = T^{kn}_{23l,\,m\pm1/2} + T^{kn}_{22l,\,m\pm1/2}\theta^{kn}_{2l,\,m\pm1/2} + S^{kn}_{l,\,m\pm1/2}\theta^{kn}_{1l,\,m\pm1/2}. \quad (3.21)$$

The finite-difference relations for the longitudinal *i*th and transverse *j*th stiffening elements are written similarly to [6, 33, 62, 63, 101].

3.5. Forces Vibrations of Three-Layer Shells with Discrete Ribbed Filler. Problems of the dynamic behavior of three-layer shells of revolution with discrete ribbed filler under axisymmetrical non-stationary loading are considered. Problem statements and numerical algorithms for solving the equations of vibrations of three-layer shells of revolution with discrete ribbed filler are presented. Numerical results of solving dynamical problems of the non-stationary behavior of three-layer shells of revolution with discrete ribbed filler (cylindrical, spherical, conic and ellipsoidal shells) over a wide range of physical, mechanical, and geometrical parameters for different types of boundary conditions and loading were found in [6, 33].

We consider problems of dynamical deformation of three-layer shells with piecewise-homogeneous filler in the cases of rigid fixing of the shell edges under internal distributed loading; one of the shell edges is rigidly fixed, and the other is free under the internal distributed loading; problems of non-stationary behavior of open three-layer spherical, conical, and ellipsoidal shells for rigid fixing of edges and free edges under internal distributed loading [6, 33].

The numerical algorithm for solving non-stationary problems for inhomogeneous three-layer shells is based on the integral-interpolation method for construction of finite-difference schemes with respect to spatial variables and a explicit finite-difference schemes of "cross" type with respect to the time coordinate. Based on the initial problem statement, we determine the solution in the smooth domain of the elastic structure (for the shells between filler discrete elements) and on the lines of spatial discontinuities (for the corresponding elements of the filler).

Every group of equations for elements of the inhomogeneous elastic structure is represented as two systems of equations. One of them is the equations of vibrations of elements of three-layer shell (for the shells, longitudinal and transverse elements of filler), the second one is the generalized Hooke's law for each of the elements. The transition from the continuous system of equations to the finite-difference one is performed in two stages. The first stage consists in finite-difference approximation of the divergent equations of vibrations in forces-moments, based on the use of the integral-differential method of approximation of the equations of vibrations. The second stage of approximation of the equations consists in the selection of energy agreed finite-dimensional approximation of the forces and moments and the corresponding deformations such that the finite-difference analog of the energy equations holds.

The algorithms for solving the problems of axisymmetric vibrations for three-layer cylindrical shells and shells of revolution with discrete filler under non-stationary loading is described below. Starting from the property that explicit finite-difference schemes are conditionally stable, investigation of the stability of the corresponding difference equations for cylindrical shells was done, and the corresponding necessary condition of stability of the finite-difference equations was obtained. The case of non-axisymmetric vibrations was considered for cylindrical shells with longitudinal-transverse discrete filler. Algorithms for obtaining the solution in the smooth domain of middle surfaces of the shells and the algorithm for obtaining solutions on the lines of spatial discontinuities (lines of the gravity center of the transverse cross-section of the longitudinal and transverse discrete elements of filler). In this case, we perform an investigation of the stability of the difference equations and obtain the necessary condition of stability.

The solutions of specific problems of the dynamical behavior of three-layer shells of different geometry under non-stationary loading were presented and regularities of occurring of wave processes in shell structures with discrete ribbed filler were investigated in [62, 63]. We stated the results and analysis of numerical solution of problems of axisymmetric vibrations of three-layer shells of revolution (cylindrical, spherical, and conical) under non-stationary loading. The problems of dynamical deformation of cylindrical shells under different boundary conditions (the case of rigid fixing of the shell edges under internal axisymmetrical distributed loading and the case where longitudinal boundary loading is applied to a free edge) were considered.

The numerical results on the vibrations of cylindrical shells found using the theory stated in [62] are compared with the results obtained using the structurally orthotropic model of three-layer shells. We consider the problem of the dynamical behavior of a three-layer cylindrical shell with filler, which is a system of ring ribs under internal normal axisymmetrical impulsive loading. Here we use the equations of vibrations of shells with discrete filler and the equations of vibrations of the

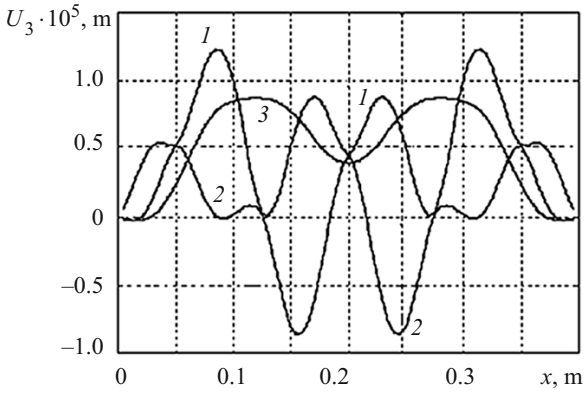

Fig. 3.2

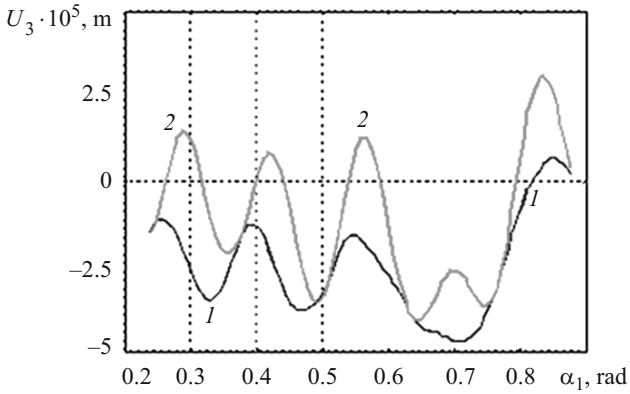

Fig. 3.3

structurally orthotropic theory of three-layer cylindrical shells. It was assumed that the shell edges are rigidly fixed, and the initial conditions are zero.

Axisymmetric vibrations of three-layer cylindrical shells were considered using the above-mentioned theories for the following geometrical, physical, and mechanical parameters: $L/h_1 = 40$, $h_1 = h_2$, $R_1/h_1 = 10$, $H_j/h_1 = 2$, $F_j = H_j h_1$, $E_1^1 = E_1^2 = E_j = 7 \cdot 10^{10}$ Pa, $\nu_1^1 = \nu_1^2 = 0.3$, $\rho_1 = \rho_2 = \rho_j = 2.7 \cdot 10^3$ kg/m^3.

The normal impulsive loading is defined by (2.13). The stiffening elements are placed at the points $x_j = [11 + (k-1) \cdot 15] \cdot \Delta x \, (k = 1, \ldots, 5, \Delta x = L/80)$. The obtained numerical results enable characterizing the SSS of the cylindrical three-layer elastic structure at an arbitrary instant. Computations were perfomred on time interval $0 \le t \le 40T$. Figure 3.2 shows the dependences of the deflection u_3 on the spatial coordinate x [m] at $t = 6T$ (the instant of achievement of the maximum of u_3). Curve *1* corresponds to the theory with discrete ribs (inner layer); curve *2* to the theory with discrete ribs (outer layer) the external layer; curve *3* to the structurally orthotropic theory of three-layer shells with filler. According to the numerical data, the qualitative difference between the obtained results is observed. Considering the discreteness of ribs (in the figures, the points connecting curves *1* and *2*) results in more dense wave generation along the structure length. Computations based on the structurally orthotropic model provide certain integral curves that take place within the limits of variation of u_3 of the inner and outer layers according to the theory with rib discreteness. Analyzing the results we see that the difference by maximal values of u_3 (according to the given theories) reaches $\approx 40\%$.

The dynamical behavior of open hemispherical three-layer shells with a free hole under internal disctributed loading $P_3(s, t)$ is investigated. It is assumed that one edge $\alpha_1 = \alpha_{10}$ of the shell is free, and the other edge $\alpha_1 = \alpha_{1N}$ is fixed. Boundary conditions for the free edge $\alpha_1 = \alpha_{10}$ have the form $T_{11}^k = 0, \overline{T}_{13}^k = 0, M_{11}^k = 0 \, (k = 1, 2)$. In the case of rigid fixing $\alpha_1 = \alpha_{1N}$, it is assumed that $u_1^k = u_3^k = \varphi_1^k = 0, k = 1, 2$. Non-stationary impulsive loading is defined by (2.13). It is also assumed that the shells are made of an orthotropic material. Computations are performed for the following geometrical, physical, and mechanical parameters: $E_1^1 = E_1^2 = 19 \cdot 10^9$ Pa, $\nu_1^1 = \nu_1^2 = 0.12$, $E_2^1 = E_2^2 = E_j = 33 \cdot 10^9$ Pa, $G_{13}^1 = G_{13}^2 = 3.69 \cdot 10^9$, $R_1 = 0.3$ m, $\rho_1 = \rho_2 = \rho_j = 1.9 \cdot 10^3$ kg/m^3, $R_1/h_1 = 30$, $h_1 = h_2$, $h_j = 2h$, $F_j = 2 \cdot 10^{-4}$ m^2, $\alpha_{10} = \pi/12$, $\alpha_{1N} = \pi/2$. Discrete stiffening elements are placed at the points $\alpha_j = [3 + (m-1) \cdot 16] \cdot \Delta\alpha, m = \overline{1, 5}, \Delta\alpha = (\alpha_{1N} - \alpha_{10})/80$. The obtained numerical results allow analyzing the SSS of spherical three-layer elastic structure at arbitrary instant (on the time interval $0 \le t \le 40T$). Figure 3.3 shows dependences of u_3 on the spatial coordinate α_1; curve *1* represents the values of u_3 for the inner spherical shell, and curve *2* represent the values of u_3 for the outer spherical shell at $t = 7T$. The points of connection of curves *1* and *2* indicate the locations of discrete ribs.

We consider the problem of axisymmetric vibrations of a rigidly fixed three-layer conic shell under internal distributed loading. Numerical convergence of the obtained results is investigated by way of example of the dynamical behavior of a rigidly fixed three-layer cylindrical shell with ribbed filler under distributed loading.

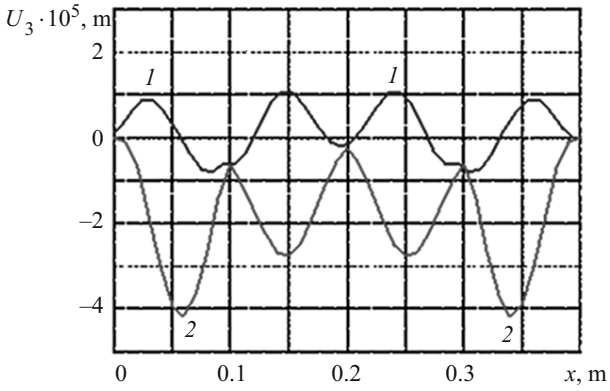

Fig. 3.4

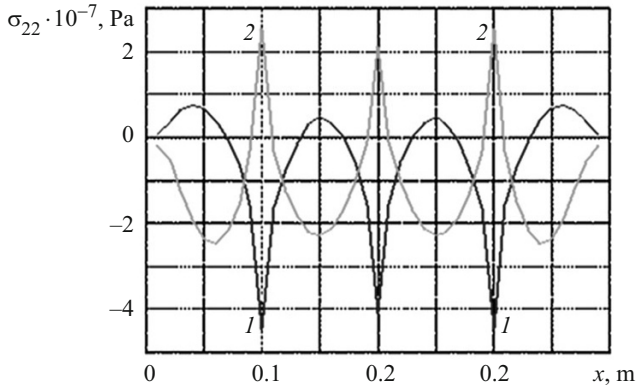

Fig. 3.5

Non-axisymmetric vibrations of cylindrical shells under distributed dynamical loading are considered in the case of cylindrical structures with both longitudinal and longitudinal-transverse discrete fillers. In particular, the problem on non-axisymmetric vibrations of a three-layer cylindrical shell with longitudinal-transverse discrete filler under normal internal loading is considered in the case of rigid fixing of edges of the initial structure. Here we use the following geometrical, physical, and mechanical parameters: $L / h_1 = 80$, $h_1 = h_2$, $R_1 / h_1 = 20$, $h_i = 2h_1$, $i = \overline{1,I}$, $h_j = h_i$, $j = \overline{1,J}$, $E_1^1 = E_1^2 = E_i = E_j = 7 \cdot 10^{10}$ Pa, $\nu_1^1 = \nu_1^2 = 0.3$, $\rho_1 = \rho_2 = \rho_i = \rho_j = 2.7 \cdot 10^3$ kg/m^3, where R_k, h_k $(k = 1, 2)$ are the radius of middle surface and the thickness of the inner and outer shells, respectively; L is the structure length. We consider the case of longitudinal-transverse discrete filler for $I = 4$ and $J = 3$, where discrete elements are arranged uniformly by special coordinates between the internal and external shells. The gravity centers of cross-sections of the discrete elements of filler are projected onto the corresponding middle surfaces of shells by the lines $y = (i-1)\pi R / 2\,(i = \overline{1,4})$ and $x_j = jL / 4\ (j = \overline{1,3})$. The normal impulsive loading is defined by (2.13).

The dependences of u_3 and σ_{22} between longitudinal ribs along the symmetry axis for the spatial coordinate x at $t = 7.5T$ are given in Figs. 3.4 and 3.5. Curves *1* correspond to the internal shell (deflection, stress), and curves *2* correspond to the external shell.

It can be clearly seen from Fig. 3.4 that the transverse discrete stiffening ribs are located ($x_j = jL / 4$, $j = \overline{1,3}$) are the points connecting curves *1* and *2*.

We analyze the obtained results (values of $u_3, \varepsilon_{11}, \varepsilon_{22}, \sigma_{11}, \sigma_{22}$) along the line of symmetry between longitudinal ribs and along the line of arrangement of longitudinal ribs for the inner and outer shells (in particular, at instances when the kinematic and static quantities reach the maximum). Comparative analysis of the values of u_3 along the rib and the value of u_3 along the line of rib symmetry shows that they differ by a factor of 1.8. Similar pattern is observed for $\varepsilon_{22}, \sigma_{22}$. A typical feature of $\varepsilon_{11}, \varepsilon_{22}, \sigma_{11}, \sigma_{22}$ is that they change abruptly at the locations of the transverse ribs $x_j = jL / 4$ $(j = \overline{1,3})$, which is shown in Fig. 3.5. This is explained by peculiarity of the model and algorithm of solving the problems of dynamical behavior of three-layer shells with discrete longitudinal-transverse filler, i.e., determination of the solution in the smooth domain of the shells and on the lines of spatial discontinuities (along the line of gravity center of cross-section of the *i*th rib (along the *OX* axis) and the *j*th rib (along the *OY* axis)).

4. Effect of Elastic Media on the Dynamics of Shell Systems. Many publications [6, 143] deal with the vibrations of ribbed open shallow shells. In contrast to known publications, below the main attention is paid to the effect of Winkler and Pasternak elastic foundation [67] on the natural frequencies and modes of vibrations of ribbed shells rectangular in plan. The investigations were performed based on the classical theory of reinforced shallow shells [3] on elastic foundation [12, 13, 95, 96]. The effect of elastic foundation is accounted for by adding the following term to the third equation of motion of ribbed isotropic shallow shells [3]:

$$C_2\left(\frac{\partial^2 u_3}{\partial x_1^2} + \frac{\partial^2 u_3}{\partial x_2^2}\right) + C_1 u_3,$$

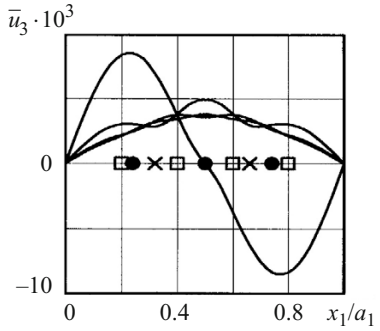

Fig. 4.1

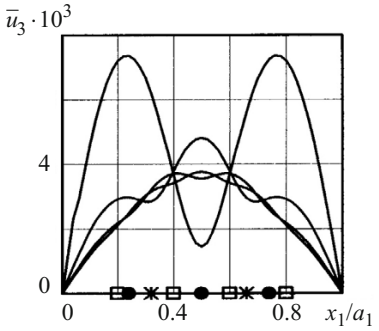

Fig. 4.2

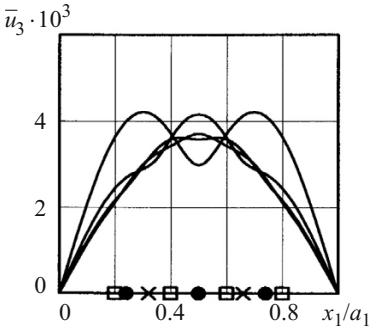

Fig. 4.3

where C_1, C_2 are the coefficients of the Winkler and Pasternak foundations, respectively. The solutions of the system of motion equations for shells with hinged edges have the form of double trigonometric series:

$$u_1 = \cos \omega t \sum_{m=0}^{\infty} \sum_{n=1}^{\infty} u_{mn} \cos \frac{\pi m x_1}{\alpha_1} \sin \frac{\pi m x_2}{\alpha_2},$$

$$u_2 = \cos \omega t \sum_{m=0}^{\infty} \sum_{n=1}^{\infty} v_{mn} \cos \frac{\pi m x_1}{\alpha_1} \sin \frac{\pi m x_2}{\alpha_2},$$

$$u_3 = \cos \omega t \sum_{m=0}^{\infty} \sum_{n=1}^{\infty} w_{mn} \cos \frac{\pi m x_1}{\alpha_1} \sin \frac{\pi m x_2}{\alpha_2}, \tag{4.1}$$

where ω is the circular frequency; α_1, α_2 are the dimensions of the shell in plan.

After substitution of (4.1) into the equations of motion of ribbed isotropic shallow shells rectangular in plan [12, 13, 95, 96] on elastic foundation, the natural frequencies can be found by finding the roots of the reduced systems of algebraic equations, and the natural modes are determined by solving the systems mentioned.

4.1. Effect of the Elastic Foundation on the Natural Frequencies and Modes of Shells. The effect of the elastic foundation on the natural frequencies and modes was analyzed for a shallow spherical shell reinforced by frames and stringers [95, 96].

Figures 4.1–4.3 show the shapes of the deflection (u_3) relative to the shell length without elastic foundation, with the Winkler and Pasternak foundations for its reinforcement by one, two, three, and four ribs, uniformly arranged along the length and width of the shell. The position of ribs is shown by (●), (×), and (□). The curves represent the minimum natural frequencies of a square shell.

It follows from Figs. 4.1–4.3 that the deflection shape changes with increase in the number of ribs. In the shell without elastic foundation and with one rib placed in the central cross-sections, the ribs twist only. If there is twice the number of ribs, then they not only twist but also bend. With further increase in the number of ribs, the deformation of the shell is one longitudinal half-wave.

The conclusions are similar for shells on elastic foundation. In the shell with one rib in the central cross-section, the ribs hardly deform. With increase in the number of ribs, the ribs not only bend, but also twist. If there are four ribs, the deformation of the shell is one longitudinal half-wave similar to the shell without elastic foundation. Comparing the results (the curves in Figs. 4.1–4.3), it can be seen that the elastic foundation has a strong effect on the deflection shape only when the shell is reinforced with one rib. If the shell is reinforced with a greater number of ribs ($n = 4$), the deflection shape of the shell with and without elastic foundation does not change.

We also calculate the first five natural frequencies depending on the coefficients of the Pasternak elastic foundation $\bar{C}_1, \bar{C}_2$ for a shell reinforced by one and two ribs in two directions. The natural frequencies increase with the coefficients $\bar{C}_1, \bar{C}_2$. With increase in $\bar{C}_1$, the intervals of variation of the coefficients $\bar{C}_2$ where the natural mode corresponding to the minimal frequency changes decrease. The natural mode corresponding to the minimum frequency which preceded by the occurrence of

multiple minimal frequencies changes abruptly in the shell reinforced with one rib in the central cross-sections and smoothly in the shell reinforced by two ribs (deflection shape tends to one half-wave).

It follows from the analysis of the results that the natural frequencies corresponding to the Pasternak elastic foundation are higher than those corresponding to the Winkler foundation. With variation of the coefficients of elastic foundation not only the natural frequencies change, but also can the natural modes. For shells on elastic foundation, there are more frequencies close to multiple ones, but having different natural modes.

Using a similar technique, we investigate the effect of elastic foundation and the number of stiffening ribs on the natural frequencies and modes for shallow cylindrical shells square in plan stiffened by frames and stringers with the same physical and mechanical characteristics [12, 13, 141–143]. The obtained results are similar to those for spherical shells.

On the basis of the conducted investigation, it is possible to conclude that for shallow cylindrical and spherical shells with a rectangular plan reinforced by a small number of sufficiently rigid ribs, it is necessary to determine the natural frequencies taking into account the discrete arrangement of the ribs. An increase in the number of ribs and the presence of the elastic foundation result not only in an increase of the natural frequencies but also in a change of the natural modes.

The effect of the Winkler elastic foundation and the number of reinforcing ribs on the minimal natural frequencies are investigated by numerical examples. We used the theory of structurally orthotropic shells [3] on elastic foundation [35]. The effect of ribs on the wave parameters can be found using the single-mode approximation:

$$u = u_{mn} \cos d_m \xi \sin n\theta \cos \omega_1 t_1,$$

$$v = v_{mn} \cos d_m \xi \sin n\theta \cos \omega_1 t_1,$$

$$w = w_{mn} \cos d_m \xi \sin n\theta \cos \omega_1 t_1. \tag{4.2}$$

After substituting (4.2) into the equations for stiffened cylindrical shell on elastic foundation [35], the natural frequencies can be found by finding the roots of a system of algebraic equations of the third order. The effect of elastic foundation and reinforcement on the natural frequencies and modes is analyzed for a ribbed cylindrical shell.

The results of calculating the minimal natural frequencies depending on the number of reinforcing ribs for shells with stringers and frames and shells reinforced by crossed system of ribs characterize the dependence of minimal natural frequencies on the coefficients of the Winkler elastic foundation $\overline{C}_1$. The natural frequencies first increase and then decrease. Thus, for example, the natural frequency of a stringer shell decrease when the number of stringers is eight. For a shell reinforced by stringers and frames, this decrease depends on the coefficient of elastic foundation. For $\overline{C}_1 < 0.05$, the natural frequencies decrease when the shell is reinforced by 16 ribs in both directions. If $\overline{C}_1 > 0.05$, the natural frequencies decrease when the shell is reinforced by eight ribs. The natural frequencies decrease because the ribs behave as attached masses. Therefore, it is necessary to select rational ribbed reinforcement. Similar investigations are described in [79, 80, 83, 85–90, 92, 107, 109, 123].

The propagation of harmonic waves in a cylindrical shell is studied in [84]. The publications [102, 117] deal with the investigation of the effect of a Winkler foundation on the propagation of harmonic waves in orthotropic cylindrical shells, and the effect of the two-parametric (Pasternak) foundation on the propagation of harmonic waves in a orthotropic cylindrical shell is studied in [7]. The performed asymptotic investigation of potential solutions of the disperse equation for long waves gives the following result:

$$V = \sqrt{\frac{E_1 E_2 h + C_1 E_1 R^2}{\rho[E_2 h + C_1 R^2 (1 - \nu_{12}\nu_{21})]}}, \quad C_1 = 0, \quad V_1 = \sqrt{\frac{E_1}{\rho}}, \quad C_1 = \infty, \quad V_2 = \sqrt{\frac{E_1}{\rho(1 - \nu_{12}\nu_{21})}}.$$

A shell without foundation has a rod-type velocity, while a shell on an absolutely rigid foundation has a plate-type velocity. For thin shells, the velocities are expressed as

$$V_2 = \sqrt{\frac{E_1}{\rho(1 - \nu_{12}\nu_{21})}}, \quad V_3 = \mu \sqrt{\frac{G_{13}}{\rho}\left[1 + \frac{C_2}{\mu^2 G_{13} h}\right]}.$$

In this case, a shell has a plate-type velocity and the coefficient C_2 affects considerably the velocity of shear waves.

In what follows, we investigate the effect of Winkler and Pasternak elastic foundation on the cut-off frequency, the number and shape of dispersion curves for harmonic waves propagating along the longitudinally reinforced closed cylindrical shell [100]. The closed circular cylindrical shell with hinged edges is reinforced by a regular system of longitudinal ribs (all ribs have the same geometrical and mechanical parameters and are arranged at the same mutual distances). The shell is on an elastic foundation characterized by the Winkler and Pasternak coefficients C_1, C_2.

The motion equations are obtained using applied theories of shells and rods [3]. In the case of presence of elastic foundation, they were derived in [26, 36, 100]. For solving the system of equations of motion [100], we use its representation as series

$$u = e^{ik\xi} \sum_{n=0}^{\infty} (u_{n1} \cos n\theta + u_{n2} \sin n\theta) \cos \omega_1 t_1,$$

$$v = e^{ik\xi} \sum_{n=0}^{\infty} (v_{n1} \sin n\theta + v_{n2} \cos n\theta) \cos \omega_1 t_1,$$

$$w = e^{ik\xi} \sum_{n=0}^{\infty} (w_{n1} \cos n\theta + w_{n2} \sin n\theta) \cos \omega_1 t_1, \tag{4.3}$$

where u_{ns}, v_{ns}, w_{ns} $(s = 1, 2)$ are unknown constants; k is the dimensionless wave parameter (associated wavelength is $\lambda = 2\pi r / k$), $\omega_1 = \omega / \omega_0$, $\omega_0 = 1 / r\sqrt{E / (1 - \nu^2)\rho_0}$.

Substituting (4.3) into the motion equations [100], we can determine u_{ns}, v_{ns}, w_{ns} from infinite systems of homogeneous linear algebraic equations, which have an exact solution. We obtained three types of dispersion equations [100].

Thus, the determination of wave parameters is reduced to finding the roots of equations of two types:

$$1 + L_n^{11} + L_n^{33} + L_n^{11} L_n^{33} + L_n^{13} L_n^{31} = 0, \tag{4.4}$$

$n = 1, \ldots, n_2$ (the general case of deformation); $n = 0 (k_1 / 2) \delta_{k_1 2 s_1}$ (the first special case of deformation); for the second special case of deformation, the equations have the form

$$1 + L_n^{22} + L_n^{44} + L_n^{22} L_n^{44} + L_n^{24} L_n^{42} = 0 \quad (n = 0, \quad \delta_{k_1 2 s_1} k_1 / 2). \tag{4.5}$$

The following notation is used: $n_2 = k_1 / 2$ (for even k_1); $n_2 = (k_1 - 1) / 2$ (for odd k_1); $2n$ is the number of nodal lines of the wave shape in the circumferential direction; $\delta_{k_1 2 s_1}$ is the Kronecker symbol; $s_1 = 1, 2, \ldots$.

The equations for determination of the cut-off frequencies can be derived from (4.4) and (4.5) with $k = 0$. The numerical data were obtained for a shell reinforced by four ribs ($k = 4$) on the inner surface. Since harmonic waves propagating along the shell are considered $0 \le \omega_i \le 0.2$, only real roots of Eqs. (4.4), (4.5) were determined. The results of determination of the cut-off frequencies and construction of dispersion curves are presented for three variants of harmonic loading of the ribbed shell: cyclically symmetric in the circumferential direction with period $2\pi / k_1$ $(n = 0)$, cyclically symmetric in the circumferential direction with period $4\pi / k_1$ $(n = k_1 / 2)$, and antisymmetric in the circumferential direction $(n = 1)$.

Within the considered range of perturbation frequencies, with increase in the coefficients of elastic foundation, the cut-off frequencies increase in comparison with the frequencies for the shell without elastic foundation. For great values of the coefficients of elastic foundation, the number of cut-off frequencies decreases. The cut-off frequencies corresponding to the Pasternak elastic foundation are higher than those corresponding to Winkler elastic foundation.

The dispersion curves for $n = 0$ and different coefficients of Winkler elastic foundation are presented in Figs. 4.4 and 4.5. Figure 4.4 corresponds to $\overline{C}_1 = 0$, while Fig. 4.5 to $\overline{C}_1 = 0.01$. As is seen from Figs. 4.4 and 4.5, with increase in the coefficient of Winkler elastic foundation, the shape of dispersion curves changes, they become smoother.

The dispersion curves for harmonic waves propagating along a longitudinally reinforced cylindrical shell on Pasternak elastic foundation ($\overline{C}_1 = 0.001$ and $\overline{C}_2 = 0.005$) are shown in Fig. 4.6. Figure 4.6 represents harmonic waves of arbitrary profile in the circumferential direction (wavelength is not multiple to the distance between ribs, i.e., the general case of the deformation).

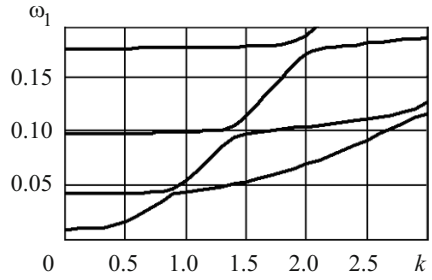

Fig. 4.4

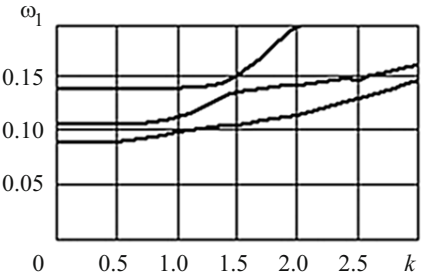

Fig. 4.5

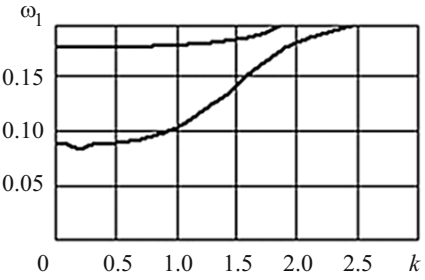

Fig. 4.6

Taking into account the discrete arrangement of ribs enables construction of dispersion curves in the special case of deformation where waves have antinode on ribs.

Analysis of the obtained results shows that with increase in the coefficients of elastic foundation, the cut-off frequencies increase, and their number in the range of perturbation frequencies decreases. The shape of dispersion curves changes with increase in the coefficients of elastic foundation, they become smoother.

A considerable number of the discretely reinforced shell structures contacting with an elastic medium undergo elastic deflections comparable with their thickness. Therefore, it is necessary to solve problems of the dynamical behavior of thin shells based on the geometrically nonlinear theory of rods and shells considering the Timoshenko hypotheses [6, 8, 9, 20, 27, 30, 81, 102, 138, 143]. The numerical algorithm for solving non-stationary problems of the theory of reinforced shells on elastic foundations is based on the application of the integral-interpolation method for construction of finite-difference schemes with respect to spatial coordinates and explicit finite-difference scheme with respect to the time coordinate [6, 33]. In deriving the equations of vibrations of stiffened shells of revolution in the presence of a medium, it was assumed that the SSS of an inhomogeneous elastic structure can be determined within the framework of the geometrically nonlinear theory of shells and rods using the Timoshenko hypotheses [6, 33]. The deformed state of the middle surface of the shell is determined by the components of the generalized vector of displacements $\overline{U} = (u_1, u_2, u_3, \varphi_1, \varphi_2)^T$. The deformed state of the gravity center of transverse cross-section of a rib directed along the axis x is determined by the generalized vector of displacements $\overline{U}_i = (u_{1i}, u_{2i}, u_{3i}, \varphi_{1i}, \varphi_{2i})^T$; for a rib directed along the axis y, it is determined by the vector $\overline{U}_j = (u_{1j}, u_{2j}, u_{3j}, \varphi_{1j}, \varphi_{2j})^T$. It is assumed that the shell and the reinforcing ribs are rigidly connected with each other.

To derive the equations of vibrations of a discretely stiffened structure, the Hamilton–Ostrogradsky variational principle is used:

$$\int_{t_1}^{t_2} [\delta(\Pi - T) - \delta A]\, dt = 0, \tag{4.6}$$

where Π is the potential energy of the system in the presence of elastic foundation, T is the kinetic energy of the system; A is the work done by the external forces.

The expression for the potential energy is

$$\Pi = \Pi_0 + \sum_{i=1}^{I} \Pi_i + \sum_{j=1}^{J} \Pi_j + \Pi_{foun},$$

where Π_0 is the potential energy of the shell, Π_i is the potential energy of the ith rib, Π_j is the potential energy of the jth rib, Π_{foun} is the potential energy of the elastic foundation (the Pasternak model).

After standard transformations in functional (4.6) considering the integral characteristics of stresses of the shell and ribs, we obtain three groups of the equations:

– the equations of vibrations of the smooth shell

$$\frac{\partial T_{11}}{\partial x}+\frac{\partial S}{\partial y}+P_1=\rho h\frac{\partial^2 u_1}{\partial t^2},\qquad \frac{\partial S}{\partial x}+\frac{\partial T_{22}}{\partial y}+\frac{T_{23}}{R}+P_2=\rho h\frac{\partial^2 u_2}{\partial t^2},$$

$$C_2\left(\frac{\partial^2 u_3}{\partial x^2}+\frac{\partial^2 u_3}{\partial y^2}\right)+\frac{\partial T_{13}}{\partial x}+\frac{\partial T_{23}}{\partial y}-\frac{T_{22}}{R}-C_1u_3+P_3=\rho h\frac{\partial^2 u_3}{\partial t^2},$$

$$\frac{\partial M_{11}}{\partial x}+\frac{\partial H}{\partial y}-T_{13}=\rho\frac{h^3}{12}\frac{\partial^2\varphi_1}{\partial t^2},\qquad \frac{\partial H}{\partial x}+\frac{\partial M_{22}}{\partial y}-T_{23}=\rho\frac{h^3}{12}\frac{\partial^2\varphi_2}{\partial t^2},\tag{4.7}$$

– the equations of vibrations of the *i*th rib along the line of gravity center of the transverse cross-section of the rib center

$$\frac{\partial T_{11i}}{\partial x}+[S]=\rho_i F_i\left(\frac{\partial^2 u_1}{\partial t^2}\pm h_{ci}\frac{\partial^2\varphi_1}{\partial t^2}\right),\qquad \frac{\partial T_{12i}}{\partial x}+[T_{22}]=\rho_i F_i\left(\frac{\partial^2 u_2}{\partial t^2}\pm h_{ci}\frac{\partial^2\varphi_2}{\partial t^2}\right),$$

$$\frac{\partial \overline{T}_{13i}}{\partial x}+[T_{23}]=\rho_i F_i\frac{\partial^2 u_3}{\partial t^2},$$

$$\frac{\partial M_{11i}}{\partial x}\pm h_{ci}\frac{\partial T_{11i}}{\partial x}-T_{13i}+[H]=\rho_i F_i\left[\pm h_{ci}\frac{\partial^2 u_1}{\partial t^2}+\left(h_{ci}^2+\frac{I_{1i}}{F_i}\right)\frac{\partial^2\varphi_1}{\partial t^2}\right],$$

$$\frac{\partial M_{12i}}{\partial x}\pm h_{ci}\frac{\partial \overline{T}_{12i}}{\partial x}+[M_{22}]=\rho_i F_i\left[\pm h_{ci}\frac{\partial^2 u_1}{\partial t^2}+\left(h_{ci}^2+\frac{I_{twi}}{F_i}\right)\frac{\partial^2\varphi_2}{\partial t^2}\right],\tag{4.8}$$

– the equations of vibrations of the *j*th rib along the line of the gravity center of the transverse cross-section of the rib center

$$\frac{\partial T_{21i}}{\partial y}+[T_{11}]=\rho_j F_j\left(\frac{\partial^2 u_1}{\partial t^2}\pm h_{cj}\frac{\partial^2\varphi_1}{\partial t^2}\right),\qquad \frac{\partial T_{22j}}{\partial y}+\frac{T_{23j}}{R_j}+[S]=\rho_j F_j\left(\frac{\partial^2 u_2}{\partial t^2}\pm h_{cj}\frac{\partial^2\varphi_2}{\partial t^2}\right),$$

$$\frac{\partial T_{23j}}{\partial y}-\frac{T_{22j}}{R_j}+[T_{13}]=\rho_j F_j\frac{\partial^2 u_3}{\partial t^2},$$

$$\frac{\partial M_{21j}}{\partial y}\pm h_{cj}\frac{\partial T_{21j}}{\partial y}+[M_{11}]=\rho_i F_i\left[\pm h_{cj}\frac{\partial^2 u_1}{\partial t^2}+\left(h_{cj}^2+\frac{I_{twj}}{F_j}\right)\frac{\partial^2\varphi_1}{\partial t^2}\right],$$

$$\frac{\partial M_{22j}}{\partial y}\pm h_{cj}\frac{\partial T_{22j}}{\partial y}-T_{23j}+[H]=\rho_j F_j\left[\pm h_{cj}\frac{\partial^2 u_1}{\partial t^2}+\left(h_{cj}^2+\frac{I_{2j}}{F_j}\right)\frac{\partial^2\varphi_2}{\partial t^2}\right].\tag{4.9}$$

The equations of vibrations (4.7)–(4.9) are supplemented by the appropriate boundary and initial conditions.

The developed and approved technique of computation of the dynamics of shells of revolution on elastic foundation in geometrically linear and nonlinear statements enables the investigation of the dynamics of discretely reinforced cylindrical [6, 8, 9, 20–22, 31, 33], spherical [6, 21, 23, 27, 33] and conic shells [30, 53] on elastic foundation.

The problem of the dynamical behavior of a discretely rib-reinforced cylindrical shell on Winkler elastic foundation ($C_2=0$ in (4.7)) under distributed impulsive loading was considered in [6]. It is assumed that the shell edges $x=0, x=L$ are rigidly fixed. Axisymmetrical vibrations of the stiffened cylindrical shell on Winkler elastic foundation were considered for the following geometrical, physical, and mechanical parameters, i.e., the steel shell with radius $R=0.1$ m, thickness $h=0.01$ m,

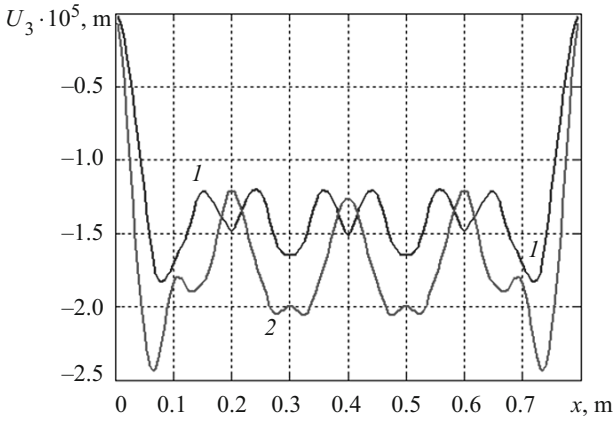

Fig. 4.7

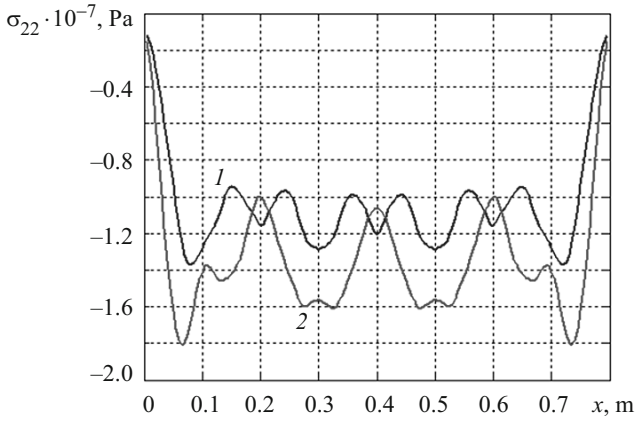

Fig. 4.8

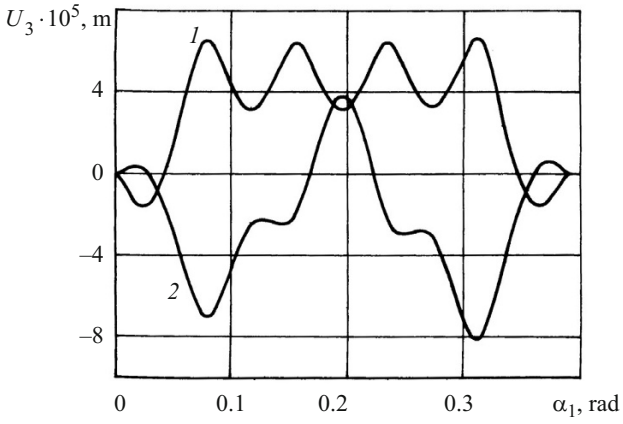

Fig. 4.9

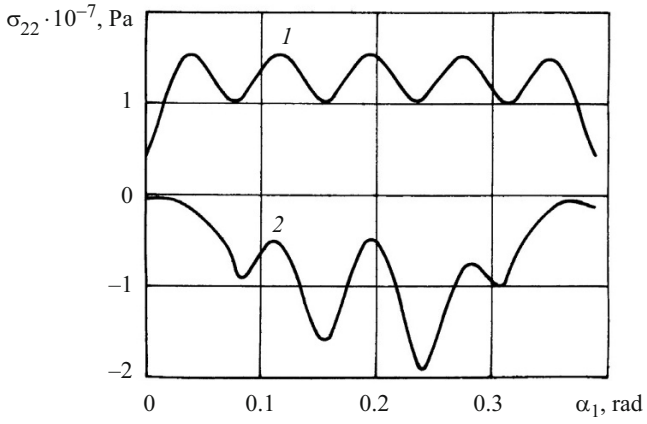

Fig. 4.10

$L/h = 80$, $R/h = 10$, Poisson's ratio is $\nu = 0.3$; density is $\rho_{sh} = 7880$ kg/m, $E = 7 \cdot 10^{10}$ Pa, $c_w = 4.6 \cdot 10^{10}$ N/m^3. Normal impulsive loading is given by (2.13).

The dependences of the deflection u_3 and stress σ_{22} on the spatial coordinate x at instant $t = 3T$ are given in Figs. 4.7 and 4.8. Curves *1* represent the presence of Winkler foundation, curves *2* represent the absence of foundation. The difference in maximal values of u_3 and σ_{22} reaches about 50%. The lines of ribs location $x_j = jL/4$ $(j = \overline{1,3})$ are clearly seen.

A stiffened spherical shell on Pasternak elastic foundation was considered in [27]. In the equations of vibrations and deformation relations, the parameters of the first quadratic form and curvature of the middle surface of the smooth shell are the following: $A_1 = R$, $A_2 = R \sin \alpha_1$, $k_1 = k_2 = R$, where R is the radius of the middle surface; α_1 is the meridional angle.

It is assumed that the shell edges are rigidly fixed in parallel cross-sections α_{10} and α_{1N} and the following boundary conditions take place: $u_1 = u_2 = \varphi_1 = 0$. The initial conditions are zero.

Distributed loading (2.13) is applied to the inner surface of the spherical shell. The problem was solved for the following geometrical, physical, and mechanical parameters: $\alpha_{10} = \pi/12$, $\alpha_{1N} = \pi/2$, $R/h = 60$, $E = 7 \cdot 10^{10}$ Pa, $\rho = 2.7 \cdot 10^3$ kg/m^3, $\nu = 0.3$, $A = 10^6$ Pa, $T = 50 \cdot 10^{-6}$ sec. The foundation coefficients are $C_1 = 0.25 \cdot 10^8$ N/m^3, $C_2 = 10^7$ N/m. The ribs are at the points $s_j = 0.2L_j$ $(L \equiv \overline{1,4})$, $L = (\alpha_{1N} - \alpha_{10})R$.

Numerical computations were performed on the time interval $t = 10T$. The dependences of u_3 and σ_{22} on the spatial coordinate are shown in Figs. 4.9 and 4.10. Curve *1* corresponds to $t = 2T$; curve *2* to $t = 9T$ (Fig. 4.9) and $t = 10T$ (Fig. 4.10).

As is seen, the reinforcing elements have a strong effect on the state of inhomogeneous structure on elastic foundation.

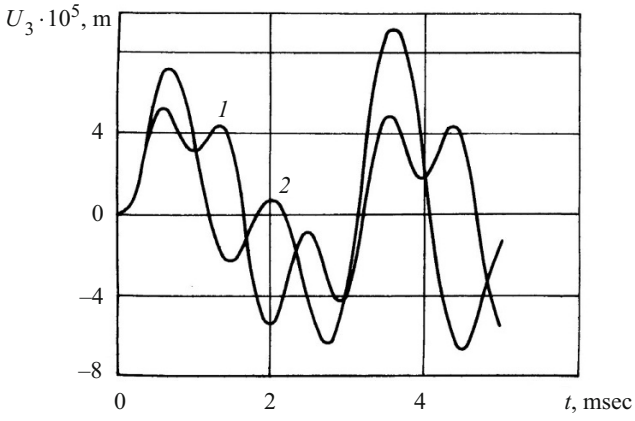

Fig. 4.11

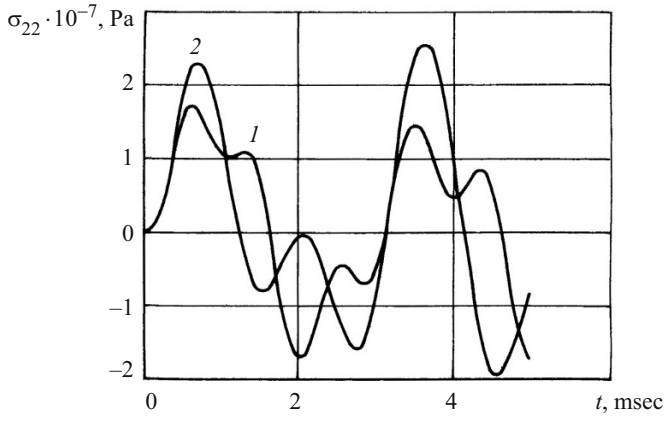

Fig. 4.12

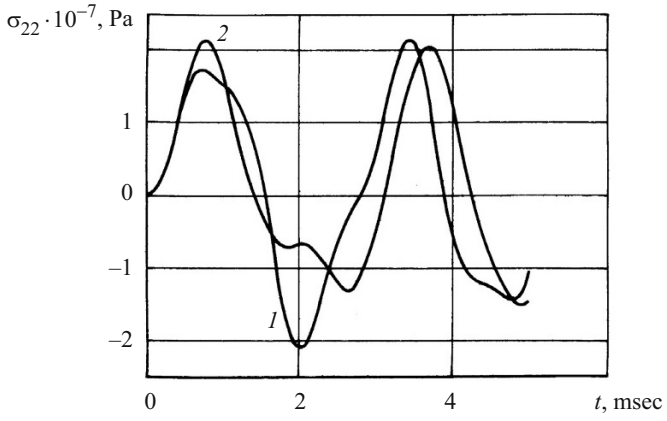

Fig. 4.13

Dependences of u_3 and σ_{22} on the time coordinate in the shell cross-section $s = L/2$ are given in Figs. 4.11 and 4.12. Here curve *1* represents the presence of elastic foundation, curve *2* represents the absence of foundation. Curves *1* and *2* coincide until the time $t = 2T$, after which they diverge in the amplitude and frequency ranges. For comparison, we present the results on the dynamical behavior of a smooth spherical shell of the same configuration (values of σ_{22}) in Fig. 4.13: curve *1* represents the absence of foundation; curve *2* represents the presence of foundation. Here the results are in agreement until $t = 4T$.

A reinforced isotropic conic shell of revolution in a Winkler elastic medium under internal impulsive loading was considered in [30]. The dynamical behavior of a conic shell of variable thickness on elastic foundation was studied in [53].

In considering the theory of conic shells, the system of coordinates (s, θ, z) is used in the equations of vibrations, where the coordinate s ($s = \alpha_1 A_1$) is measured from the left edge of the shell with the radius of the middle surface R_0 (truncated conical shells). The coefficients of the first quadratic form and curvature of the coordinate surface are the following: $A_1 = 1$, $A_2 = R_s$, $k_1 = 0$, $k_2 = \cos\beta / R_s$, where β is the the cone angle; s is the current coordinate; $R_s = R_0 = s \cdot \sin\beta$. We assumed that the shell edges are rigidly fixed in the cross-section $s = s_0$ and $s = s_N$. The initial conditions are zero. The distributed loading (2.13) is applied to the inner surface of the conic shell.

The problem is solved for the following geometrical, physical, and mechanical parameters: $s_0 = 0$, $s_N = 0.4$ m, $R_0 / h = 60$, $E = 7 \cdot 10^{10}$ Pa, $\rho = 2.7 \cdot 10^3$ kg/m^3, $\nu = 0.3$, $A = 10^6$ Pa, $T = 50 \cdot 10^{-6}$ sec. The foundation coefficient $C_1 = 0.25 \cdot 10^8$ N/m^3. The ribs are located at the points $s_j = 0.1Lj$, $j \equiv \overline{1,3}$, $L = s_N - s_0$.

Numerical computations were performed on time interval $t = 20T$. Curves of u_3 and σ_{22} depending on the spatial coordinate s and the cone angle β at instant $t = 4T$ are given in Figs. 4.14 and 4.15. Curve *1* corresponds to $\beta = \pi/6$; curve *2* corresponds to $\beta = \pi/12$. As is seen, the reinforcing elements ($s_j = 0.1Lj$, $j \equiv \overline{1,3}$, $L = s_N - s_0$) have a strong effect on the SSS of the inhomogeneous structure on elastic foundation.

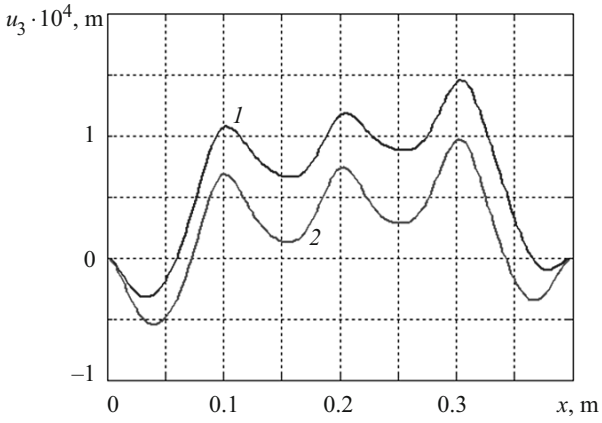

Fig. 4.14

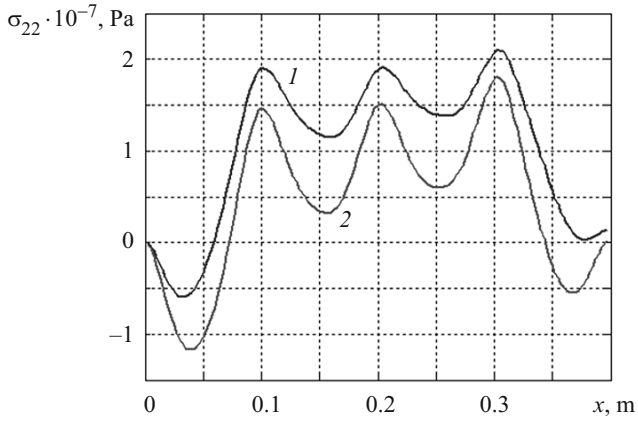

Fig. 4.15

Numerical results on the behavior of the reinforced conic shell with and without elastic foundation were compared. The difference in the values of u_3 and σ_{22} in the amplitude and frequency ranges begin to be significant starting from time $t = 2T$. For a smooth conic shell, this difference begins to be significant at $t = 4T$.

Analysis of the numerical results on the axisymmetric vibrations of discretely stiffened shells of revolution on Winkler and Pasternak foundation under impulsive loading shows that the difference from elastic medium can reach 20–30%, and even 50–70%.

We formulated a problem statement and developed a numerical algorithm for solving dynamical problems for inhomogeneous shell structures on an elastic foundation of bilateral action, which is modeled by three-component water-saturated soil. The tests [38, 39, 65] show that the model [38, 39] quite correctly describes the deformation of multicomponent liquid media. For solving coupled dynamical problems for the shell–soil system, we constructed the appropriate MacCormack finite-difference schemes [70].

4.2. Influence of Soil on Vibrations of Cylindrical Shell. Let us consider the process of deformation of a infinitely long thin cylindrical shell in soil medium under internal impulsive loading [6, 20 – 22, 31].

The motion of soil medium is described by a system of equations for Euler variables [70]:

$$\frac{\partial}{\partial t}(\rho V) + \frac{1}{r}\frac{\partial}{\partial r}\left[r(\rho V^2 + P) - \frac{1}{r}P\right] = 0, \qquad \frac{\partial \rho}{\partial t} + \frac{1}{r}\frac{\partial}{\partial t}[r(\rho V) = 0], \tag{4.10}$$

where r is the spatial variable; t is the time coordinate; V is the velocity; ρ is the density; P is pressure.

We used the equation of state of soil medium according to the model of nonlinear multicomponent liquid medium [38, 39]:

$$\frac{\rho_0}{\rho}\sum_{i=1}^{3}\alpha_i\left[\frac{\gamma(P-P_0)}{\rho_0 C_0^2}+1\right]^{-1/\gamma_i}, \qquad \rho_0 = \sum_{i=1}^{3}\alpha_i\rho_0, \qquad \sum_{i=1}^{3}\alpha_i = 1, \tag{4.11}$$

where index “1” refers to air, index “2” refer to water, and index “3” refer to solid component; α_i is the volume fraction of components; γ_i is the isotropic index in gaseous, liquid, and solid components of the medium; c_{i0} is the sound velocity in the components of medium at atmospheric pressure P_0; ρ_{i0} are the densities of medium components.

The velocity of sound for the pressure P is determined from the condition $c = (dp/d\rho)^{1/2}$ and has the form

$$c = \frac{\displaystyle\sum_{i=1}^{3}\alpha_i\left[\frac{\gamma_i(P-P_0)}{\rho_0 c_{i0}^2}+1\right]^{-1/\gamma_i}}{\left[\rho_0\displaystyle\sum_{i=1}^{3}\frac{\alpha_i}{\rho_0 c_{i0}^2}\left[\frac{\gamma_i(P-P_0)}{\rho_0 c_{i0}^2}+1\right]^{-(1+\gamma_i)/\gamma_i}\right]^{1/2}}. \tag{4.12}$$

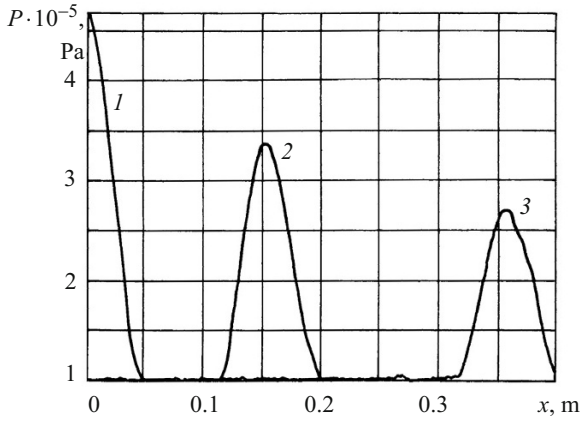

Fig. 4.16

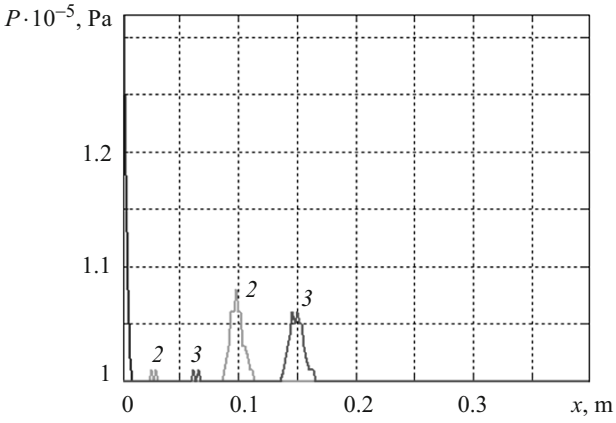

Fig. 4.17

The equation of motion of a thin shell of radius R and thickness h has the form

$$\rho_{sh} h\ddot{u}_3 = \frac{Eh}{1-\nu^2}\frac{u_3}{R^2} + P_3 - P_r(t), \tag{4.13}$$

where $P_3(t)$ is loading on the inner part of the shell; $P_r(t)$ is the soil pressure on the shell; u_3 is the radial displacement of the shell; ρ_{sh}, E, ν are the physical and mechanical parameters of the shell material.

The coupling of the problem is provided by setting the no-flow condition at the deformed interface between the shell and the soil medium:

$$\dot{u}_3 = V_r, \tag{4.14}$$

where V_r is the velocity of the boundary of the soil medium.

Equations (4.13), (4.14) and the conditions of unperturbed motions at infinity are used as boundary conditions for the problem of the dynamics of soil medium.

The algorithm for solving the problem of interaction of a cylindrical shell and soil medium (Eqs. (4.10)–(4.12)) is based on the MacCormack finite-difference scheme [70].

We consider a cylindrical shell in soil medium under internal impulsive loading $P_3(t)$ (Eqs. (4.10)–(4.13)). Computations are performed for steel shell with radius $R = 0.1$ m, thickness $h = 0.01$ m. The elastic modulus of the shell material is $E = 201$ GPa; Poisson's ratio is $\nu = 0.3$; density is $\rho_{sh} = 7880\,\text{kg/m}^3$. Loading $P_3(t)$ is defined by (2.13).

The problem was solved for two types of water-saturated soils. The characteristics of soil components are the following:

1) air $\rho_1 = 1.2$ kg/m^3, $c_1 = 330c_1$ m/sec, $\gamma_1 = 1.4$;

2) water $\rho_2 = 10^3$ kg/m^3, $c_2 = 1500$ m/sec, $\gamma_2 = 7$;

3) solid component $\rho_3 = 2650\,\text{kg/m}^3$, $c_3 = 4500$ m/sec, $\gamma_3 = 4$.

Regularities of propagation of the pressure P wave with respect to spatial coordinate r at different time instants are given in Fig. 4.16 (variant 1 is for soil components $\alpha_1 = 0$, $\alpha_2 = 0.4$, $\alpha_3 = 0.6$). Curves *1*, *2*, *3* correspond to times $t_1 = 0.35\cdot10^{-4}$ sec, $t_2 = 0.125\cdot10^{-3}$ sec, $t_3 = 0.25\cdot10^{-3}$ sec. Similar curves for variant 2 are shown in Fig. 4.17 for $\alpha_1 = 0.01$, $\alpha_2 = 0.39$, $\alpha_3 = 0.6$. As is seen, the gaseous component content α_1 affects considerably the pressure distribution with respect to spatial and time coordinates. The maximum of $P_0(t)$ in variant 1 is three times greater than in variant 2. Air affects considerably the shape of the pressure impulse; smearing of the impulse occurs (curves *2* and *3*). The velocity of propagation of pressure wave changes considerably in comparison with variant 1 (the absence of α_1). Curves *1*, *2*, *3* correspond to times $t_1 = 0.6\cdot10^{-4}$ sec, $t_2 = 0.125\cdot10^{-2}$ sec, $t_3 = 0.188\cdot10^{-2}$ sec. Slower damping of the pressure wave in comparison with variant 1 is also observed.

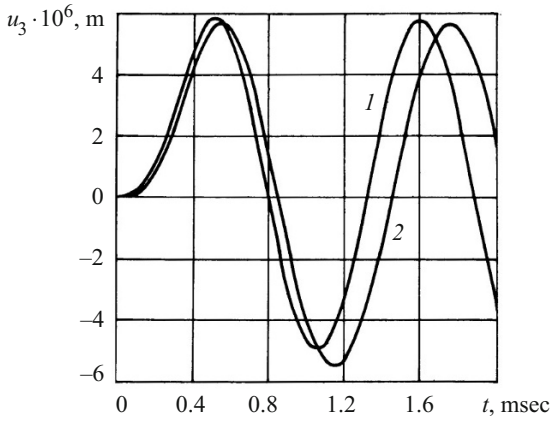

Fig. 4.18

As a particular case of Eqs. (4.13) the an infinite cylindrical shell on Winkler elastic foundation under impulsive interval loading $P_3(t)$ is considered. In this case, the equations of vibrations have the form

$$-T_{22} / R - c_w u_3 + P_3(t) = \rho h \ddot{u}_3 . \tag{4.15}$$

Loading $P_3(t)$ is defined by (2.13).

The objective of performing the computations according to Eqs. (4.15) was the maximal possible equality of the shell deflections u_3 with the computations according to Eqs. (4.13). Starting from the similarity of Eqs. (4.13) and (4.15), it is possible to derive a formula for the Winkler coefficients c_w in the case of specific type of vibrations of the shell–medium system:

$$c_w = \max P_0 / u_3(t^*), \tag{4.16}$$

where $P_0(t)$, $u_3(t)$ are determined by solving problem (4.13)–(4.15); t^* is the time of achievement of $\max P_0(t)$. Since it is impossible to achieve complete coincidence of the results by two models, we use, as a validity criterion, the maximal possible coincidence of the values of u_3 during the first period of vibrations (Fig. 4.18).

Similar investigations were perfumed for a spherical shell on Winkler elastic foundation and the coupled problem for nonlinear soil medium and spherical shell [6, 21, 23]. Such structures of equations for spherical shells on elastic foundation and in soil medium allow estimating the coefficient c_w of Winkler elastic foundation by formula (4.16). It follows from data of the conducted computations that the effect of the elastic foundation on the shell SSS begins to be significant after the stress σ_{22} achieves the maximal value.

The problem statement is presented in [20] and the equations of forced vibrations of longitudinal-transverse reinforced cylindrical shells in soil medium within the framework of the Timoshenko structural-orthotropic model under non-stationary loading are obtained in [137]. An infinite axisymmetrical cylindrical shell reinforced by ribs whose directions coincide with the lines of principal curvatures of its middle surface is considered. For the smooth shell, the following distribution of displacements across the thickness is used: $u_1^z(x, z) = u_1(x) + z\varphi_1(x)$, $u_3^z(x, z) = u_3(x)$.

The SSS of a rib directed along the axis x can be described by the vector of displacements of the gravity center of the transverse cross-section $\overline{U}_{pi} = (u_{1pi}, u_{3pi}, \varphi_{1pi})$. For a rib directed along the axis y, we have $\overline{U}_{pj} = (u_{1pj}, u_{3pj}, \varphi_{1pj})$.

Using the shell–rib interface conditions [20] and the Hamilton–Ostrogradsky variational principle of stationarity [6, 33] (after standard transformations in the variational functional), we obtained the equations of vibrations of a structurally orthotropic cylindrical shell [20]:

$$\rho_{sh} h \left(1 + \frac{F_1}{l_1 h} + \frac{F_2}{l_2 h} \right) \ddot{u}_3 = -\left(\frac{Eh}{1-\nu^2} + \frac{EF_2}{l_2} \right) \frac{u_3}{R^2} + P_3(t) - P_r(t). \tag{4.17}$$

Consider the deformation of an infinitely long stiffened cylindrical shell in soil medium under internal impulsive loading. We describe the motion of the soil medium by the system of equations for Euler variables (4.10). The equation of state of

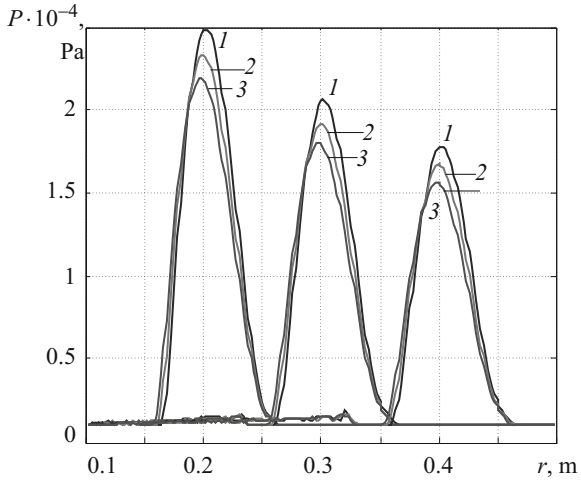

Fig. 4.19

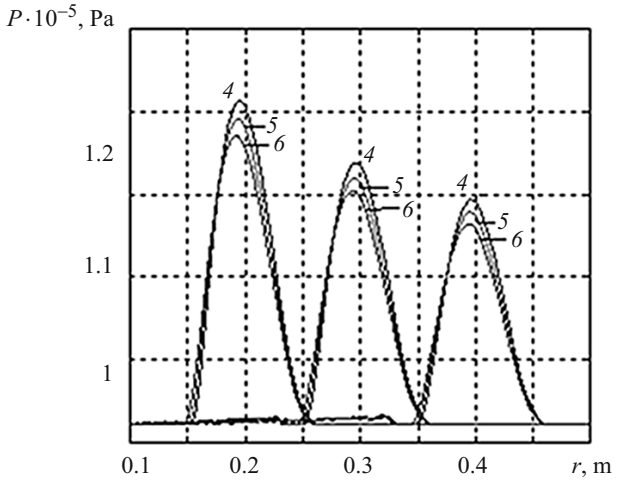

Fig. 4.20

the soil medium follows from the model of nonlinear multicomponent liquid medium (4.11). The sound velocity for the pressure P_1 is determined from the condition $c = (dp/d\rho)^{1/2}$ and it has the form (4.12). As a particular case, we obtain an equation of vibrations of a structurally orthotropic shell with regular longitudinal reinforcement:

$$\rho_{sh} h\left(1+\frac{F_1}{l_1 h}\right)\ddot{u}_3 = -\frac{Eh}{1-\nu^2}\frac{u_3}{R^2} + P_3(t) - P_r(t). \tag{4.18}$$

In Eqs. (4.17), (4.18), $P_3(t)$ is the loading on the internal part of the shell; $P_r(t)$ is the soil pressure onto the shell; u_3 is the radial displacement of the shell; ρ_{sh}, E, ν are physical and mechanical parameters of the material of the shell and ribs (in the case of isotropic material for shell and ribs).

The coupling of the problem is provided by the no-flow condition (4.14) at the interface between the shell and the soil medium. Equations (4.17), (4.18) (4.14) and the conditions of unperturbed motion at infinity are used as the boundary conditions for the problem of the dynamics of soil medium.

The algorithm for solving the problem on the interaction of a cylindrical shell with soil medium is based on the MacCormack finite-difference scheme [70].

We consider an infinitely long longitudinally reinforced cylindrical shell in soil medium under internal impulsive loading (4.10). Computations were performed for a steel shell of radius $R = 0.1$ m; thickness $h = 0.01$ m. The modulus of elasticity of the shell material is $E = 210$ GPa, Poisson's ratio is $\nu = 0.3$; density is $\rho_{sh} = 7880$ kg/m^3.

For the soil medium, the following characteristics of the component were used:

1) for air $\rho_1 = 1.2$ kg/m^3, $c_1 = 330$ m/sec, $\gamma_1 = 1.4$;

2) for water $\rho_2 = 10^3$ kg/m^3, $c_2 = 1500$ m/sec, $\gamma_2 = 7$;

3) for the solid component $\rho_3 = 2650$ kg/m^3, $c_3 = 4500$ m/sec, $\gamma_3 = 4$.

According to the equations of vibrations of a stiffened shell within the framework of the structurally orthotropic model, it is seen that the effect of longitudinal reinforcements manifests only in the inertial term. Therefore, we analyze wave processes starting from the reduced mass of the reinforced shell $m = \rho_{sh} h[1 + F_1/(l_1 h)]$. We will characterize the process using the ratio m/m_0, where $m_0 = \rho_{sh} h$.

Regularities of propagation of the pressure P wave with respect to the spatial coordinate r for different time instants for $\alpha_1 = 0, \alpha_2 = 0.3, \alpha_3 = 0.7$ (depending on the value of m/m_0) are shown in Fig. 4.19. Curves *1–3* correspond to $m/m_0 = 1$, 1.2, 1.4, respectively, at the times of passing the distances $r = 2r_0$, $r = 3r_0$, $r = 4r_0$. Similar dependences for $m/m_0 = 1.6$, 1.8, 2 are given in Fig. 4.20 (curves *4–6*).

As is seen from Fig. 4.19, values of the pressure for $m/m_0 = 1$ differ by more than 10% from those for $m/m_0 = 1.4$. The situation is similar in Fig. 4.20.

4.3. Dynamics of a Spherical Shell in Soil Medium. Consider a closed spherical shell in infinite soil medium [6, 21, 23]. The propagation of spherical waves in the medium is described by the following system of equations for Euler variables [70]:

$$\frac{\partial}{\partial t}(\rho U)+\frac{1}{r^2}\frac{\partial}{\partial r}\left[r^2(\rho U^2+P)\right]-\frac{2}{r}P=0,$$

$$\frac{\partial \rho}{\partial t}+\frac{1}{r^2}\frac{\partial}{\partial r}\left[r^2(\rho U)\right]=0. \tag{4.19}$$

In Eqs. (4.19), r is the spatial variable; t is the time coordinate; U is velocity; ρ is density; P is pressure.

The equations of state of the soil medium follow from the model of nonlinear multicomponent liquid medium [38, 39, formulas (4.11)].

The equations of vibrations of a thin spherical shell of radius R and thickness h have the form

$$\rho_{sh} h\ddot{u}_3 = -\frac{T_{11}}{R}-\frac{T_{22}}{R}+P_3(t)-P_r(t),$$

$$T_{11}=\frac{Eh\nu}{1-\nu^2}\frac{u_3}{R^2}, \qquad T_{22}=\frac{Eh}{1-\nu^2}\frac{u_3}{R^2}, \tag{4.20}$$

where $P_3(t)$ is the loading on the inner surface of the cylindrical shell; $P_r(t)$ is the soil pressure on the shell; u_3 is the radial displacement of the shell; ρ_{sh}, E, ν are physical and mechanical parameters of the shell material.

The coupling of the problem for the shell–soil system is provided by the no-flow conditions at the deformed interface between the shell and soil medium:

$$\dot{u}_3 = U_r, \tag{4.21}$$

where U_r is the velocity of the boundary of the soil medium.

We use Eqs. (4.20), (4.21) and the conditions of the absence of perturbations of displacements at infinity as the boundary conditions for the problem of the dynamics of soil medium.

The algorithm for solving the problem of interaction of the spherical shell with soil medium (Eqs. (4.19) – (4.21)) is based on the MacCormack finite-difference scheme [70].

At the predictor step, the difference equations have the form

$$\tilde{\rho}_k = \rho_k^n - \frac{\tau}{r_k^2}\left[\frac{(r^2\rho^n V^n)_{k+1}-(r^2\rho^n V^n)_k}{\Delta r}\right],$$

$$(\tilde{\rho}\tilde{V})_k = (\rho^n V^n)_k - \frac{\tau}{r_k^2}\left\{\frac{[r^2\rho(V^2+P)^n]_{k+1}-[r^2(\rho V^2+P)^n]}{\Delta r}-2P_k^n r_k\right\}$$

$$F(\tilde{P}_k,\tilde{\rho}_k)=0. \tag{4.22}$$

At the corrector step, the equations are written as

$$\rho_k^{n+1} = 0.5\left\{\rho_k^n+\tilde{\rho}_k-\frac{\tau}{r_k^2}\left[\frac{(r^2\tilde{\rho}\tilde{V})_k-(r^2\tilde{\rho}\tilde{V})_{k-1}]}{\Delta r}\right]\right\},$$

$$(\rho V)_k^{n+1} = 0.5\left\{(\rho^n V^n)_k+(\tilde{\rho}^n\tilde{V}^n)_k-\frac{\tau}{r_k^2}\left[\frac{[r^2(\tilde{\rho}\tilde{V}^2+\tilde{P})^n]_k-[r^2(\tilde{\rho}\tilde{V}^2+\tilde{P})^n]_{k-1}}{\Delta r}-2\tilde{P}_k r_k\right]\right\},$$

$$F(P_k^{n+1}, \rho_k^{n+1}) = 0. \tag{4.23}$$

To determine the desired quantities at the interface between the spherical shell and the soil medium, we use the following procedure. Represent the equations of vibrations of the shell (4.20) as

$$\frac{\partial V_0}{\partial t} = H, \qquad H = \frac{1}{\rho_{sh}}\left[-\frac{\sigma_{11}}{R} - \frac{\sigma_{22}}{R} + \frac{P_3(t) - P_0}{h}\right]. \tag{4.24}$$

At the predictor step, we approximate Eqs. (4.21) by the following relations: $\widetilde{V}_0 = V_0^n + \tau H_0(t^n)$, where $H_0(t^n) = \dfrac{1}{\rho_{sh}}\left[-\dfrac{\sigma_{11}^n}{R} - \dfrac{\sigma_{22}^n}{R} + \dfrac{P_3(t^n) - P_0^n}{h}\right]$.

The values of $\widetilde{\rho}_0, \widetilde{P}_0$ are determined by the formulas

$$\widetilde{\rho}_0 = \rho_0^n - \frac{\tau}{r_0^2}\left[\frac{-3r_0^2(\rho_0^n V_0^n) + 4r_1^2(\rho_1^n V_1^n) - r_2^2(\rho_2^n V_2^n)}{2\Delta r}\right],$$

$$F(\widetilde{P}_0, \widetilde{\rho}_0) = 0. \tag{4.25}$$

At the corrector step, Eqs. (4.20) are approximated by the finite-difference relations

$$V_0^{n+1} = 0.5[V_0^n + \widetilde{V}_0 + \tau H_1(t^{n+1})],$$

$$H_1(t^{n+1}) = \frac{1}{\rho_{sh}}\left[-\frac{\sigma_{11}^{n+1}}{R} - \frac{\sigma_{22}^{n+1}}{R} + \frac{P_3(t^{n+1}) - \widetilde{P}_0}{h}\right]. \tag{4.26}$$

The values of ρ_0^{n+1} and P_0^{n+1} are determined by the following formulas:

$$\rho_0^{n+1} = 0.5\left\{\rho_0^n + \widetilde{\rho}_0 - \frac{\tau}{r_0^2}\left[\frac{-3r_0^2(\widetilde{\rho}_0\widetilde{V}_0) + 4r_1^2(\widetilde{\rho}_1\widetilde{V}_1) - r_2^2(\widetilde{\rho}_2\widetilde{V}_2)}{2\Delta r}\right]\right\},$$

$$F(P_0^{n+1}, \rho_0^{n+1}) = 0.$$

The function $F(P, \rho)$ in (4.22) – (4.26) has the form

$$F(P, \rho) = \sum_{i=1}^{3} \alpha_i \left[\frac{\gamma_i(P - P_0)}{\rho_{i0} c_{i0}^2} + 1\right]^{-1/\gamma_i} - \frac{\rho_0}{\rho}. \tag{4.27}$$

To determine the pressure P from given values of density ρ we use the Newton–Raphson iteration procedure. Since the MacCormack difference scheme (4.22), (4.23) is explicit, we use the stability condition $(|V| + c)\tau / \Delta r < 1$, where c is the local sound velocity in the soil medium.

Numerical Results. Consider a closed spherical shell in soil medium under internal impulsive loading $P_3(t)$ (2.13). The difference equations (4.22)–(4.26) correspond to Eqs. (4.19) – (4.21). Computations were performed for a steel shell of radius $R = 0.1$ m, thickness $h = 0.01$ m. The elasticity modulus for the shell material is $E = 210$ GPa, Poisson's ratio is $\nu = 0.3$; density $\rho_{sh} = 7880\ \text{kg/m}^3$.

The problem was solved for three types of water-saturated soils. The characteristics of soil components are the following:

1) air $\rho_1 = 1.2\ \text{kg/m}^3$, $c_1 = 330$ m/sec, $\gamma_1 = 1.4$;

2) water $\rho_2 = 10^3\ \text{kg/m}^3$, $c_2 = 1500$ m/sec, $\gamma_2 = 7$;

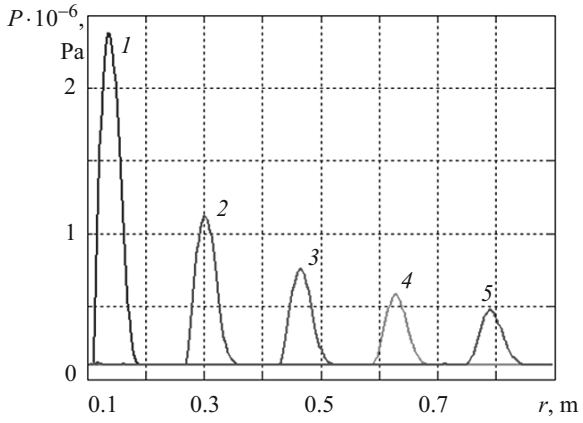

Fig. 4.21

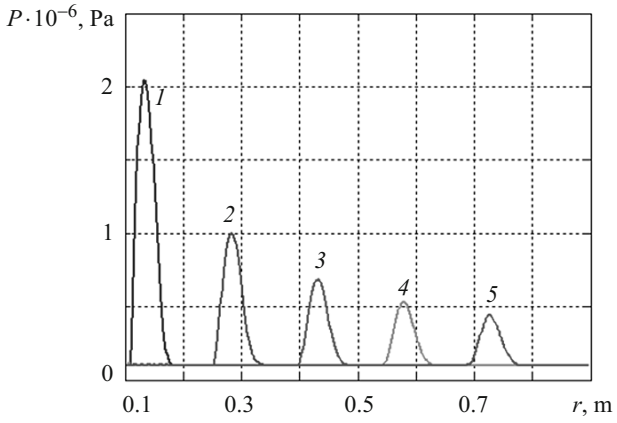

Fig. 4.22

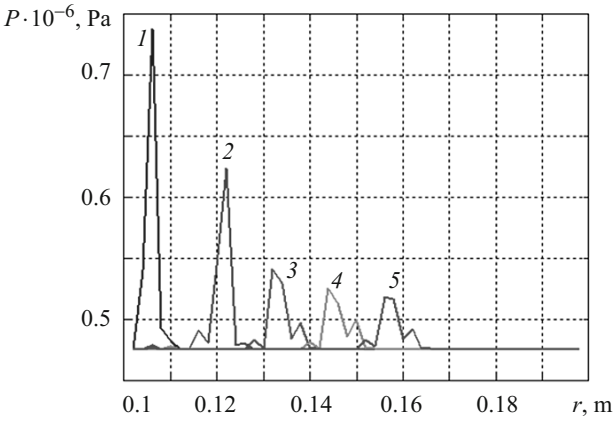

Fig. 4.23

3) solid component $\rho_3 = 2650\,\text{kg/m}^3$, $c_3 = 4500$ m/sec, $\gamma_3 = 4$.

The regularities of propagation of the pressure wave P by the spatial coordinate r at different instants are presented in Fig. 4.21 (variant 1 corresponds to the following components of soil $\alpha_1 = 0$, $\alpha_2 = 0.4$, $\alpha_3 = 0.6$). Curves *1–5* correspond to $t_1 = T$, $t_2 = 3T$, $t_3 = 5T$, $t_4 = 7T$, $t_5 = 9T$.

Similar dependences are presented in Fig. 4.22 for variant 2 ($\alpha_1 = 0$, $\alpha_2 = 0.6$, $\alpha_3 = 0.4$). As is seen, the velocity of the pressure wave P in variant 1 ($\alpha_3 = 0.6$) is higher than in with variant 2 ($\alpha_3 = 0.4$). At $t = 9T$, the pressure wave P reaches the distance $r = 8R$ in the first variant of soil and the distance $r \approx 7.4R$ in the second variant. The amplitudes of the pressure waves P differ too. In case 1, the amplitude of the pressure wave P at instant $t = T$ is $P \approx 2.4$ MPa. In case 2 ($\alpha_3 = 0.4$, medium is less rigid than in variant 1) the pressure wave P at instant $t = T$ is $P \approx 2.0$ MPa. The amplitudes of the pressure wave at other instants differ too.

The dependences of pressure waves P along the coordinate r are given for the third variant of soil ($\alpha_1 = 0.01$, $\alpha_2 = 0.39$, $\alpha_3 = 0.6$) in Fig. 4.23. As is seen, the content of gaseous component α_1 influences considerably the distribution of pressure with respect to spatial and time coordinates. The maximum of $P_0(t)$ for $r = R$ (at the interface between the spherical shell and the soil medium) more than three times lower than in variants 1 and 2. Air affects considerably the shape and magnitude of the pressure wave P, the shape of impulse pressure broadens. The velocity of the pressure wave P also changes considerably in comparison with variants 1 and 2 (for $\alpha_1 = 0$). At time $t = 9T$ the pressure wave passes the distance $r \approx 1.55R$ (unlike variant 1 where $r = 8R$).

4.4. Cylindrical Shell in Two-Layer Soil Medium. Consider a stiffened infinite cylindrical shell in two-layer soil medium [54]. We assume that the distributed impulsive loading $P_3(t)$ is applied to the inner surface of the stiffened cylindrical shell for $r = r_0$ (Fig. 4.24).

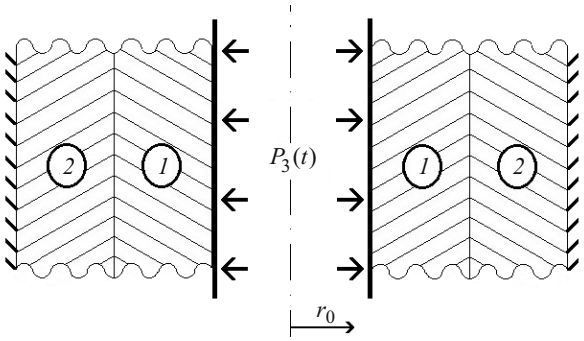

Fig. 4.24

The motion equations of the stiffened thin cylindrical shell of radius R and thickness h have the form (4.13). To describe the behavior of the layers of soil medium, we use the model of nonlinear multi-component liquid medium according to (4.11) [38, 39].

The motion of the two-layer soil medium in the case of propagation of cylindrical waves is described by the system of equations for Euler coordinates [70] (4.10). The motion equations of soil medium (4.10) are supplemented by the equation of state (4.11). The coupling of the problem is provided by the no-flow condition at the deformed interface between the shell and the soil medium (4.14).

We use Eqs. (4.13), (4.14) for $r = r_0$ and the conditions of non-perturbed motion at infinity as the boundary conditions for the problem of the dynamics of soil medium. On the boundary of contacts of soils with different densities, we set the conditions of continuity of velocity.

The algorithm for solving the problem of propagation of cylindrical waves in two-layer soil medium is based on the MacCormack finite-difference scheme [70].

At the predictor step, the difference equations have the following form:

$$\widetilde{\rho}_k = \rho_k^n - \frac{\tau}{r_k}\left[\frac{(r\rho^n V^n)_{k+1} - (r\rho^n V^n)_k}{\Delta r}\right],$$

$$(\widetilde{\rho}\widetilde{V})_k = (\rho^n V^n)_k - \frac{\tau}{r_k}\left\{\frac{[r(\rho V^2 + P)^n]_{k+1} - [r(\rho V^2 + P)^n]_k}{\Delta r} - P_k^n\right\},$$

$$F(\widetilde{P}_k, \widetilde{\rho}_k) = 0. \tag{4.28}$$

At the corrector step, we write the equations as

$$\rho_k^{n+1} = 0.5\left\{\rho_k^n + \widetilde{\rho}_k - \frac{\tau}{r_k}\left[\frac{(r\widetilde{\rho}\widetilde{V})_k - (r\widetilde{\rho}\widetilde{V})_{k-1}}{\Delta r}\right]\right\},$$

$$(\rho V)_k^{n+1} = 0.5\left\{(\rho^n V^n)_k + (\widetilde{\rho}\widetilde{V})_k - \frac{\tau}{r_k}\left[\frac{[r(\widetilde{\rho}\widetilde{V}^2 + \widetilde{P})]_k - [r(\widetilde{\rho}\widetilde{V}^2 + \widetilde{P})]_{k-1}}{\Delta r} - \widetilde{P}_k\right]\right\},$$

$$F(P_k^{n+1}, \rho_k^{n+1}) = 0. \tag{4.29}$$

To determine the pressure P (from the given density ρ in the equation of state of soil medium), we use the Newton–Raphson iteration procedure. Since the MacCormack difference scheme (4.28), (4.29) is explicit, we use the stability condition $(|V| + c)\tau / \Delta r < 1$, where c is the local sound velocity (4.12).

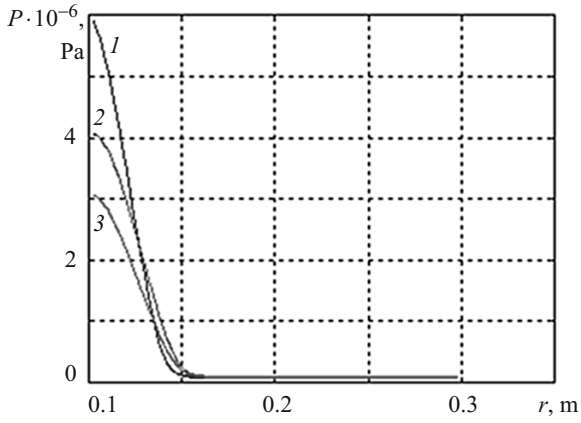

Fig. 4.25

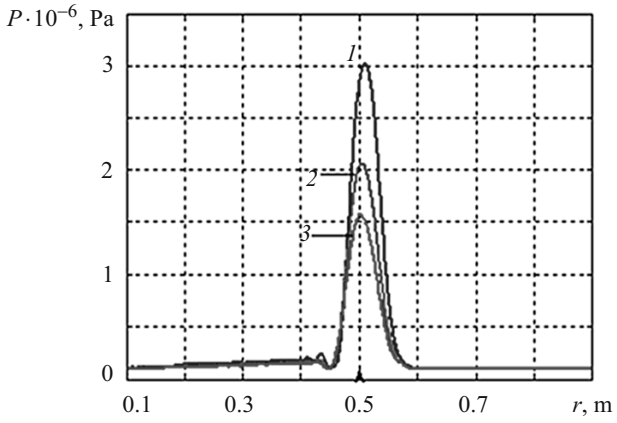

Fig. 4.26

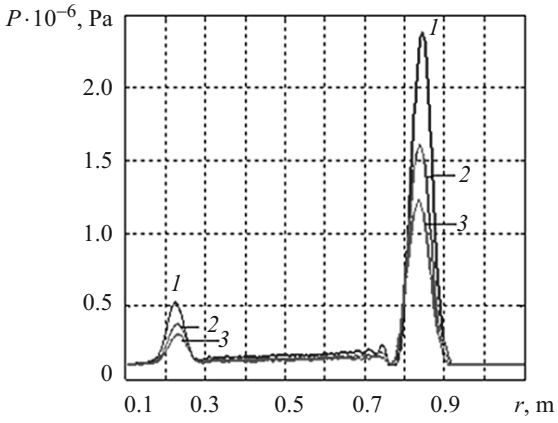

Fig. 4.27

It was assumed that the stiffened cylindrical shell has the following parameters: radius $R = 0.1$ m; the modulus of elasticity $E = 210$ GPa; Poisson's ratio $\nu = 0.3$; density $\rho = 7.88\cdot10^3$ kg/m^3. The shell thickness h was varied. Three cases were considered: $h/R = 0.05$, $h/R = 0.1$, $h/R = 0.15$. The loading $P_3(t)$ (2.13) applied to the inner surface of the shell is given for $r = r_0$.

The first layer $r_0 \le r \le 5r_0$ is characterized by the parameters $\alpha_1 = 0$, $\alpha_2 = 0.7$, $\alpha_3 = 0.3$. The second layer $5r_0 \le r \le \infty$ by the parameters $\alpha_1 = 0$, $\alpha_2 = 0.3$, $\alpha_3 = 0.7$. In both cases, in the equation of state of soil medium we set $\rho_2 = 10^3$ kg/m^3, $\rho_3 = 2650$ kg/m^3, $\gamma_2 = 7$, $\gamma_3 = 4$.

The dependences of the pressure wave P on the spatial coordinate r at certain instants are presented in Fig. 4.25. Curve *1* corresponds to $h/R = 0.05$ for $t = 0.625T$. Curves *2* and *3* correspond to $h/R = 0.1$ and $h/R = 0.15$ for $t = 0.75T$. The dependences of the wave pressure P at the instant $t = 6.25T$ of reaching the interface $r = 5r_0$ are shown in Fig. 4.26. As the pressure wave passes the interface (from less dense medium to more dense medium), a reflected wave occurs.

The main pressure wave in the three cases of the ratio h/R is presented on the right-hand side of Fig. 4.27. The reflected pressure wave, moving towards the plane, is shown on the left-hand side of Fig. 4.27. Figure 4.27 corresponds to time $t = 10T$. After reaching the reinforced edge, the reflected wave is damped. The effect of reflection from the shell is not observed. This is attributed to the specific features of the computational mathematical model. The notation in Figs. 4.26 and 4.27 is similar to that in Fig. 4.25.

4.5. Wave Processes in Soil Medium of Periodic Structure. Consider an infinite cylindrical cavity in soil medium of periodic structure [42]. Assume that distributed impulsive loading $P_3(r_0, t)$ is applied to the inner surface of the cavity for $r = r_0$ (Fig. 4.28).

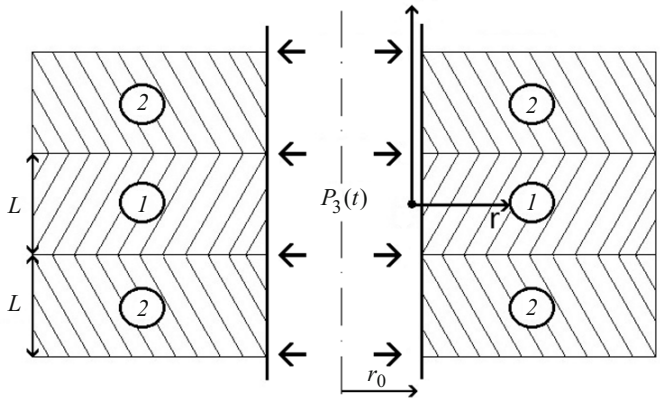

Fig. 4.28

Let us use the model of nonlinear multicomponent liquid medium according to formula (4.11) to describe the behavior of the layers of the soil medium. The motion of the soil medium of periodic structure in the case of propagation of cylindrical waves is described by the system of equations for Euler coordinates [70]:

$$\frac{\partial}{\partial t}(\rho u)+\frac{\partial}{\partial x}(\rho u^2+P)+\frac{1}{r}\frac{\partial}{\partial r}(r\rho uv)=0,$$

$$\frac{\partial}{\partial t}(\rho v)+\frac{\partial}{\partial x}(\rho uv)+\frac{1}{r}\frac{\partial}{\partial r}[r(\rho v^2+P)]-\frac{P}{r}=0,$$

$$\frac{\partial \rho}{\partial t}+\frac{\partial}{\partial x}(\rho u)+\frac{1}{r}\frac{\partial}{\partial r}(r\rho v)=0. \tag{4.30}$$

The system of equations (4.30) has the following vector form:

$$\frac{\partial \overline{F}}{\partial t}+\frac{\partial \overline{A}}{\partial x}+\frac{1}{r}\frac{\partial}{\partial r}(r\overline{B})+\frac{\overline{C}_0}{r}=0, \tag{4.31}$$

$$\overline{F}=\begin{pmatrix}\rho u\\ \rho v\\ \rho\end{pmatrix},\quad \overline{A}=\begin{pmatrix}\rho u^2+P\\ \rho uv\\ \rho u\end{pmatrix},\quad \overline{B}=\begin{pmatrix}\rho uv\\ \rho v^2+P\\ \rho v\end{pmatrix},\quad \overline{C}_0=\begin{pmatrix}0\\ -P\\ 0\end{pmatrix}, \tag{4.32}$$

where u is the velocity of displacement of medium particles along the axis x; v is the velocity of displacements of particles along the axis r; ρ is the density of the corresponding soil layer; P is the pressure of the corresponding point of the soil medium (x, r).

The motion equations of soil medium (4.30) – (4.32) are supplemented by the equation of state (4.11). We use Eqs. (4.30) for $r=r_0$ and the conditions of non-perturbed motion at infinity as the boundary conditions for the problem of the dynamics of soil medium of periodic structure. We set the conditions of continuity of velocities at the interface between soils with different densities.

The algorithm for solving the problem of the propagation of cylindrical waves in soil medium of periodic structure (Eqs. (4.31)–(4.33)) is based on the MacCormack finite-difference scheme [70].

At the predictor step, the difference equations have the form

$$\tilde{\overline{F}}_1=\overline{F}^n_{k,l}-\Delta t\left[\frac{\overline{A}_{k,l}-\overline{A}_{k,l-1}}{\Delta x}+\frac{\overline{B}_{k,l}-\overline{B}_{k,l-1}}{\Delta r}+\overline{C}_{k,l}\right]^n. \tag{4.33}$$

At the corrector step, the difference equations have the form

$$\overline{F}_{k,l}^{n+1} = 0.5\left\{ \overline{F}_{k,l}^{n} - \overline{\overline{F}}_{k,l} - \Delta t\left[\frac{\widetilde{A}_{k,l+1} - \widetilde{A}_{k,l}}{\Delta x} + \frac{\widetilde{B}_{k+1,l} - \widetilde{B}_{k,l}}{\Delta r} + \widetilde{C}_{k,l} \right] \right\}. \tag{4.34}$$

In scalar form Eqs. (4.33), (4.34) are written as

– at the predictor step

$$(\widetilde{\rho u})_{k,l} = (\rho u)_{k,l}^{n} - \Delta t\left[\frac{(\rho u^2 + P)_{k,l}^{n} - (\rho u^2 + P)_{k,l-1}^{n}}{\Delta x} + \frac{1}{r_k}\frac{(r\rho uv)_{k,l}^{n} - (r\rho uv)_{k-1,l}^{n}}{\Delta r} \right],$$

$$(\widetilde{\rho v})_{k,l} = (\rho v)_{k,l}^{n} - \Delta t\left[\frac{(\rho uv)_{k,l}^{n} - (\rho uv)_{k,l-1}^{n}}{\Delta x} + \frac{1}{r_k}\frac{[r(\rho v^2 + P)]_{k,l}^{n} - [r(\rho v^2 + P)]_{k,l-1}^{n}}{\Delta r} - \frac{P_{k,l}^{n}}{r_k} \right],$$

$$\widetilde{\rho}_{k,l} = \rho_{k,l}^{n} - \Delta t\left[\frac{(\rho u)_{k,l}^{n} - (\rho u)_{k,l-1}^{n}}{\Delta x} + \frac{1}{r_k}\frac{(r\rho v)_{k,l}^{n} - (r\rho v)_{k-1,l}^{n}}{\Delta r} \right],$$

$$\widetilde{p}_{k,l} = F(P_{k,l}^{n}, \widetilde{\rho}_{k,l}), \tag{4.35}$$

– at the corrector step

$$(\rho u)_{k,l}^{n+1} = 0.5\left\{ (\rho u)_{k,l}^{n+1} + (\widetilde{\rho u})_{k,l} - \Delta t\left[\frac{(\widetilde{\rho u}^2 + \widetilde{p})_{k,l+1} - (\widetilde{\rho u}^2 + \widetilde{p})_{k,l}}{\Delta x} + \frac{1}{r_k}\frac{(r\widetilde{\rho u v})_{k+1,l} - (r\widetilde{\rho u v})_{k,l}}{\Delta r} \right] \right\},$$

$$(\rho v)_{k,l}^{n+1} = 0.5\left\{ (\rho v)_{k,l}^{n} + (\widetilde{\rho v})_{k,l}^{n} - \Delta t\left[\frac{(\widetilde{\rho u v})_{k,l+1} - (\widetilde{\rho u v})_{k,l}}{\Delta x} + \frac{1}{r_k}\frac{[r(\widetilde{\rho v}^2 + \widetilde{P})]_{k+1,l} - [r(\widetilde{\rho v}^2 + \widetilde{P})_{k,l}}{\Delta r} - \frac{\widetilde{P}_{k,l}}{r_k} \right] \right\},$$

$$\rho_{k,l}^{n+1} = 0.5\left\{ \rho_{k,l}^{n} + \widetilde{\rho}_{k,l} - \Delta t\left[\frac{(\widetilde{\rho u})_{k,l+1} - (\widetilde{\rho u})_{k,l}}{\Delta x} + \frac{1}{r_k}\frac{(r\widetilde{\rho v})_{k+1,l} - (r\widetilde{\rho v})_{k,l}}{\Delta r} \right] \right\},$$

$$\widetilde{P}_{k,l}^{n+1} = F(P_{k,l}^{n}, \widetilde{\rho}_{k,l}^{n+1}). \tag{4.36}$$

To determine the pressure value P from the given values of density ρ, we use the Newton–Raphson iteration procedure in Eq. (4.11). Since the MacCormack difference scheme (4.33), (4.35) is explicit, we use the stability condition

$$\max((|u| + c)\tau / \Delta x, (|v| + c)\tau / \Delta r) < 1,$$

where c is the local velocity of sound in soil medium (4.12).

Numerical Results. Consider the problem of propagation of cylindrical waves in soil medium of periodic structure (Fig. 4.28). We assume that the loading $P_3(r_0, t)$(2.13) is applied to the surface of cylindrical cavity for $r = r_0$. We set $r_0 = 0.1$ m, $L / r_0 = 4$. The results of numerical computations of the dependence of pressure waves P on the distance r from the edge of the cylindrical cavity for $r = r_0$ are given in Figs. 4.29 and 4.30. Four groups of dependences of the pressure waves for different times are shown (*A* corresponds to *T*; *B* corresponds to 3.5*T*; *C* corresponds to 6.5*T*; *D* corresponds to 9.5*T*). The dependences of the pressure P on the coordinate r for variant 1 for $x = L / 2$ according to Fig. 4.28 ($\alpha_1 = 0$, $\alpha_2 = 0.3$, $\alpha_3 = 0.7$) are presented in Fig. 4.29. Curves *1* correspond to this variant of soil. Curves *2* correspond to the pressure P in the soil layer 2 for $x = L / 2$ according to Fig. 4.28 ($\alpha_1 = 0$, $\alpha_2 = 0.7$, $\alpha_3 = 0.3$). Curves *3* correspond to the pressure at the interface of media (Fig. 4.28).

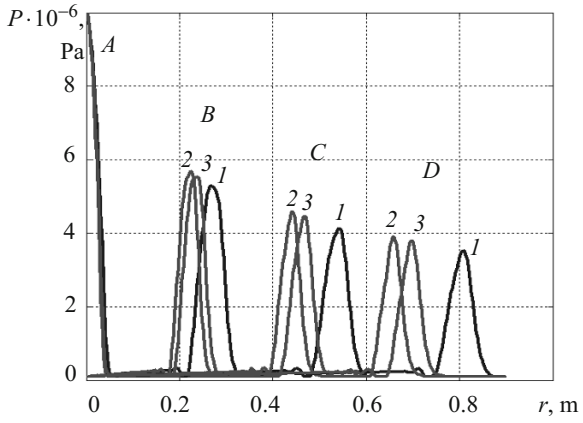

Fig. 4.29

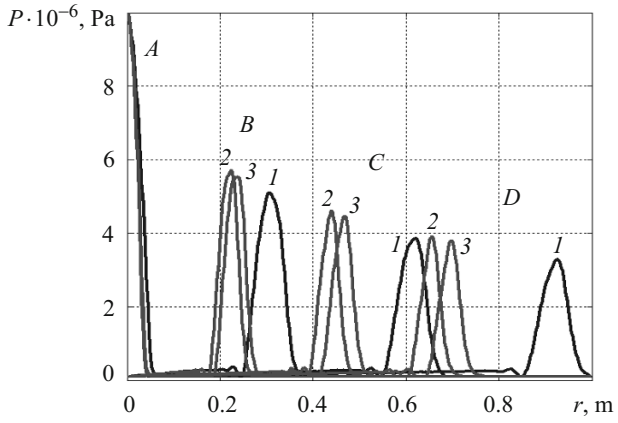

Fig. 4.30

Similar results for soil with the following parameters are presented in Fig. 4.30: for the first layer $\alpha_1 = 0, \alpha_2 = 0.2, \alpha_3 = 0.8$ (curve *1*); for the second layer $\alpha_1 = 0, \alpha_2 = 0.8, \alpha_3 = 0.2$ (curves *2*); curves *3* correspond to the pressure at the interface. In both cases, $\rho_2 = 10^3$ kg/m^3, $\rho_3 = 2650$ kg/m^3, $\gamma_2 = 7, \gamma_3 = 4$.

As follows from Figs. 4.29 and 4.30 for $\alpha_1 = 0, \alpha_2 = 0.3, \alpha_3 = 0.7$ and $\alpha_1 = 0, \alpha_2 = 0.2, \alpha_3 = 0.8$, the velocity of the pressure wave considerably exceed the velocities of the pressure waves for other parameters of soil medium. The velocity of the pressure wave *P* at the interface between media *1* and *2* (Fig. 4.28) is closer to the velocity of the pressure wave in soil with lower density (curves *3* in Figs. 4.29 and 4.30). Considerable damping of the pressure waves in space (*r*) and time (*t*) is observed in layers of medium and at the interface.

4.6. Wave Processes in Cylindrical Shell–Soil Medium System of Periodic Structure. Let us consider a stiffened infinite cylindrical cavity in soil medium of periodic structure [29, 41]. Assume that distributed impulsive loading $P_3(r_0, t)$ is applied to the internal surface for $r = r_0$ of the shell (Fig. 4.31).

Let us solve the problem of dynamical interaction of the cylindrical shell with soil medium of periodic structure under internal distributed non-stationary loading. We represent the equations of vibrations of the cylindrical shell (on which the soil medium acts) according to the model of shells with the Timoshenko hypotheses [41]:

$$\frac{\partial T_{11}}{\partial x} = \rho h \frac{\partial^2 u_1}{\partial t^2}, \qquad \frac{\partial M_{11}}{\partial x} - T_{13} = \rho \frac{h^3}{12} \frac{\partial^2 \varphi_1}{\partial t^2},$$

$$\frac{\partial T_{13}}{\partial x} - \frac{T_{22}}{R} + P_3(x, t) - P_r(x, r_0, t) = \rho h \frac{\partial^2 u_3}{\partial t^2}. \tag{4.37}$$

In Eqs. (4.37), u_1, u_3, φ_1 are the components of the generalized vector of displacements of the middle surface of the cylindrical shell; $T_{11}, T_{22}, T_{13}, M_{11}$ are the integral (over the thickness) forces andmoments of the cylindrical shell; $P_3(x, t)$ is the loading on the inner surface of the cylindrical shell; $P_r(x, r_0, t)$ is the soil pressure on the shell.

The motion of the medium of periodic structure in the case of cylindrical symmetry is described by the system of equations for Euler coordinates [70]:

$$\frac{\partial}{\partial t}(\rho u) + \frac{\partial}{\partial x}(\rho u^2 + P) + \frac{1}{r}\frac{\partial}{\partial r}(r\rho uv) = 0,$$

$$\frac{\partial}{\partial t}(\rho v) + \frac{\partial}{\partial x}(\rho uv) + \frac{1}{r}\frac{\partial}{\partial r}[r(\rho v^2 + P)] - \frac{P}{r} = 0,$$

$$\frac{\partial \rho}{\partial t} + \frac{\partial}{\partial x}(\rho u) + \frac{1}{r}\frac{\partial}{\partial r}(r\rho v) = 0. \tag{4.38}$$

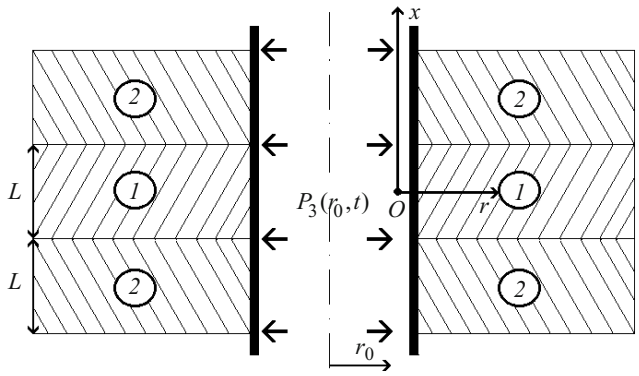

Fig. 4.31

The system of equations (4.38) has the following vector form:

$$\frac{\partial \overline{F}}{\partial t}+\frac{\partial \overline{A}}{\partial x}+\frac{1}{r}\frac{\partial}{\partial r}(r\overline{B})+\frac{\overline{C}_0}{r}=0,$$

$$\overline{F}=\begin{pmatrix}\rho u\\ \rho v\\ \rho\end{pmatrix},\quad \overline{A}=\begin{pmatrix}\rho u^2+P\\ \rho uv\\ \rho u\end{pmatrix},\quad B=\begin{pmatrix}\rho uv\\ \rho v^2+P\\ \rho v\end{pmatrix},\quad \overline{C}_0=\begin{pmatrix}0\\ -P\\ 0\end{pmatrix}, \tag{4.39}$$

where u is the velocity of displacement of particles along the axis x; v is the velocity of displacement of particles along the axis r; ρ is the density of the corresponding soil layer; P is the pressure of the corresponding point of soil medium (x, r).

The equations of state of soil medium for every layer follow from the model of nonlinear multicomponent medium (4.11) [38, 39].

The coupling of the problem for the shell–soil system of periodic structure is provided by the no-flow conditions at the deformed interface between the shell and the soil medium:

$$\dot{u}_1=u,\qquad \dot{u}_3=\nu, \tag{4.40}$$

where u, ν are the velocities of the boundary of the soil medium.

The symmetry conditions for kinematical and force quantities are set at the interface of inhomogeneous soil layers. We use Eqs. (4.38), (4.40) and conditions of the absence of perturbations of displacements at infinity as the boundary conditions for the problem of the dynamics of soil layer.

To solve the initial equations of the theory of vibrations of shells with the Timoshenko hypotheses [137], we use the integral-interpolation method for construction of difference schemes for hyperbolic equations [69]. The two-step MacCormack scheme [70] is used for numerical solution of problems of the dynamical behavior of soil medium:

at the predictor step:

$$\widetilde{\overline{F}}_1=\overline{F}^n_{k,l}-\Delta t\left[\frac{\overline{A}_{k,l}-\overline{A}_{k,l-1}}{\Delta x}+\frac{\overline{B}_{k,l}-\overline{B}_{k,l-1}}{\Delta r}+\overline{C}_{k,l}\right]^n,\qquad \Phi(\widetilde{P}_k,\widetilde{\rho}_k)=0, \tag{4.41}$$

at the corrector step:

$$\overline{F}^{n+1}_{k,l}=0.5\left\{\overline{F}^n_{k,l}-\widetilde{\overline{F}}_{k,l}-\Delta t\left[\frac{\widetilde{A}_{k,l+1}-\widetilde{A}_{k,l}}{\Delta x}+\frac{\widetilde{B}_{k+1,l}-\widetilde{B}_{k,l}}{\Delta r}+\widetilde{C}_{k,l}\right]\right\},$$

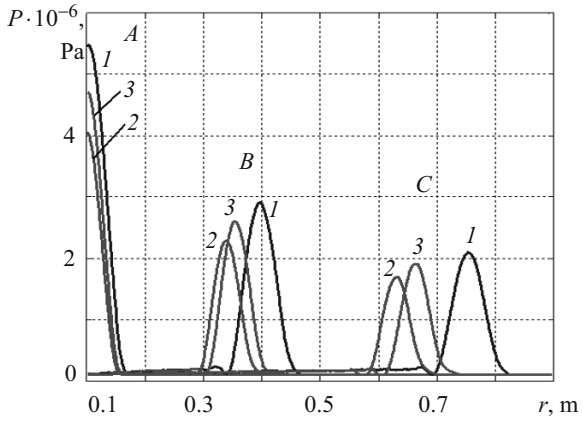

Fig. 4.32

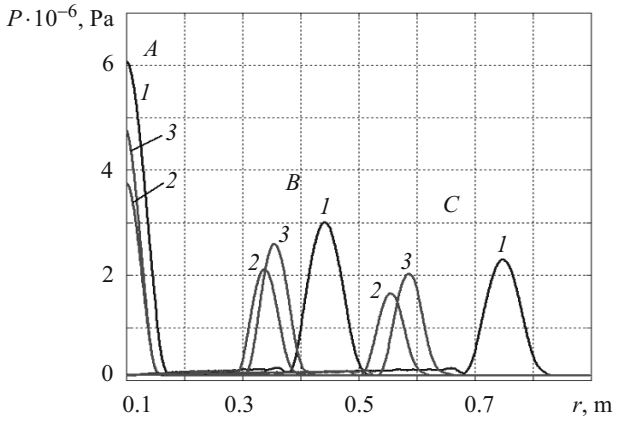

Fig. 4.33

$$\Phi(P_k^{n+1}, \rho_k^{n+1}) = 0.$$

To determine the pressure P from the given values of density ρ, the Newton–Raphson iteration iteration procedure is used in Eq. (4.41). Since the MacCormack difference scheme (4.41) is explicit, we use the stability condition

$$\max((|u|+c)\tau/\Delta x,\ (|v|+c)\tau/\Delta r) < 1,$$

where c is the local velocity of sound in soil medium (4.12).

Numerical Results. Consider the problem of propagation of cylindrical waves in stiffened soil medium of periodic structure (Fig. 4.31). Assume that loading (2.13) is applied to the inner surface of the stiffened cylindrical cavity for $r = r_0$. It is assumed that $r_0 = 0.1$ m, $L/r_0 = 4$, $r_0/h = 10$. The results of numerical computations of dependences of pressure waves P on the distance r from the edge of the stiffened cylindrical shell for $r = r_0$ are shown in Figs. 4.32 and 4.33, where three groups of dependences of pressure waves for different times are presented; A, B, C correspond to $0.75T$, $4T$, $8T$ (variant 1), C corresponds to $2T$ (variant 2).

The dependences of the pressure values P on the coordinate r for variant 1 are presented in Fig. 4.32. Curves *1* correspond to the soil with parameters $\alpha_1 = 0$, $\alpha_2 = 0.3$, $\alpha_3 = 0.7$ in the cross-section $x = 0$ according to Fig. 4.31. Curves *2* correspond to the values of P in the soil layer with parameters $\alpha_1 = 0$, $\alpha_2 = 0.7$, $\alpha_3 = 0.3$ in the cross-section $x = L$. Curves *3* are the values of pressure P at the interfaces of layers for $x = L/2$.

Similar computational data are given in Fig. 4.33 for variant 2. The first soil layer has parameters $\alpha_1 = 0$, $\alpha_2 = 0.2$, $\alpha_3 = 0.8$ (curves *1* corresponds to the cross-section $x = 0$); the second layer corresponds to $\alpha_1 = 0$, $\alpha_2 = 0.8$, $\alpha_3 = 0.2$ (curves *2* are given in the cross-section $x = L$); curves *3* correspond to the pressure P at the interfaces of layers ($x = L/2$). For both cases, it is assumed that $\rho_2 = 10^3$ kg/m^3, $\rho_3 = 2650$ kg/m^3, $\gamma_2 = 7$, $\gamma_3 = 4$ in formula (4.11).

The results of computations are in qualitative agreement with the computational results for non-stiffened soil medium of periodic structure (see 4.5). The presence of reinforcing shell in the cylindrical cavity decreases the amplitudes of pressure waves in the corresponding cross-sections in comparison with the results [29]. Here the amplitudes of pressure waves depend explicitly on the parameters of the soil layer. The results also differ with respect to the time coordinate. The amplitude of the wave P (curve *1*) in the cross-section $r/r_0 = 7.5$ occurs at $t = 8T$ in variant 1 and at $t = 7T$ in variant 2. The situation is similar for the other variants of computations.

Similar problems are considered in [78, 81, 91, 93, 103, 108, 134–136, 139].

Conclusions. We have reviewed publications on the experimental investigation of the dynamics of inhomogeneous cylindrical shells under different non-stationary loading. The performed analysis of experimental investigations allows stating that for further development and refining of theoretical methods of determining the SSS and vibrations of inhomogeneous shells under dynamical loading, it is necessary to expand and develop experimental investigations of the dynamics of shells.

It is important to derive equations based on nonlinear refined equations of three-layer shells of revolution. Nonlinear dynamical problems for three-layer shells of revolution with continuous or piecewise-inhomogeneous filler under independent kinematic and static hypothesis for each layer with considering transverse and normal deformations in the filler have been developed substantially. This approach is used when the difference of physical and mechanical properties of layers is significant. Here the order of the governing system of equations depends on the number of layers. The satisfactory agreement of the results of theoretical and experimental investigations for three-layer objects with continuous and piecewise-inhomogeneous filler allows us to state that the relevant theory has been developed adequately.

We considered three-layer shells of revolution with discrete ribbed filler under impulsive loading. The equations of dynamical deformation of a three-layer elastic shell structure with discrete filler were derived using the Timoshenko hypotheses in geometrically nonlinear approximation. By means of numerical methods, we solved the problems of the dynamical behavior of three-layer shells of revolution with discrete filler under impulsive loading and discovered new mechanical effects.

It is of interest to find analytical solutions, according to the classical theory of shells and rods, for the dynamical characteristics of open cylindrical and spherical shells stiffened by a regular system of discrete ribs and resting on Winkler and Pasternak foundations.

It is necessary to note that the majority of discretely stiffened shell structures contacting with an elastic medium undergo deflections comparable with their thickness. Therefore, it is necessary to investige the problems of the dynamical behavior of thin ribbed shells based on the geometrically nonlinear theory of rods and shells with the Timoshenko hypotheses. The developed and tested technique of investigation of the dynamics of shells of revolution on elastic foundation in geometrically linear and nonlinear statements enables investigation of the dynamics of discretely stiffened shells of revolution on Winkler and Pasternak elastic foundation. Such shell structures are widely used in aircraftss, where they perform both new functional purpose and are subject to new types of non-stationary loading.

Numerical algorithms for solving coupled dynamic problems for inhomogeneous shell structures on an elastic foundation of bilateral action modeled by a three-component water-saturated soil have been developed. The algorithm for solving problems of the interaction of cylindrical and spherical shells with soil medium is based on the MacCormack finite-difference scheme. As a particular case, we considered cylindrical and spherical shells on Winkler elastic foundation under impulsive internal loading. In this case, the equations of vibrations are similar to the equations of vibrations of the shell–medium system. On this basis, it is possible to obtain a formula for Winkler coefficients in the case of each particular variant of vibrations of the shell–medium system.

We investigated a two-layered soil medium with a stiffened infinite cylindrical cavity. Distributed impulsive loading is applied to the internal surface of the supporting cylindrical shell. In the case of propagation of cylindrical waves, the motion of the two-layer medium is described by a system of equations for Euler coordinates. The dependences of pressure waves at instants of reaching the interfaces of soil medium and their interaction have been presented.

The problem for a closed spherical shell in soil medium under internal impulsive loading is solved and the propagation of waves depending on the content of the medium is studied. We consider an infinite cylindrical cavity in soil medium of periodic structure, where distributed impulsive loading is applied to the internal surface. The dependences of pressure on the spatial variable for different times and variants of soil layers have been presented.

An infinite cylindrical cavity in soil medium of periodic structure supported by a cylindrical shell, to the internal surface of which distributed impulsive loading is applied has been investigated. The presence of the supporting shell in the cylindrical cavity affects how the amplitudes of the pressure waves decrease in the corresponding cross-sections of layers. The amplitudes of pressure waves explicitly depend on the parameters of soil layers. It should be noted that the development of modern well technologies, where shell structures of casing pipes subject to different types of dynamical loading are used, requires both development of computational methods and solution of new engineering problems.

REFERENCES

1. Ya. Aleksandrov, L. E. Bruker, A. M. Kurshin, and A. P. Prusakov, *Design of Three-Layer Panels* [in Russian], Oborongiz, Moscow (1960).
2. S. A. Ambartsumyan, *Theory of Anisotropic Shells* [in Russian], Fizmatgiz, Moscow (1961).

3. I. Ya. Amiro and V. A. Zarutskii, *Theory of Ribbed Shells*, Vol. 2 of the five-volume series *Methods of Shell Design* [in Russian], Naukova Dumka, Kyiv (1980).
4. I. I. Anik'ev, V. I. Gulyaev, G. M. Ivanchenko, P. Z. Lugovoi, et al., "On the effect of quasi-total internal reflection of elastic waves by the interfaces of elastic media," *PMTF*, **41**, 1, 21–27 (2000).
5. A. S. Vol'mir, *Stability of Deformable Systems* [in Russian], Nauka, Moscow (1967).
6. K. G. Golovko, P. Z. Lugovoi and V. F. Meish, *Dynamics of Inhomogeneous Shells under Non-Stationary Loading* [in Russian], Kievskii Universitet, Kiev (2012).
7. K. G. Golovko, P. Z. Lugovoi, and Yu. N. Podilchuk, "On the effect of elastic foundation on propagation of harmonic waves in orthotropic cylindrical shell," *Mat. Met. Fiz.-Mekh. Polya*, **50**, 1, 98–106 (2007)
8. K. G. Golovko P. Z. Lugovoi, and V. F. Meish, "Wave processes in stiffened cylindrical shells on elastic foundation under impulsive loading," *Bulletin of NTUU* (*KPI*), *Ser. Girnitstvo*, No. 14, P. 17–21 (2007).
9. K. G. Golovko, P. Z. Lugovoi, and V. F. Meish, "Solving dynamic problems for reinforced cylindrical shells on a Winkler foundation under impulsive loads," *Sist. Tekhnol.*, *Vip.: Mat. Probl. Tekhn. Mekh.*, No. 4 (45), 3–7 (2006).
10. V. A. Zarutskii and V. F. Sivak, "Experimental investigation of dynamics of shells (survey)," *Int. Appl. Mech.*, **35**, No. 3, 3–11 (1999).
11. V. O. Kononenko, A. M. Nosachenko, and A. I. Telalov, *Investigation of Vibrations of Fiberglass Shells* [in Russian], Naukova Dumka, Kiev (1974).
12. V. G. Kravets, P. Z. Lugovoi, and P. Ya. Prokopenko, "Effect of reinforcement and elastic foundation on oscillations of rectangular in plan planar ribbed cylindrical shells," *Bulletin of NTUU* (*KPI*), *Ser. Girnitstvo*, No. 20, 20–26 (2011).
13. V. D. Kubenko, P. Z. Lugovoi, and N. Ya. Prokopenko, "Influence of reinforcement on the natural frequencies of shallow cylindrical shells with rectangular planform on an elastic foundation," *Probl. Obchysl. Mekh. Mitsn.*, **16**, 151–156 (2011).
14. L. A. Latanskaya, V. F. Meish, and V. A. Kairov, "Mathematical modeling of stress–strain state of three-layer spherical shells with piecewise-continuous filler under impulsive loading," *Probl. Obchysl. Mekh. Mitsn.*, No. 14, 216–223 (2010).
15. L. A. Latanskaya and V. F. Meish, "Numerical solution of dynamical axisymmetric problems of the theory of ellipsoidal shells with piecewise-homogeneous filler," *Visn. Dnipropetr. Nats. Univ.*, *Ser. Mekhanika*, **2**, No. 11, 110–116 (2007).
16. V. N. Loginov, *Electric Measurement of Mechanical Quantities* [in Russian], Energiya, Moscow (1976).
17. V. D. Lomtadze, *Engineering Geology*, *Engineering Geodynamics* [in Russian], Nedra, Leningrad (1977).
18. P. Z. Lugovoi, M. O. Lisyuk, M. I. Mikhailova, I. I. Akinfeev, and E. O. Sushchenko, "Effects of total internal reflection of explosive waves in a cylindrical shell with liquid," *Bulletin of NTUU* (*KPI*), *Ser. Girnitstvo*, No. 12, 7–13 (2005).
19. P. Z. Lugovoi, M. O. Lisyuk, M. I. Mikhailova, and I. I. Akinfeyev, "Theoretical and experimental investigation of waves propagation in orthotropic cylindrical shells," *Vest. Kremench. Gos. Politekhn. Univ.*, No. 5 (34), 105–106 (2005).
20. P. Z. Lugovoi, V. F. Meish, and Yu. A. Meish, "Dynamical interaction of structurally orthotropic cylindrical shells with elastic foundation," in: *Mathematical Problems of Technical Mechanics* [in Russian], No. 1(24), DDTU, Dneprodzerzhinsk (2014), pp. 8–13.
21. P. Z. Lugovoi, V. F. Meish, and Yu. A. Meish, "Dynamical behavior of cylindrical and spherical shells in soil medium," *Vest. Nats. Transp. Univ.*, Part 2, NTU, Kiev, No. 19, 249–254 (2009).
22. P. Z. Lugovoi, V. F. Meish, and Yu. A. Meish, "Numerical solution of nonlinear problems of the theory of stiffened cylindrical shells under non-stationary loading," in: *Proc. 2nd Int. Conf. on Mathematics in Modern Technical University* [in Ukrainian], NTUU (KPI), Kiev (2013), pp. 52–55.
23. P. Z. Lugovoi and V. F. Meish, "Wave processes in the spherical shell–soil medium system under impulsive loading," *Vest. Nats. Transp. Univ.*, Part 1, No. 15, 93–98 (2007).
24. P. Z. Lugovoi, "Dynamics of shell structures under impulsive loading (survey)," *Int. Appl. Mech*., **26**, No. 8, P. 3–20 (1990).
25. P. Z. Lugovoi, "Dynamics of thin-wall structures under non-stationary loading (survey)," *Int. Appl. Mech*., **37**, No. 5, 44–74 (2001).

26. P. Z. Lugovoi and N. Ya. Prokopenko, “On dispersion curves for harmonic waves propagating along longitudinally reinforced cylindrical shells on elastic foundation,” in: *Trans. Dneprodzerzhinsk State Technical University* [in Ukrainian], No. 1(24), Dneprodzerzhinsk (2014), pp. 140–143.
27. P. Z. Lugovoi, K. G. Golovko, and V. F. Meish, “Dynamical behavior of spherical shells on elastic foundation under impulsive loading,” *Syst. Tekhnol.*, No. 4 (51), 9–13 (2007).
28. P. Z. Lugovoi and V. F. Meish, “Numerical modeling of dynamical behavior and strength computation of multilayered shells under impulsive loading,” *Probl. Prochn.*, No. 4, 86–96 (2000).
29. P. Z. Lugovoi, V. F. Meish, and Yu. A. Meish, “Dynamical behavior of a cylindrical shell interacting with three-component soil medium of periodic structure,” in: *Nonstationary Processes of Deformation*, *Caused by Fields of Different Nature* [in Ukrainian], Inst. Prikl. Probl. Mekh. Mat. NANU, Lvov (2012), pp. 99–102.
30. P. Z. Lugovoi, V. F. Meish, and Yu. A. Meish, “On solving axisymmetric problems of dynamics of stiffened conic shells on elastic foundation,” *Probl. Vych. Mekh. Prochn. Konstr.*, No. 13, 142–148 (2009).
31. P. Z. Lugovoi, V. F. Meish, and Yu. A. Meish, “Numerical solution of the problem of the dynamical interaction of inhomogeneous cylindrical shells with elastic soil medium,” *Probl. Vych. Mekh. Prochn. Konstr.*, No. 23, 124–134 (2014).
32. P. Z. Lugovoi, V. F. Meish, Yu. A. Meish, and G. M. Zabolotny, “Forced vibrations of five-layer cylindrical shells with longitudinal-transverse reinforcement under distributed loading,” in: *Methods for Solving Applied Problems of Solid Mechanics* [in Russian], No. 12, DNU, Dnepropetrovsk (2011), pp. 203–209.
33. P. Z. Lugovoi, V. F. Meish, and E. A. Shtantsel’, *Non-Stationary Dynamics of Inhomogeneous Shell Structures* [in Russian], Kiev. Univ., Kiev (2005).
34. P. Z. Lugovoi, V. P. Mukoid, and V. F. Meish, *Dynamics of Shell Structures under Explosive Loads* [in Russian], Naukova Dumka, Kiev (1991).
35. P. Z. Lugovoi and N. Ya. Prokopenko, “Effect of elastic foundation on the natural frequencies of a ribbed cylindrical shell,” *Probl. Vych. Mekh. Prochn. Konstr.*, No. 23, 135–146 (2014).
36. P. Z. Lugovoi, N. Ya. Prokopenko, and K. G. Golovko, “Dispersion curves for harmonic waves propagating along longitudinally reinforced cylindrical shells on elastic foundations,” in: *Mathematical Problems of Technical Mechanics* [in Russian], No. 2 (22), DDTU, Dneprodzerzhinsk (2013), pp. 99–104.
37. P. Z. Lugovoi, V. F. Sivak, K. G. Golovko, and N. I. Kritskaya, “Experimental investigation of the effect of continuum on the dynamical characteristics of a stiffened cylindrical shell under impulsive loading,” *Probl. Vych. Mekh. Prochn. Konstr.*, No. 18, 120–125 (2012).
38. V. M. Lyakhov, *Waves in Soils and Porous Multicomponent Media* [in Russian], Nedra, Moscow (1982).
39. V. M. Lyakhov, *Fundamentals of Dynamics of Explosion in Soils and Liquid Media* [in Russian], Nedra, Moscow (1974).
40. V. F. Meish and N. V. Kravchenko, “Application of difference schemes of approximation of Richardson type for solving dynamical problems of the theory of discretely reinforced multilayered cylindrical shells,” *Bulletin of Kiev National University*, *Ser. Phys.&Math.*, No. 3, 115–121 (2004).
41. V. F. Meish, “Wave processes in the system cylindrical shell – soil medium of periodic structure under impulsive loading,” *Bulletin of NTUU* (*KPI*), *Ser. Girnitstvo*, No. 27, 15–21 (2015).
42. V. F. Meish, “Numerical solving of the problems of cylindrical wave propagation in soil media of periodic structure,” *Bulletin of NTUU* (*KPI*), *Ser. Girnitstvo*, No. 25, 9–16 (2014).
43. V. F. Meish and N. V. Arnauta, “Forced Vibrations of five-layerd shells with discrete ribs under non-stationary loading,” issue 4 (57), *Mathematical Problems of Technical Mechanics* [in Russian], Dnepropetrovsk (2008), pp. 120–124.
44. V. F. Meish and N. V. Arnauta, “Computation of axisymmetric vibrations of reinforced cylindrical shells under longitudinal boundary loading,” *Probl. Vych. Mekh. Prochn. Konstr.*, No. 15, P. 89–96 (2010).
45. V. F. Meish and N. V. Arnauta, “Computation of axisymmetric vibrations of three-layer cylindrical shells with discrete ribs under non-stationary loading,” *Mathematical Problems of Technical Mechanics* [in Russian], Dnepropetrovsk, No. 3 (62), 40–44 (2009).
46. V. F. Meish and N. V. Arnauta, “Numerical algorithm for computation of axisymmetric vibrations of reinforced three-layer cylindrical shells using Richardson finite-difference approximations,” *Probl. Vych. Mekh. Prochn. Konstr.*, No. 14, 246–253 (2010).

47. V. F. Meish, N. V. Arnauta, and G. M. Zabolotnyi, "Forced vibrations of longitudinally stiffened multilayered cylindrical shells under nonstationary loading," in: *Methods for Solving Applied Problems of Solid Mechanics* [in Russian], DNU, Dnepropetrovsk, No. 10 (2009), pp. 199–205.
48. V. F. Meish and N. V. Kravchenko, "Forced vibrations of multilayered spherical shells with reinforced hole under non-stationary loading," *Teor. Prikl. Mekh.*, No. 37, 146–150 (2003).
49. V. F. Meish and N. V. Kravchenko, "Computation of the stress-strain state of the multilayered shells with discrete inhomogeneities under non-stationary loading," *Bulletin of Kiev National University*, *Ser. Phys.&Math.*, No. 3, 210–216 (2002).
50. V. F. Meish and N. V. Kravchenko, "Non-axisymmetric oscillations of inhomogeneous multilayered discretely reinforced cylindrical shells under non-stationary loading," *Int. Appl. Mech*., **39**, No. 9, 88–95 (2003).
51. V. F. Meish and N. V. Kravchenko, "Application of difference approximations of Richardson type for solving dynamical problems of the theory of discretely reinforced multilayered cylindrical shells," *Bulletin of Kiev National University*, *Ser. Phys.&Math.*, No. 3, 115–121 (2004).
52. V. F. Meish and L. A. Latanskaya, "Axisymmetric vibrations of three-layer cylindrical shells with piecewise-continuous filler under non-stationary loading," *Vest. Donetsk. Nats. Univ.*, *Ser. A*, *Estest. Nauki*, No. 1, 161–164 (2008).
53. V. F. Meish, P. Z. Lugovoi, and V. M. Melnik, "Dynamical behavior of a conic shell of variable thickness on elastic foundation," *Probl. Vych. Mekh. Prochn. Konstr.*, No. 19, 219–225 (2012).
54. V. F. Meish and Yu. A. Meish, "Mathematical modeling of wave processes in a cylindrical shell–two-layer soil system," *Bulletin of NTUU* (*KPI*), *Ser. Girnitstvo*, No. 22, 3–8 (2012).
55. V. F. Meish and Yu. A. Meish, "Statement and numerical algorithm for solving problems of forced vibrations in the theory of three-layer cylindrical shells with piecewise-homogeneous filler," *in: Mathematical Problems of Technical Mechanics* [in Russian], No. 2(25), DDTU, Dneprodzerzhinsk (2003), pp. 21–26.
56. V. F. Meish and Yu. A. Meish, "Numerical solution of problems of the forced vibrations of three-layer cylindrical shells with piecewise-homogeneous filler," *Vest. Nats. Transp. Univ.*, No. 8, 432–437 (2003).
57. V. F. Meish, Yu. A. Meish, and E. A. Shtantsel', "Dynamical behavior of three-layered beams within applied theories under nonstationary loading," *Mathematical Problems of Technical Mechanics* [in Russian], No. 4 (51), DDTU, Dneprodzerzhinsk (2007), pp. 27–34.
58. V. F. Meish, V. F. Mukoid, and E. A. Shtantsel', "Comparative analysis of dynamical behavior of three-layer cylindrical shells with inhomogeneous filler within the framework of applied theories," *Bulletin of Kiev National University*, *Ser. Phys.&Math.*, No. 3, 163–168 (2000).
59. V. F. Meish, V. K. Stryuk, and L. V. Kot, "Non-stationary behavior of the three-layered discretely reinforced shells of revolution under longitudinal impulsive loading," *Bulletin of Kiev National University*, *ser. Phys.&Math.*, No. 3, 171–175 (1999).
60. V. F. Meish, Yu. A., Khamrenko and A. P. Mukoid, "Dynamical behavior of three-layer ellipsoidal shell of revolution under axisymmetric non-stationary loading, *Bulletin of Kiev National University*, *Ser. Phys.&Math.*, No. 3, 71–76 (1998).
61. V. F. Meish, Yu. A. Khamrenko, and N. A. Shulga, "Non-stationary vibrations of cylindrical shells under axisymmetric loading," *Int. Appl. Mech.*, **35**, No. 8, 3–9 (1999).
62. V. F. Meish and S. E. Shtantsel', "Non-axisymmetric vibrations of three-layer shells with inhomogeneous filler under dynamical loading," *Bulletin of Kiev National University*, *Ser. Phys.&Math.*, No. 5, 342–347 (2001).
63. V. F. Meish and S. E. Shtantsel', "Construction of numerical algorithm for solving dynamical problems of theory of three-layer shells with inhomogeneous filler," *Mathematical Problems of Technical Mechanics* [in Russian], No. 2 (13), DDTU, Dneprodzerzhinsk (2001), pp. 97–102.
64. V. F. Meish, N. A. Shul'ga, and Yu. A. Khamrenko, "On the theory of non-stationary axisymmetric vibrations of three-layer shells of revolution," Dop. NAN Ukrainy, No. 9, 69–73 (1999).
65. I. A. Luchko, V. A. Plaksii, N. S. Remez, et al., *Mechanical Effect of an Explosion in Soil* [in Russian], Naukova Dumka, Kyiv (1989).
66. E. S. Osternik, "Experimental investigations of deformations of the normal and the method of implementing boundary conditions for layered plates," in: *Proc. 8th All-Union Conf. on the Theory of Plates and Shells* [in Russian], Nauka, Moscow (1973), pp. 596–602.

67. A. V. Perel'muter and V. I. Slivker, *Computational Models of Buildings and Potentials of Their Analysis* [in Russian], Stal', Kiev (2000).
68. S. A. Rumyantsev, *Dynamics of Transient Processes and Self-Synchronization of Motions of Vibration Machines* [in Russian], UrO RAN, Ekaterinburg (2003).
69. A. A. Samarskii, *Theory of Difference Schemes* [in Russian], Nauka, Moscow (1977).
70. C. A. Fletcher, *Computational Techniques for Fluid Dynamics*, Vol. 2, Springer-Verlag, Berlin (1988).
71. A. N. Guz, V. A. Zarutskii, I. Ya. Amiro, et al., *Experimental Investigations of Thin-Wall Structures* [in Russian], Naukova Dumka, Kiev (1984).
72. H. Altenbach, "An alternative determination of transverse shear stiffnesses for sandwich and laminated plates" *Int. J. Solids Struct.* **37,** 3503–3520 (2000).
73. H. Altenbach, "Theories for laminated and sandwich plates: A review," *Mech. Comp. Mater.*, **34**, No. 3, 243–252 (1998).
74. E. Carrera, "Historical review of zig-zag theories for multilayered plates and shells," *Appl. Mech. Rev.*, **56,** No. 3, 287–309 (2003).
75. E. Carrera, "Theories and finite elements for multilayered, anisotropic, composite plates and shells," *J. Arch. Comput. Meth. Eng.*, **9**, No. 2, 87–140 (2002).
76. E. Carrera, "Developments, ideas, and evaluations based upon Reissner's Mixed Variational Theorem in the modeling of multilayered plates and shells," *Appl. Mech. Rev.*, **54,** 301–329 (2001).
77. E. Carrera, "On the use of the Murakami's zig-zag function in the modeling of layered plates and shells," *Comp. Struct.*, **82,** 541–554 (2004).
78. K. Cichocki, "Effects of underwater blast loading on structures with protective elements," *Int. J. Impact Eng.*, **22**, No. 6, 609–617 (1999).
79. Ö. Civalec, "Geometrically nonlinear dynamic and static analysis of shallow spherical shell resting on two-parameters elastic foundations," *Int. J. Press. Vess. Piping*, **113,** 1–9 (2014).
80. B. Collet and J. Pouget, "Nonlinear modulation of wave packets in a shallow shell on an elastic foundation," *Wave Motion*, **34** (1), 112–118 (2001).
81. K. G. Golovko, P. Z. Lugovoi, and V. F. Meish, "Solution of axisymmetric dynamic problems for cylindrical shells on an elastic foundation," *Int. Appl. Mech.*, **43,** No. 12, 1390–1395 (2007).
82. Ya. M. Grigorenko, A. Ya. Grigorenko, and G. G. Vlaikov, *Problems of Mechanics for Anisotropic Inhomogeneous Shells on the Basis of Different Models*, S.P. Timoshenko Institute of Mechanics, Technical center of the National Academy of Science of Ukraine, Kiev (2009).
83. K. Guler and Z. Celep, "Static and dynamic responses of a rigid circular plate on a tensionless Winkler foundation," *J. Sound Vibr.*, **276**, No. 1–2, 449–458 (2004).
84. V. I. Gulyaev, P. Z. Lugovoi, and N. A. Lysyuk, "Propagation of harmonic waves in a cylindrical shell (Timoshenko model)," *Int. Appl. Mech.*, **39**, No. 4, 472–478 (2003).
85. A. P. Gupta and N. Bfardwaj, "Vibration of rectangular orthotropic elliptic plates on quadratically varying thickness on elastic foundation," *J. Vibr. Acoust.*, **126,** No. 1, 132–140 (2004).
86. Hiroyuki Matsunaga, "Vibration and stability of thick plates on elastic foundation," *J. Eng. Mech.*, **126**, No. 1, 27–34 (2000).
87. Yi. Huang and He Fang-she, "Free vibrations of shallow spherical shells on elastic foundation," *Chin. J. Geotechn. Eng.*, **16**, No. 5, 36–46 (1994).
88. Hui-Shen Shen, "Large deflection of Reissner–Mindlin plates on elastic foundations," *J. Eng. Mech.*, **124**, No, 10, 1080–1089 (1998).
89. Hui-Shen Shen, "Postbuckling of orthotropic plates on two-parameter elastic foundation," *J. Eng. Mech.*, **121**, No. 1, 50–56 (1995).
90. Kadir Guller, "Circular elastic plate resting on tensionless Pasternak foundation," *J. Eng. Mech.*, **130**, No. 10, 1251–1254 (2004).
91. N. Kambouchev, L. Noels, and R. Rodovitzky, "Numerical simulation of the fluid–structure interaction between air blast waves and free – standing plates," *Comp. Struct.*, **85,** 923–931 (2007).
92. A. A. Khathan, "Large-deformation analysis of plates on unilateral elastic foundation," *J. Eng. Mech.*, **120**, No. 8, 1820–1827 (1994).

93. V. D. Kubenko and P. S. Kovalchuk, “Stability and nonlinear vibrations of closed shells of cylindrical shape interacting with flowing fluid,” *Int. Appl. Mech.*, **51**, No. 1, 19–79 (2015).
94. P. Z. Lugovo, I. Yu. Podil’chuk, and V. F. Sivak, “Experimental study of the behavior of a cylindrical shell under impulsive loading with ambient humidity taken into account,” *Int. Appl. Mech.*, **46,** No. 4, 418–421 (2010).
95. P. Z. Lugovo and N. Ya. Prokopenko, “Vibrations of ribbed shallow rectangular shells on an elastic foundation,” *Int. Appl. Mech.*, **46,** No. 8, 912–918 (2010).
96. P. Z. Lugovoi and N. Ya. Prokopenko, “Influence of reinforcement and elastic foundation on the vibrations of shallow shells with rectangular planform,” *Int. Appl. Mech*., **47,** No. 6, 714–719 (2011).
97. P. Z. Lugovoi, V. F. Meish, and K. G. Golovko, “Solving axisymmetric dynamic problems for reinforced shells of revolution on an elastic foundation,” *Int. Appl. Mech.*, **45,** No. 2, 193–199 (2009).
98. P. Z. Lugovoi, V. V. Sivak, and V. F. Sivak, “Experimental research of the vibrations of a cylindrical shell filled with some medium and subjected to impulsive loading,” *Int. Appl. Mech.*, **45,** No. 11, 1232–1235 (2009).
99. P. Z. Lugovoi, V. V. Sivak, and V. F. Sivak, “Stress distribution in a glassfiber-reinforced plastic shell structure under impulsive transverse loading,” *Int. Appl. Mech*., **45,** No. 4, 443–447 (2009).
100. P. Z. Lugovoi and N. Ya. Prokopenko, “Influence of an elastic foundation on the dispersion of harmonic waves in longitudinally reinforced cylindrical shells,” *Int. Appl. Mech.*, **51**, No. 5, 583–590 (2015).
101. P. Z. Lugovoi, V. F. Meish, and S. E. Shtantsel’, “Forced nonstationary vibrations of a sandwich cylindrical shell with cross-ribbed core,” *Int. Appl. Mech*., 2005, **41**, No. 2, 161–167 (2005).
102. P. Z. Lugovoj, “Propagation of harmonic waves in an orthotropic cylindrical shells on elastic foundation,” *Int. Appl. Mech.*, **40**, No. 3, 297–303 (2004).
103. F. Marconi, “Investigation of the interaction of a blast wave with an internal structure,” *AIAA J.*, **32**, No. 8, 1561–1567 (1994).
104. V. F. Meish and Yu. A. Khamrenko, “Comparative analysis of the dynamic responses of transiently loaded sandwich shells predicted by various applied theories,” *Int. Appl. Mech*., **39**, No. 7, 856–861 (2003).
105. V. F. Meish and N. V. Kravchenko, “Nonaxisymmetric vibrations of discretely reinforced inhomogeneous multilayer cylindrical shells under nonstationary loads,” *Int. Appl. Mech.*, **39**, No. 9, 1066–1072 (2003).
106. V. F. Meish and A. M. Mikhlyak, “Forced vibrations of three-layer elliptic cylindrical shells under distributed loads,” *Int. Appl. Mech.*, **46**, No. 2, 195–200 (2010).
107. I. Mirsky and G. Herrmann, “Nonaxially symmetric motions of cylindrical shells,” *J. Acoust. Soc. Amer.*, **28**, No. 2, 277–203 (1973).
108. Moon-Hee Nam and Kwan-Hee Lee, “Unsymmetrically loaded cylindrical tank on elastic foundation,” *J. Eng. Mech.*, **126,** No. 12, 1257–1261 (2000).
109. Nam-H. Kim, C. Fu, Chung, and Moon-Young Kim, “Exact solutions for free vibration analysis of non-symmetric curved beam on two-types of elastic foundation,” *J. Eng. Mech.*, **126**, No. 1, 71–77 (2000).
110. A. K. Noor and W. S. Burton, “Assessment of computational models for multilayered composite shells,” *Appl. Mech. Rev.*, **43**, No. 4, 67–97 (1990).
111. A. K. Noor, W. S. Burton, and C. W. Bert, “Computational models for sandwich panels and shells,” *Appl. Mech. Rev.*, **49**, No. 3, 155–200 (1996).
112. A. K. Noor, W. S. Burton, and J. M. Peters, “Assessment of computation models for multilayered composite cylinders,” *Int. J. Solids Struct.*, **27**, No. 10, 1269–1286 (1991).
113. A. K. Noor and W. S. Burton, “Assessment of shear deformation theories for multi-layered composite plates,” *Appl. Mech. Rev.*, **42** (1), 1–13 (1989).
114. N. J. Pagano, “Free edge stress fields in composite laminates,” *Int. J. Solids Struct.*, **14,** 401–406 (1978).
115. N. J. Pagano, “Exact solutions for composite laminates in cylindrical bending,” *J. Comp. Mater.*, **3,** 389–411 (1969).
116. N. J. Pagano, “Exact solutions for rectangular bidirectional composites and sandwich plates,” *J. Comp. Mater.*, **4**, 20–34 (1970).
117. D. N. Paliwal and Singh Satyendra, “Free vibrations of orthotropic cylindrical shell on elastic foundation,” *AIAA J.*, **37,** No. 9, 1135–1139 (1999).
118. M. S. Qatu, “Accurate theory for laminated composite deep thick shells, *Int. J. Solids Struct.*, **36**, No. 19, 2917–2941 (1999).

119. M. S. Qatu, “Recent research advances in the dynamic behavior of shells: 1989–2000, Part 1: Laminated Composite Shells,” *Appl. Mech. Rev.*, **55**, No. 4, 325–350 (2002).
120. M. S. Qatu, *Vibration of Laminated Shells and Plates*, Elsevier, Amsterdam (2004).
121. M. S. Qatu R. W. Sullivan, and W. Wang, “Recent research advances in the dynamic behavior of composite shells: 2000–2009,” *Comp. Struct.*, **93**, No. 1, 14–31 (2010).
122. M. S. Qatu, “Free vibration of laminated composite rectangular plates,” *Int. J. Solids Struct.*, **28**, No. 8, 941–954 (1991).
123. Qui Ping, Wang Xin-zhi, and Yeh Kai-yuah, “Bifurcation and chaos of the circular plates on the nonlinear elastic foundation,” *Appl. Math. Mech.*, **24**, No. 8, 880–885 (2003).
124. J. N. Reddy and R. A. Arciniega, “Shear deformation plate and shell theories: From Stavsky to present,” *Mech. Adv. Mater. Struct.*, **11,** 535–582 (2004).
125. J. N. Reddy, and C. F. Liu, “A higher-order shear deformation theory of laminated elastic shells,” *Int. J. Eng. Sci.*, **23**, 669–683 (1985).
126. J. N. Reddy, “On refined computational models of composite laminates,” *Int. J. Numer. Meth. Eng.*, **27**, 361–382 (1989).
127. J. N. Reddy, “A simple higher order theory for laminated composite plates,” *J. Appl. Mech.*, **51**, 745–752 (1984).
128. T. A. Rose, P. D. Smith, and G. S. Mays, “Effectiveness of walls designed for the protection of structures against air blast from high explosives,” in: *Proc. of the Institution of Civil Engineers: Structures and Buildings*, **110**, No. 1, 78–85 (1995).
129. S. Saicit Tamero lu, “Vibrations of clamped rectangular plates on elastic foundation subjected to uniform compressive forces,” *J. Eng. Mech.*, **122**, No. 8, 714–718 (1996).
130. H. Y. Sheng and J.Q. Ye, “A three-dimensional state space finite element solution for laminated composite cylindrical shells,” *Comp. Meth. Appl. Mech. Eng.*, **192**, No. 22–24, 2441–2459 (2003).
131. X. P. Shi, “Rectangular thick plate with free edges on Pasternac foundation,” *J. Eng. Mech.*, **120**, No. 5, 971–988 (1994).
132. N. A. Shulga and V. F. Meish, “Forced vibration of three-layered spherical and ellipsoidal shells under axially symmetric loads,” *Mech. Comp. Mater.*, **39**, No. 5, 625–636 (2003).
133. Yu. V. Skosarenko, “Natural vibrations of ribbed cylindrical shell interaction with elastic foundation,” *Int. Appl. Mech.*, **50**, No. 5, 111–128 (2014).
134. Yu. V. Skosarenko, “Stress–strain state of ribbed cylindrical shell interaction with elastic foundation under shot-time loads,” *Int. Appl. Mech.*, **51**, No. 1, 112–122 (2015).
135. K. P. Soldatos, “Mechanics of cylindrical shells with non-circular cross section,” *Appl. Mech. Rev.*, **49**, No. 8, 237–274 (1999).
136. K. P. Soldatos, “A refined laminated plate and shell theory with applications,” *J. Sound Vibr.*, **144**, No. 3, 109–129 (2000).
137. S. P. Timoshenko, D. X. Young, and Weaver, Jr., *Vibration Problems in Engineering*, John Wiley and Sons, New York (1974).
138. H. S. Turkmen, “Structural response of laminated composite shells subjected to blast loading: comparison of experimental and theoretical methods,” *J. Sound Vibr.*, **249**, No. 4, 663–678 (2002).
139. X. Wang and Z. Zhong, “Three-dimensional solution of smart laminated anisotropic circular cylindrical shells with imperfect bonding,” *Int. J. Solids Struct.*, **40**, No. 22, 5901–5921 (2003).
140. C. P. Wu and J. Y. Lo, “Three-dimensional elasticity solutions of laminated annular spherical shells,” *J. Eng. Mech.*, **126**, No. 8, 882–885 (2000).
141. V. A. Zarutskii and N. Ya. Prokopenko, “Influence of discrete longitudinal ribs on harmonic waves in cylindrical shells,” *Int. Appl. Mech.*, **39**, No. 4, 457–469 (2003).
142. V. A. Zarutskii and N. Ya. Prokopenko, “Vibrations and stability of shallow ribbed shells with a rectangular planform,” *Int. Appl. Mech.*, **38**, No. 6, 335–340 (2002).
143. V. A. Zarutskii, P. Z. Lugovoi, and V. F. Meish, “Dynamic problems and stress strain state of inhomogeneous shell structures under stationary and nonstationary loads,” *Int. Appl. Mech.*, **45**, No. 3, 245–272 (2009).